Auxiliary-Field Monte Carlo Methods for Interacting Fermions: Application to the Nuclear Shell Model

Thesis by

Gladys Hau-Wan Lang

In Partial Fulfillment of the Requirements

For the Degree of

Doctor of Philosophy

California Institute of Technology

Pasadena, California

1993

(Submitted May 14, 1993)

Abstract

This thesis presents the path-integral formulation of the nuclear shell model using the Hubbard-Stratonovich transformation, which linearizes the two-body interaction by auxiliary fields. The path-integral was evaluated via Monte Carlo. The method scales favorably with valence-nucleon number and shell-model basis: full-basis calculations can be done up to the rare-earth region, which cannot be treated by other methods. Observables are calculated for the ground state and in a thermal ensemble. Dynamical correlations are obtained, from which strength functions are extracted through the Maximum Entropy method. Examples in the *s-d* shell, where exact diagonalization can be carried out, compare well with exact results. The "sign problem", which is generic to fermion Monte Carlo calculations, is proved to be absent in a wide class of interactions including the attractive pairing-plus-multipole interactions. The formulation is general for interacting fermion systems and is well suited for parallel computation. The method has been implemented on the Intel Touchstone Delta System, achieving better than 99% parallelization.

To my parents

and

Sidney

ACKNOWLEGEMENTS

I am deeply indebted to Prof. Steve Koonin who suggested this thesis project, guided me through it, and also worked closely with me in it. At times when seemingly insurmountable obstacles were met, Steve has always been optimistic and gave me great encouragement. I am also grateful to Dr. David Dean, Dr. Calvin Johnson and Dr. Erich Ormand, who have collaborated in this project, for their hard work and contribution in making it successful.

Thanks go to people who helped me through the graduate studies. Prof. William A. Goddard has given me valuable advice during my second year at Caltech in the study of Hubbard Models. Dr. Hong Q. Ding introduced me to the field of parallel computation, and has given me much help. I have also to thank Heidi Lorenz-Wirzba and other staff members at the Caltech Concurrent Supercomputing Facilities, who have mantained the the parallel computing facilities, including the Hypercubes and the Intel Gamma and Delta System, on which most of my graduate work relies.

I have to thank the Caltech community for making graduate life here easier and more pleasant, especially, the staff at the Kellogg Radiation Laboratory, at the physics departmental office, and at the Registration office.

TABLE OF CONTENTS

I. INTRODUCTION

A. Interacting fermions

Interacting fermions are ubitquitous: nucleons in nuclei, electrons in atoms and condensed matter, quarks in hardrons. They consitute a large part of the physical problems in understanding matter. The exact treatment of the interacting fermions from first principles quantum mechanics is unrealistic apart from extremely simple systems, such as two-body system and three-body non-relativistic problems. Approximations have to be sought.

The idea of quasi-particles (independent particles dressed with effective mass and charge from interaction with the medium) proved to be successful in the early development of many branches of physics. In solid-state systems, the picture of independent electrons and holes moving in conduction and/or covalent bands give rise to a successful description of metals and semiconductors, where interactions between the particles are either unimportant, or can be handled within perturbation (scattering) calculations. In the nucleus, the independent particle picture of the early nuclear shell model explained a vast amount of nuclear data, such as abundances, and spins [1]. However, as the understanding becomes more sophisticated, there are examples where the simple picture is invalid. For example, in transition metals and magnetic materials, (or more specifically the high-temperature superconducting oxides), there is a strong correlation among electrons, and treatments that account for many-body effects are necessary. One example is the Hubbard model [2] in which the effect of Columb repulsion is simplified to a constant on-site repulsion for electrons on the same atomic orbital. Similarly, quantitative predictions for nuclear excitation spectra, transition rates, and electromagnetic moments can only be made by considering the residual interaction of the valence nucleons.

In these examples, the Hubbard model and the nuclear shell model, although the model space is drastically truncated to incorporate only the physically significant degrees of freedom, exact solutions of the model can only be had in simple or small systems: 4×4 lattice in the Hubbard model, 0s-1d nuclei in the nuclear shell model. The major limit is the combinatorial scaling of the Fock space with the single particle basis and number of valence particles in exact diagonalization calculations. It is a general challenge to develop methods to calculate strongly interacting many-fermions systems, where perturbation expansions are invalid. Different quantum Monte Carlo methods have been proposed in the last twenty years to treat quantum problems with stochastic methods [3] rather than direct diagonalization. Attempts like the Green's function Monte-Carlo method and related path-integral Monte-Carlo method, are limited in application to fermionic system, mainly due to the existence of nodes in femionic wavefunctions that arise from the antisymmetry properties in particle exchange [4]. Since the exchange symmetry is non-local, it is difficult to handle it in a local approach like the Green's function method. Results are usually obtained in the fixed node approximation [4], which generates an upper bound for the ground state energy.

The auxiliary field Monte Carlo method (AFMC) [5] was proposed as a way of handling interacting fermions. It is based on a Monte Carlo evaluation of a path-integral obtained by the Hubbard-Stratonovich transformation of the partition operator. The many-body wavefunction is represented by a set of single-particle wavefunctions evolving in fluctuating external fields. The method therefore enforces the Pauli principle exactly by using the Slater-determinant of single-particle wavefunctions, and involves a mild scaling of storage and computation time with the single-particle basis. The method is also applicable to bosonic systems, although it was most noted for handling fermion systems, which are difficult to deal with by other methods. Both finite temperature and ground state properties can be obtained. The AFMC method has

been applied to condensed matter systems such as the Hubbard Model, yielding much information about the electron correlations and magnetic properties.

Inspired by the success of the AFMC method in the Hubbard systems, we have applied the method to the nuclear shell model, which involves a a general two-body interaction rather than a simple on-site repulsion. Through these studies, we hope to develop a new method for studying the nuclear shell model, as well as to understand the power and limits of the auxiliary field Monte Carlo method for treating general fermionic systems. To put the work in better perspective, I will first review the nuclear shell model and what we hope to get from the Monte Carlo calculations. A detailed discussion of the nuclear shell model can be found in [6] and a review of the status of the model can be found in [1] [7].

B. The nuclear shell model

The early nuclear shell model describes nucleons as moving independently in an effective spherical potential generated by the interaction among them. The introduction of a strong $l \cdot s$ spin orbit force established the success of the model by its explanation of magic nuclei and the prediction of spin and parity for simple nuclei. Fig. 1 depicts the schematic single-particle orbitals with spin-orbit coupling, labelled by orbital and total angular momentum (l, j) [8]. The model explains the magic proton and neutron numbers observed in the nuclear abundances: the numbers correspond to the closing of major shells, above which a large gap exists for excitations, leading to especially stable 0^+ nuclei. It also predicts the spin and parity of nuclei where a single valence nucleon exists outside a closed shell, the values being just the spin and parity of the orbital. Predictions for more complicated nuclei can be made by considering the residual-interaction (i.e., that not included by the effective potential) among the valence nucleons outside a closed inert core of shells. Thus, the

nuclear shell model is a drastic truncation of the original problem, in which nucleons interact through a short range attraction and hard core repulsion, to a model space of valence nucleons in limited discrete orbitals, interacting with a much more tractable effective interaction.

However, exact calculations can still only be carried out in small nuclei or in systems with very few valence nucleons, because of the exponential growth of the dimension of the Fock space with the number of active orbitals or the number of valence nucleons. Various approximations has been used to treat more complicated nuclei, including mean-field methods: Hartree-Fock and Hartree-Fock-Bogoliubov method with various projection schemes for particle number and angular momentum. Boson approximations (interacting boson models) have been suggested for the lowest 0^+ and 2^+ nucleon pairs, to further truncate the shell model space [9]. These approximations were good for some nuclei.

The development of high performance computers extended the domain of nuclei that can be treated by exact diagonalization. The most successful examples are the systematic studies of *s-d* shell nuclei by Brown and Wildenthal [10] using a full-basis diagonalization of the *s-d* shell (i.e. keeping all the possible configurations of the valence nucleons in the *s-d* shell). The 63 matrix elements in the two-body Hamiltonian are fitted to 400 energy levels in different nuclei. Forty-seven linear combinations of the matrix elements are well determined from the fit, with the remaining less-well-determined combinations taken from G-matrix calculation. This set of matrix elements, with a simple scaling of $A^{-0.3}$, can well describe all A=21-35 nuclei, correctly giving the lowest six to ten levels for each possible spin. Quadrupole moments, electric form factors and strength functions are also found to be in good agreement with experimental values. The method demonstrated the power of the shell model when full-basis calculations can be carried out in a truncated space that is large enough, usually consisting of at least one major shell for each nucleon type. However,

full-basis calculations cannot be carried out in higher shells, except for cases in which either the proton or neutron shell is closed. For example, the largest calculation in the s-d shell is ^{28}Si, where the number of $J = 0$, $T = 0$ states is 839. For the ^{60}Zn in the middle of the next shell, (i.e., the f-p shell), the corresponding number is 5,053,574. Therefore, while the exact diagonalization method has established the success of the microscopic nuclear shell approach, it is not feasible for medium and large nuclei [11].

I propose in this thesis the auxiliary field Monte-Carlo Method as another route to the nuclear shell model. Full-basis ground state calculations will fit in present-day high performance computers (e.g., the Delta system), for nuclei up to the rare-earth region, because of the moderate scaling of the computational effort (see next section). Finite temperature and ground state properties can be calculated within the same framework. It is a stochastic method and would be especially suitable for implementation on a parallel computer where each processor represents an independent Metropolis walker. The applications demonstrated below have been implemented on the Touchstone Delta (512 i860 nodes) and Gamma system (64 nodes) at Caltech.

C. Organization

The presentation is organized as follows. Section II introduces the Hubbard-Stratonovich (HS) transformation of the partition operator $\exp(-\beta\hat{H})$ to a path integral in auxiliary fields, and briefly reviews previous work of this method on interacting fermions. Particular attention is paid to the Monte Carlo studies on Hubbard model and comparison is made with the nuclear problem. The transformation requires that the Hamiltonian $\hat{H}$ be cast as a quadratic form in an appropriate set of one-body operators. Section III discusses two ways in which this can be achieved, using either particle density or pairing operators. The symmetries of the nuclear shell model, including rotation and isospin, determine the particular choice for the set of operators

there. The partition operator can be used to extract information about the system at finite temperature or in its ground state. In section IV, after a brief review of the known formula for calculating static observables in the ground-state projector formalism and the grand-canonical ensemble, various new methods are introduced for treating the canonical ensemble, which is important for nuclear systems. Section V discusses the measurement of dynamical correlations and extraction of strength functions which can yield information about the ground state and excited states. Section VI describes the computational algorithms for implementations and compares the efficiency of different sampling schemes. Applications to nuclei in different shells are discussed in Section VII. Finally, I will conclude in section VIII. Much of the material in section II to section VIII is in a preprint submitted to Physical Review C. This project was done in collaboration with D. J. Dean, C. W. Johnson, S. E. Koonin, and W. E. Ormand.

II. AUXILIARY-FIELDS PATH INTEGRAL

Given some many-body Hamiltonian $\hat{H}$, we seek a tractable expression for the imaginary time evolution operator:

$$\hat{U} = \exp(-\beta \hat{H}) \,. \tag{2.1}$$

Here, β has units of inverse energy and β^{-1} can be interpreted as a temperature. It is also clear that $\hat{U}$ can be interpreted as the quantum evolution operator for an imaginary time β. (Here and throughout, we take $\hbar = 1$ and all nuclear energies are measured in units of MeV and temperature measured in units of $(\mathrm{MeV})^{-1}$.) We will refer to $\hat{U}$ as the evolution operator hereafter. The operator $\hat{H}$ is usually a generalized Hamiltonian and might contain terms beyond the true Hamiltonian, such as $-\mu\hat{N}$ in the grand-canonical ensemble or $-\omega\hat{J}_z$ if we are 'cranking' the system.

There are two formalisms for extracting information from the evolution operator: the "thermal" formalism (on which we will concentrate) and the "zero-temperature" formalism (to which the thermal formalism reduces in the limit $\beta \to \infty$). In the thermal formalism, we begin with the partition function

$$Z = \hat{\mathrm{Tr}} \exp(-\beta \hat{H}) \tag{2.2}$$

and then construct the thermal observable of an operator $\hat{O}$:

$$\left\langle \hat{O} \right\rangle = \frac{1}{Z} \hat{\mathrm{Tr}} \left[\hat{O} \exp(-\beta \hat{H}) \right] \,. \tag{2.3}$$

Here, the trace $\hat{\mathrm{Tr}}$ is over many-body states of fixed (canonical) or all (grand-canonical) particle number. In the zero-temperature formalism we begin with a trial wavefunction ψ_0 and use the evolution operator to project out the ground state, assuming that ψ_0 is not orthogonal to the ground state. The expectation value of $\hat{O}$ is then given by

$$\left\langle \hat{O} \right\rangle = \lim_{\beta\to\infty} \frac{\left\langle \psi_0 \left| \exp(-\frac{\beta}{2}\hat{H})\hat{O}\exp(-\frac{\beta}{2}\hat{H}) \right| \psi_0 \right\rangle}{\left\langle \psi_0 \left| \exp(-\beta\hat{H}) \right| \psi_0 \right\rangle} . \tag{3.4}$$

In this section, we describe how to write $\hat{U}$ in a form that allows Eqs. (2.3) or (2.4) to be evaluated.

A. Path integral formulation of the evolution operator

We restrict ourselves to generalized Hamiltonians that contain at most two-body terms. The Hamiltonian $\hat{H}$ can then be written as a quadratic form in some set of 'convenient' operators $\hat{\mathcal{O}}_\alpha$:

$$\hat{H} = \sum_\alpha \epsilon_\alpha \hat{\mathcal{O}}_\alpha + \frac{1}{2}\sum_\alpha V_\alpha \hat{\mathcal{O}}_\alpha^2, \tag{3.5}$$

where we've assumed that the quadratic term is diagonal in the $\hat{\mathcal{O}}_\alpha$. The meaning of 'convenient' will become clear shortly, but typically it refers to one-'body' operators, either one-particle ('density') or one-quasiparticle ('pairing'). The strength of the two-body interaction is characterized by the real numbers V_α.

For $\hat{H}$ in the quadratic form (2.5), one can write the evolution operator $\hat{U}$ as a path integral. The exponential is first split into N_t 'time' slices, $\beta = N_t\Delta\beta$, so that

$$\hat{U} = \left[\exp(-\Delta\beta\hat{H})\right]^{N_t} . \tag{3.6}$$

Then perform the Hubbard-Stratonovich (HS) transformation on the two-body term for the n'th time slice to give [12],

$$\exp\left(-\Delta\beta\hat{H}\right) \simeq \int_{-\infty}^{\infty} \prod_\alpha d\sigma_{\alpha n} \left(\frac{\Delta\beta|V_\alpha|}{2\pi}\right)^{1/2} \exp\left(-\Delta\beta\sum_\alpha (\frac{1}{2}|V_\alpha|\sigma_{\alpha n}^2 + s_\alpha V_\alpha \sigma_{\alpha n}\hat{\mathcal{O}}_\alpha + \epsilon_\alpha\hat{\mathcal{O}}_\alpha)\right) , \tag{3.7}$$

where the phase factor s_α is ± 1 if $V_\alpha < 0$ and is $\pm i$ if $V_\alpha > 0$. Each real c-number $\sigma_{\alpha n}$ is the *auxiliary field* associated with $\hat{\mathcal{O}}_\alpha$ at time slice n.

The approximation (2.7) is valid through order $\Delta\beta$, since the corrections are commutator terms of order $(\Delta\beta)^2$. The evolution operator is then

$$\hat{U} = \left[\exp\left(-\Delta\beta\hat{H}\right)\right]^{N_t} \simeq \int \mathcal{D}^{N_t}[\sigma] G(\sigma) \exp\left(-\Delta\beta h_\sigma(\tau_{N_t})\right) \ldots \exp\left(-\Delta\beta h_\sigma(\tau_1)\right) \quad (3.8)$$

where the integration measure is

$$\mathcal{D}^{N_t}[\sigma] = \prod_{n=1}^{N_t} \prod_{\alpha} d\sigma_{\alpha n} \left(\frac{\Delta\beta|V_\alpha|}{2\pi}\right)^{\frac{1}{2}} , \quad (3.9a)$$

the Gaussian factor is

$$G(\sigma) = \exp\left(-\sum_{\alpha n} \frac{1}{2}|V_\alpha|\sigma_{\alpha n}^2\right) , \quad (3.9b)$$

and the one-body Hamiltonian is

$$\hat{h}_\sigma(\tau_n) = \sum_\alpha \left(\epsilon_\alpha + s_\alpha V_\alpha \sigma_{\alpha n}\right) \hat{O}_\alpha . \quad (3.10)$$

It is sometimes convenient to employ a continuum notation,

$$\hat{U} = \int \mathcal{D}[\sigma] \exp\left(-\frac{1}{2}\int_0^\beta d\tau \sum_\alpha |V_\alpha| \sigma_\alpha^2(\tau)\right) \times \left[\mathcal{T} \exp\left(-\int_0^\beta d\tau\, \hat{h}_\sigma(\tau)\right)\right] , \quad (3.11)$$

where $\mathcal{T}$ denotes time-ordering and

$$\mathcal{D}[\sigma] = \lim_{N_t\to\infty} \mathcal{D}^{N_t}[\sigma] , \quad (3.12)$$

$$\mathcal{T} \exp\left(-\int_0^\beta d\tau\, \hat{h}_\sigma(\tau)\right) = \lim_{N_t\to\infty} \prod_{n=1}^{N_t} \exp\left(-\Delta\beta\, \hat{h}_\sigma(\tau_n)\right) . \quad (3.13)$$

In the limit of an infinite number of time slices Eq. (2.8) is exact. In practice one has a finite number of time slices and the approximation is valid only to order $\Delta\beta$. The case of only one time slice is known as the Static Path Approximation (SPA); previous work on the SPA and its extensions can be found in [13] and [14].

Rewriting the evolution operator as a path integral can make the model space tractable. Consider the case where the $\hat{O}_\alpha$ are density operators. Then Eq. (2.1) is

an exponential of two-body operators; it acts on a Slater-determinant to produce a sum of many Slater-determinants. In contrast, the path-integral formulation (2.8) contains only exponentials of one-body operators which, by Thouless' theorem [15], takes a Slater-determinant to another single Slater-determinant. Therefore, instead of having to keep track of a very large number of determinants (often many thousands for modern matrix-diagonalization shell model codes such as OXBASH [16]), we need deal only with one Slater-determinant at a time. Of course, the price to be paid is the evaluation of a high-dimensional integral. However, the number of auxiliary fields grows only quadratically with the size of the single particle basis while the corresponding number of Slater-determinants grows exponentially. Furthermore, the integral can be evaluated stochastically, making the problem ideal for parallel computation.

B. Monte Carlo evaluation of the path integral

Formulating the evolution operator as a path integral over auxiliary fields reduces the problem to quadrature. For a limited number of auxiliary fields, such as in the SPA with only a quadrupole-quadrupole interaction, the integral can be evaluated by direct numerical quadrature. However, for more general cases (typically hundreds of fields), the integral must be evaluated stochastically using Monte Carlo techniques.

Using the one-body evolution operator defined by

$$\hat{U}_\sigma(\tau_2,\tau_1) = \mathcal{T}\exp\left(-\int_{\tau_1}^{\tau_2} d\tau\, \hat{h}_\sigma(\tau)\right) , \tag{3.14}$$

we can write Eq. (2.3) or (2.4) as

$$\left\langle \hat{O} \right\rangle = \frac{\int \mathcal{D}[\sigma]\, G(\sigma) \left\langle \hat{O}(\sigma) \right\rangle \zeta(\sigma)}{\int \mathcal{D}[\sigma]\, G(\sigma)\, \zeta(\sigma)} . \tag{3.15}$$

For the zero-temperature formalism

$$\zeta(\sigma) \equiv \left\langle \psi_0 \left| \hat{U}_\sigma(\beta,0) \right| \psi_0 \right\rangle \tag{3.16}$$

and

$$\langle O(\sigma) \rangle = \frac{\left\langle \psi_0 \left| \hat{U}_\sigma(\beta,\beta/2)\, \hat{O}\, \hat{U}_\sigma(\beta/2,0) \right| \psi_0 \right\rangle}{\left\langle \psi_0 \left| \hat{U}_\sigma(\beta,0) \right| \psi_0 \right\rangle} , \tag{3.17}$$

while for the thermal formalism (canonical and grand-canonical),

$$\zeta(\sigma) \equiv \hat{\mathrm{Tr}}[\hat{U}_\sigma(\beta,0)] , \tag{3.18}$$

and

$$\left\langle \hat{O} \right\rangle_\sigma = \frac{\hat{\mathrm{Tr}}\left[\hat{O}\, \hat{U}_\sigma(\beta,0)\right]}{\hat{\mathrm{Tr}}\, \hat{U}_\sigma(\beta,0)} . \tag{3.19}$$

To evaluate the path integral via Monte Carlo techniques, we must choose a normalizable positive-definite weight function W_σ, and generate an ensemble of statistically independent fields $\{\sigma_i\}$ such that the probability density to find a field with values σ_i is W_{σ_i}. Defining the 'action' by

$$\mathcal{S}_\sigma = \sum_\alpha \frac{1}{2} |V_\alpha| \int_0^\beta d\tau\ \sigma_\alpha(\tau)^2 - \ln \zeta(\sigma) , \tag{3.20}$$

the required observable is then simply

$$\left\langle \hat{O} \right\rangle = \frac{\int \mathcal{D}[\sigma] \left\langle \hat{O} \right\rangle_\sigma e^{-\mathcal{S}_\sigma}}{\int \mathcal{D}[\sigma]\, e^{-\mathcal{S}_\sigma}} = \frac{\frac{1}{N} \sum_i \left\langle \hat{O} \right\rangle_i \Phi_i}{\frac{1}{N} \sum_i \Phi_i} , \tag{3.21}$$

where N is the number of samples,

$$\Phi_i = e^{-\mathcal{S}_i} / W_i \tag{3.22}$$

and $\mathcal{S}_i \equiv \mathcal{S}_{\sigma_i}$, etc. Ideally W should approximate $\exp(-S)$ closely. However, $\exp(-S)$ is generally not positive and can even be complex. In some cases, Φ_i may oscillate violently, giving rise to a very small denominator in Eq. (2.21) to be cancelled by a very small numerator. While this cancellation is exact analytically, it is only approximate

in the Monte Carlo evaluation so that this 'sign problem' leads to large variances in the evaluation of the observable.

There are several possible schemes for both the choice of W and the sampling of the fields. We typically choose $W = |\exp(-S)|$ and generate the samples via random walk (Metropolis) methods.

C. Discrete Hubbard-Stratonovich transformation

The idea of a discrete HS transformation was first proposed and implemented in Monte Carlo calculations of the Hubbard Model [17] , which is described by the Hamiltonian

$$\hat{H} = \sum_{<ij>} t\ a^{\dagger}_{i\sigma} a_{j\sigma} + \sum_{i} U\ n_{i\uparrow} n_{i\downarrow}. \tag{3.23}$$

Here $a^{\dagger}_{i\sigma}, a_{j\sigma}$ are the fermion creation and annihilation operators for localized electron orbitals on lattice sites i and j. The first term in the Hamiltonain describes the hopping of electrons to nearest neighboring sites while the second term approximates the Columb repulsion of electrons by a simple on-site repulsion. To linearize the on-site repulsion, one field, x_i, is introduced per site. In the continuous HS transformation

$$e^{-\Delta\beta\sum_i U n_{i\uparrow} n_{i\downarrow}} = \int \prod_i \sqrt{\Delta\beta/4\pi} dx_i e^{-\frac{1}{4}\Delta\beta x_i^2} e^{-\Delta\beta U \sum_i \{x_i(n_{i\uparrow}-n_{i\downarrow})+(n_{i\uparrow}+n_{i\downarrow})\}}. \tag{3.24}$$

However, since the occupation number $n_{i\sigma}$, is discrete, either 0 or 1, there is a discrete transformation that can also linearize the action:

$$e^{-\Delta\beta\sum_i U n_{i\uparrow} n_{i\downarrow}} = \frac{1}{2} \sum_{x_1=\pm 1} \cdots \sum_{x_N=\pm 1} e^{-\Delta\beta V(x)} \tag{3.25}$$

where

$$V(x) = U \sum_i \lambda_i (n_{i\uparrow} - n_{i\downarrow}) x_i, \tag{3.26}$$

and

$$\lambda_i = 2\tanh^{-1}\sqrt{\tanh(\Delta\tau U/2)}/\Delta\beta\ U. \tag{3.27}$$

A similar discrete transformation can also be carried out when the on-site interaction is attractive. In these discrete HS transformations, the auxiliary fields are like spin variables with discrete values. In all comparative studies of discrete and continuous HS transformation, the discrete version has been found to perform better in Monte Carlo calculations in having small de-correlation length in the random walk.

For a general fermionic interaction, as in the nuclear shell model, the two-body interaction is give by (2.5) where $\hat{\mathcal{O}}_\alpha$ is a general operator bilinear in the fermion creation and annilhilation operator. The operator is not described by simple discrete values and therefore an exact transformation like that in (2.25) cannot be found. Noting that (2.8) is an approximation good to the order $\Delta\beta$ due to the corrections by commutator terms, it is sufficient to consider a transformation good to a certain order in $\Delta\beta$. Expanding the $\exp(\Delta\beta(\frac{1}{2}g\hat{\mathcal{O}}^2))$ and seeking approximation to a finite order,

$$\int dy\ f(\sigma)e^{\Delta\beta(g\sigma\hat{\mathcal{O}})} \simeq \exp\left(\Delta\beta\frac{1}{2}g\hat{\mathcal{O}}^2\right) \tag{3.28a}$$

$$\int dy\ f(\sigma)\left(1+\Delta\beta(g\hat{\mathcal{O}}^2)+(\Delta\beta)^2/2g^2\hat{\mathcal{O}}^4+...\right) = 1+\frac{1}{2}\Delta\beta g\hat{\mathcal{O}}^2+\frac{1}{8}(\Delta\beta)^2g^2\hat{\mathcal{O}}^2+... \tag{3.28b}$$

we can use a finite sum of delta-functions for $f(\sigma)$, by matching the expression order by order in $\Delta\beta$, up to the order desired. This will give rise to a discrete sum from the integration of the delta-functions. For example, to reproduce the left-hand side of (2.28b) to first order, the requirement on $f(\sigma)$ is

$$\int f(\sigma)d\sigma = 1 \tag{3.29a}$$

$$\int f(\sigma)\sigma\ d\sigma = 0 \tag{3.29b}$$

$$\int f(\sigma)\sigma^2 \, d\sigma = 1/(g \, \Delta\beta). \tag{3.29c}$$

We can therefore choose two delta-functions

$$f(\sigma) = \frac{1}{2}\delta(\sigma - \sqrt{1/(g \, \Delta\beta)}) + \frac{1}{2}\delta(\sigma + \sqrt{1/(g \, \Delta\beta)}). \tag{3.30}$$

To reproduce the left-hand side to the $(\Delta\beta)^2$ term, we can choose

$$f(\sigma) = \frac{2}{3}\delta(\sigma) + \frac{1}{6}\delta(\sigma - \sqrt{\frac{3}{(g \, \Delta\beta)}}) + \frac{1}{6}\delta(\sigma + \sqrt{\frac{3}{(g \, \Delta\beta)}}). \tag{3.31}$$

More delta-functions will be needed to reproduce the higher-order terms.

I will compare the discrete and continuous HS transformation in the nuclear shell model in section VI, and come to the conclusion that the continuous HS transformation performs as well as the discrete transformation after an efficient random walk is introduced in the former case. The new random walk is found to be at least ten times more efficient than the conventional sampling scheme used in the continuous HS transformation, when applied to *sd* shell nuclei. The conclusion that the discrete transformation is better for Monte Carlo calculations in the Hubbard Model, may be due to the inefficient sampling scheme used on the previous continuous transformation studies.

D. Previous application in nuclear physics

Calculations using the auxiliary field path-integral have been mainly done in the static path approximation (SPA) by direct numerical integration [13]. The level density, quadrupole deformation, and strength functions was calculated for exactly solvable models like the Lipkin model, monopole pairing force and quadrupole interaction in the Elliott SU(3) model, where analytical results exist and the SPA was shown to give a good description at high temperature. This can be understood from the fact that the lowest-order corrections are the comutators among different quadratic forms

and the one-body part of the Hamiltonian in (2.5), which are of order β^2 . When compared to the mean field approximation, SPA is found to give a higher level density at high temperature, close to the exact result, but it converges to the value for the mean field approximation at low temperature. Therefore while SPA can account for the thermal fluctuations at high temperature, it misses important quantum fluctuations at low temperature, since time-dependent fields are left out.

The RPA-SPA approximation [14] is an attempt to incorporate the quantum fluctuations of the finite-frequency Fourier component of the fields by taking account into the curvature of the free-energy around the static path. In the simplest case where there is only one quadratic term in the Hamiltonian, the auxiliary field is described by just $\sigma(t)$. When a resolution of $\Delta\beta$ is used for the imaginary time, the free energy can be expressed in the Fourier component of the fields,

$$\tilde{\sigma}_i = \sum_{t_j} e^{i\omega_i t_j}\sigma(t_j), \tag{3.32}$$

and free energy is approximated by

$$F(\tilde{\sigma}_0, \tilde{\sigma}_1, \tilde{\sigma}_2, ...) \simeq F(\tilde{\sigma}_0, 0, 0, 0, ..) + \frac{1}{2}\sum_{i\neq 0}\frac{\partial^2}{\partial\tilde{\sigma}_i^2}|_{\tilde{\sigma}_0}\tilde{\sigma}_i^2 \tag{3.33}$$

when this expression is substituted into the path integral, the Gaussian integration over the finite Fourier components can be carried out analytically, leaving the integration over the static field $\tilde{\sigma}_0$ to be done numberically. Notice that the Gaussian integration over $\tilde{\sigma}_i$ contributes a factor depending on $\tilde{\sigma}_0$. This method has been applied to a pure pairing interaction and was shown to improve the SPA. However, the approximation breaks down at low temperatures where the static path is unstable to quantum fluctuations, in which case a negative curvature for some Fourier components appears and invalidates the Gaussian approximation. Both the SPA and RPA-SPA methods via direct integration fashion have been limited to simple interactions with a few quadratic terms, due to the limited number of integrations that can be carried out.

E. Previous applications in Hubbard Model

Monte Carlo calculations for many time slices have been applied to several Hubbard-type systems with on-site repulsion [3], including the Hubbard model (2.23) in various dimensions, the Emery model (also known as three-band Hubbard model), and the Anderson model. The 3-D Hubbard model was originally proposed for studying transitional metals where strong correlation exist among electrons. After the discovery of copper-oxide superconductors, the 2-D Hubbard model has been under intensive study with the expectation that it captures the physics on the Cu-O plane. Since the parameter U/t of the superconducting system lies in an intermediate region where analytical expansions break down, the auxiliary-field Monte Carlo calculations have played an important role in giving exact results in finite lattices, resulting in much understanding of the system. We will concentrate on the applications to the 2-D Hubbard model, where many results are available.

The systems studied in the 2-D Hubbard model range from the 4×4 lattices to 16×16 lattices, with parameter U/t ranging from 0 to 10. Since one wants to study the properties of the bulk system, it is desirable to make the lattice as large as possible to avoid finite size effects. Extrapolation is usually done in the lattice size for physical observables to reach the continuum limit. In particular, the magnetic and pairing susceptibility should diverge as the system size tends to infinity to signal a phase transition. Both the zero-temperature formalism and grand canonical ensemble are used in the Monte Carlo calculations. A resolution of $\Delta\beta = 0.125/t$ is necessary to obtaining an accuracy of several percent. For the above system sizes, it takes $\beta \geq 10/t$ to reach the ground state, amounting to 80 time slices in the path-integral. Numerical instability easily sets in, due to the long propagation of matrices. In the ground state formalism, the calculation can be stabilized by orthogonalization of the single particle wavefunctions as they are propagated [5]. In the grand canonical

ensemble, a modified Gram-Schmidt factorization [22] is introduced which separates the diverging singular values of the matrix. These methods enable calculations to be carried out with many time slices to reach the ground state.

Various physical observables have been obtained from the calculations, including the momentum distribution, double occupany, magnetic correlation and susceptibility, and pairing correlation and susceptibility. Dynamical imaginary time correlations were also measured from which strength functions were reconstructed by various methods. Among these is the MaxEnt method [18] [19] [20], which seems to be the most successful. We will also use this method for the nuclear problem. A brief description of MaxEnt is given in Appendix C.

The major problem met in these calculations is the sign problem associated with negative contributions to the path integral. In the half-filled 2-D Hubbard model, where one electron occupies each lattice site on average, the particle-hole symmetry enforces positivity in the path-integral. In this case, stable calculations have been done up to 16×16 lattices for the ground state. Unfortunately, the average sign deteriorates quickly as the system is doped away from half-filling. Calculations at low temperacture is particularly difficult as the average sign decreases exponentially with the inverse temperature β. The problem is also more severe for larger systems. For the physically interesting region relevant for superconductivity, where $0.7 < \langle n \rangle < 0.95$ per lattice site, it is difficult to go beyond an 8×8 lattice with $\beta = 8/t$. It is interesting to note that the average sign increases again at doping level $\langle n \rangle = 0.5$, allowing more stable calculations there.

F. Comparison of application to the Hubbard model and nuclear shell model

As noted above, since the Hubbard model is studied to understand the bulk material, a large lattice is desirable. For a lattice size of 16×16, the number of single

particle states is already 256, which corresponds to the matrix dimension in the calculation. In comparision, the calculation of a nuclear shell model can involve smaller matrices; the matrix size for *sd, fp* and rare-earth nuclei are only 12, 20 and 44 for full-basis, one oscillator shell calculations. Hubbard model calculations also need many time slices to reach the ground state. The main reason is the presence of different scales in the Hamilitonian caused by a large U/t ratio, and a large commutator term (which gives rise to a correction for a finite number of time slices) from the repulsion and hopping term, which are diagonal in conjugate base. On the other hand, the nuclear shell model is found to behave much better in the extrapolation to continuous path integral. A $\Delta\beta$ value of 1/8 MeV^{-1} with $\beta = 3$, which amounts to 24 time slices, can result in good ground state calculations for *s-d* shell nuclei. In the examples we have studied, there is no need for matrix stabilization. These two factors, smaller matrix size and smaller number of time slices used, are favorable to nuclear shell-model calculations.

On the other hand, since the shell model calculations involve interactions among all single particle states (versus the on-site repulsion in the Hubbard model), the number of auxiliary fields introduced in each time slice is N_s^2 versus N_s, where N_s is the number of single particle states. Therefore the shell model calculations in general involve a higher dimensional integral in the auxiliary fields, although this factor would not introduce much more time in the Monte Carlo algorithm. The more time consuming part in the nuclear shell model calculation comes from the exponentiation and multiplication of matrices which are not sparse, as they are in the Hubbard model calculations.

The Hubbard model suffers from severe sign problem away from half-filling due to the strong repulsive character of the interaction (c.f. the attractive Hubbard model which has no sign problem). We analyze the sign problem in Section VII and find that an interaction with a strong enough pairing character leads to positive definite

path integral. The nuclear-shell model is characterized by strong pairing interaction. We have found that a phenomenological pairing plus attractive multipole interaction, including the popular Pairing Plus Quadrupole interaction, gives rise to positive definite path integral. This characteristic is particularly favorable for Monte Carlo calculations of the nuclear shell model.

Finite size and shell structure are two important features that distinguish the studies of nuclei from bulk system such as Hubbard model. The grand canonical ensemble is used to study thermal or ground state properties in the Hubbard model, because the particle number fluctuation is not significant in a large system. In nuclei, particularly for small and medium sizes, grand canonical ensemble gives only the average properties of neighboring nuclei which can be very different from each other. In this respect, we introduce several methods in calculating canonical ensemble observables in the auxiliary-field Monte Carlo in Section III.

III. DECOMPOSITIONS OF THE HAMILTONIAN

To realize the HS transformation, the two-body parts of $\hat{H}$ must be cast as a quadratic form in one-body operators $\mathcal{O}_\alpha$. As these latter can be either density operators or pair creation and annihilation operators (or both), there is considerable freedom in doing so. In the simplest example, let us consider an individual interaction term,

$$\hat{H} = a_1^\dagger a_2^\dagger a_4 a_3 \ , \tag{3.1}$$

where $a_i^\dagger, a_i$ are anti-commuting fermion creation and annihilation operators. In the pairing decomposition, we write (using the upper and lower bracket to indicate the grouping)

$$\hat{H} = \overbrace{a_1^\dagger a_2^\dagger} \underbrace{a_4 a_3} \tag{3.2a}$$

$$= \frac{1}{4}(a_1^\dagger a_2^\dagger + a_3 a_4)^2 - \frac{1}{4}(a_1^\dagger a_2^\dagger - a_3 a_4)^2 + \frac{1}{2}[a_1^\dagger a_2^\dagger, a_3 a_4] \ . \tag{3.2b}$$

The commutator is a one-body operator that can be put directly in the one-body Hamiltonian $\hat{h}_\sigma$. The remaining two quadratic forms in pair-creation and -annihilation operators can be coupled to auxiliary fields in the HS transformation.

In the density decomposition, there are two ways to proceed: we can group (1,3) and (2,4) to get

$$\hat{H} = \overbrace{a_1^\dagger a_3} \underbrace{a_2^\dagger a_4} - a_1^\dagger a_4 \delta_{23} \tag{3.3a}$$

$$= -a_1^\dagger a_4 \delta_{23} + \frac{1}{2}[a_1^\dagger a_3, a_2^\dagger a_4] + \frac{1}{4}(a_1^\dagger a_3 + a_2^\dagger a_4)^2 - \frac{1}{4}(a_1^\dagger a_3 - a_2^\dagger a_4)^2 \ , \tag{3.3b}$$

or group (1,4) and (2,3) to get

$$\hat{H} = -\overbrace{a_1^\dagger a_4}\underbrace{a_2^\dagger a_3} + a_1^\dagger a_3 \delta_{24} \,. \tag{3.4a}$$

$$= a_1^\dagger a_3 \delta_{24} - \frac{1}{2}[a_1^\dagger a_4, a_2^\dagger a_3] - \frac{1}{4}(a_1^\dagger a_4 + a_2^\dagger a_3)^2 + \frac{1}{4}(a_1^\dagger a_4 - a_2^\dagger a_3)^2 \,. \tag{3.4b}$$

Again the commutator terms are one-body operators, but now the quadratic forms are squares of density operators that conserve particle number. We refer to Eq. (3.3) as the 'direct' decomposition and Eq. (3.4) as the 'exchange' decomposition.

For any general two-body Hamiltonian, we can choose the pairing or density decompositions for different parts of the two-body interaction. Moreover, even within a pure density break-up decomposition, there is still freedom to choose between the direct and exchange formulations. Although the exact path integral result is independent of the scheme used, different schemes will lead to different results under certain approximations (e.g., mean field or SPA). The choice of decomposition will also affect the rate of convergence of our numerical result as $N_t \to \infty$, as well as the statistical precision of the Monte Carlo evaluation. Most significantly, it affects the fluctuation of Φ in Eq. (2.21) and thus determines the stability of the Monte Carlo calculation. (See Section VI below.)

In the application of these methods to the nuclear shell model, it is particularly convenient to use quadratic forms of operators that respect rotational invariance, isospin symmetry, and the shell structure of the system. We introduce these in the following subsections for both the density and pairing decompositions.

A. Density decomposition

We begin by ignoring explicit isospin labels, and by writing the rotationally invariant two-body Hamiltonian for a fermionic system as

$$\hat{H}_2 = \frac{1}{2}\sum_{abcd}\sum_J V_J(ab,cd)\sum_M A_{JM}^\dagger(ab)A_{JM}(cd)$$

$$= \frac{1}{4} \sum_{abcd} \sum_{J} [(1+\delta_{ab})(1+\delta_{cd})]^{1/2} V_J^A(ab,cd) \sum_{M} A_{JM}^{\dagger}(ab) A_{JM}(cd) \qquad (3.5)$$

where the sum is taken over all proton and neutron single-particle orbits (denoted by a, b, c, d) and the pair creation and annihilation operators are given by

$$A_{JM}^{\dagger}(ab) = \sum_{m_a m_b} (j_a m_a j_b m_b | JM) a_{j_b m_b}^{\dagger} a_{j_a m_a}^{\dagger} = -[a_{j_a}^{\dagger} \times a_{j_b}^{\dagger}]^{JM} \qquad (3.6a)$$

$$A_{JM}(ab) = \sum_{m_a m_b} (j_a m_a j_b m_b | JM) a_{j_a m_a} a_{j_b m_b} = [a_{j_a} \times a_{j_b}]^{JM} \, . \qquad (3.6b)$$

The $V_J(ab,cd)$ are the angular-momentum coupled two-body matrix elements of a scalar potential $V(\vec{r}_1, \vec{r}_2)$ defined as

$$V_J(ab,cd) = \langle [\psi_{j_a}(\vec{r}_1) \times \psi_{j_b}(\vec{r}_2)]^{JM} | V(\vec{r}_1, \vec{r}_2) | [\psi_{j_c}(\vec{r}_1) \times \psi_{j_d}(\vec{r}_2)]^{JM} \rangle \, , \qquad (3.7)$$

(independent of M) while the anti-symmetrized two-body matrix elements of $V_J^A(ab,cd)$ are given by

$$V_J^A(ab,cd) = [(1+\delta_{ab})(1+\delta_{cd})]^{-1/2} \left[V_J(ab,cd) - (-1)^{j_c+j_d-J} V_J(ab,dc) \right] \, . \qquad (3.8)$$

Before continuing with the discussion regarding the density decomposition, we note that for fermionic systems the two-body Hamiltonian is completely specified by the set of anti-symmetrized two-body matrix elements $V_J^A(ab,cd)$ that are the input to many standard shell model codes such as OXBASH [16]. Indeed, we can add to the $V_J^A(ab,cd)$ any set of (unphysical) symmetric two-body matrix elements $V_J^S(ab,cd)$ satisfying

$$V_J^S(ab,cd) = (-1)^{j_c+j_d-J} V_J^S(ab,dc), \qquad (3.9)$$

without altering the action of $\hat{H}_2$ on any many-body fermionic wave function. Note, however, that although the $V_J^S(ab,cd)$ do not alter the eigenstates and eigenvalues of the full Hamiltonian, they can (and do) affect the character of the decomposition of

$\hat{H}_2$ into density operators, as is shown below. In what follows, we define the set of two-body matrix elements $V_J^N(ab,cd)$ that may possess no definite symmetries as

$$V_J^N(ab,cd) = V_J^A(ab,cd) + V_J^S(ab,cd)\ , \tag{3.10}$$

allowing us to write the two-body Hamiltonian as

$$\hat{H}_2 = \frac{1}{4}\sum_{abcd}\sum_{J}[(1+\delta_{ab})(1+\delta_{cd})]^{1/2}\, V_J^N(ab,cd)\sum_{M} A_{JM}^{\dagger}(ab)A_{JM}(cd)\ . \tag{3.11}$$

To obtain the density decomposition of $\hat{H}_2$, we perform a Pandya transformation to recouple (a,c) and (b,d) into density operators with definite multipolarity

$$\hat{\rho}_{KM}(ab) = \sum_{m_a,m_b}(j_a m_a, j_b m_b|KM)a^{\dagger}_{j_a m_a}\tilde{a}_{j_b m_b}\ , \tag{3.12}$$

where $\tilde{a}_{j_a m_a} = (-1)^{j_a+m_a}a_{j_a m_a}$. Then $\hat{H}_2$ can be rewritten as

$$\hat{H}_2 = \hat{H}_2' + \hat{H}_1'\ ; \tag{3.13}$$

$$\hat{H}_2' = \frac{1}{2}\sum_{abcd}\sum_{K} E_K(ac,bd)\sum_{M}(-1)^M\hat{\rho}_{K-M}(ac)\hat{\rho}_{KM}(bd) \tag{3.14}$$

where the particle-hole matrix elements of the interaction are

$$\begin{aligned} E_K(ac,bd) = (-1)^{j_b+j_c}\sum_{J}(-1)^J(2J+1)\begin{Bmatrix} j_a & j_b & J \\ j_d & j_c & K \end{Bmatrix} \\ \times \quad \frac{1}{2}V_J^N(ab,cd)\sqrt{(1+\delta_{ab})(1+\delta_{cd})} \end{aligned} \tag{3.15}$$

and $\hat{H}_1'$ is a one-body operator given by

$$\hat{H}_1' = \sum_{ad}\epsilon_{ad}'\hat{\rho}_{00}(a,d)\ , \tag{3.16a}$$

with

$$\epsilon_{ad}' = -\frac{1}{4}\sum_{b}\sum_{J}(-1)^{J+j_a+j_b}(2J+1)\frac{1}{\sqrt{2j_a+1}}V_J^N(ab,bd)\sqrt{(1+\delta_{ab})(1+\delta_{cd})}\ . \tag{3.16b}$$

Note that adding symmetrized matrix elements is equivalent to using the exchange decomposition for some parts of the interaction. The freedom in choosing the combinations of direct and exchange decomposition is then embodied in the arbitrary symmetrized part of the matrix elements.

Introducing the shorthand notation $i = (ac), j = (bd)$, we can write Eq. (3.14) as

$$\hat{H}_2' = \frac{1}{2}\sum_{ij}\sum_{K} E_K(i,j)(-1)^M \hat{\rho}_{KM}(i)\hat{\rho}_{K-M}(j) \,. \tag{3.17}$$

Upon diagonalizing the matrix $E_K(i,j)$ to obtain eigenvalues $\lambda_{K\alpha}$ and associated eigenvectors $v_{K\alpha}$, we can represent $\hat{H}_2'$ as

$$\hat{H}_2' = \frac{1}{2}\sum_{K\alpha} \lambda_K(\alpha)(-1)^M \hat{\rho}_{KM}(\alpha)\hat{\rho}_{K-M}(\alpha) \,, \tag{3.18}$$

where

$$\hat{\rho}_{KM}(\alpha) = \sum_i \hat{\rho}_{KM}(i) v_{K\alpha}(i) \,. \tag{3.19}$$

Finally, if we define

$$\hat{Q}_{KM}(\alpha) \equiv \frac{1}{\sqrt{2(1+\delta_{M0})}} \left(\hat{\rho}_{KM}(\alpha) + (-1)^M \hat{\rho}_{K-M}(\alpha)\right) \,, \tag{3.20a}$$

$$\hat{P}_{KM}(\alpha) \equiv -\frac{i}{\sqrt{2(1+\delta_{M0})}} \left(\hat{\rho}_{KM}(\alpha) - (-1)^M \hat{\rho}_{K-M}(\alpha)\right) \,, \tag{3.20b}$$

then $\hat{H}_2'$ becomes

$$\hat{H}_2' = \frac{1}{2}\sum_{K\alpha} \lambda_K(\alpha) \sum_{M\geq 0} \left(\hat{Q}^2_{KM}(\alpha) + \hat{P}^2_{KM}(\alpha)\right) \,. \tag{3.21}$$

This completes the representation of the two-body interaction as a diagonal quadratic form in density operators. We then couple auxiliary fields $\sigma_{KM}(\alpha)$ to $\hat{Q}_{KM}$ and $\tau_{KM}(\alpha)$ to $\hat{P}_{KM}$ in the HS transformation. (The latter is not to be confused with the "imaginary time" τ.) In the treatment thus far, protons and neutrons were not distinguished from each other. Although the original Hamiltonian $\hat{H}_2$ conserves proton

and neutron numbers, we ultimately might deal with one-body operators $\rho_{KM}(a_p, b_n)$ and $\rho_{KM}(a_n, b_p)$ (n,p subscript denoting neutron and proton) that individually do not do so. The one-body Hamiltonian $\hat{h}_\sigma$ appearing in the HS transformation then mixes neutrons and protons. The single-particle wavefunctions in a Slater determinant then contain both neutron and proton components and neutron and proton numbers are not conserved separately in each Monte Carlo sample; rather the conservation is enforced only statistically.

It is, of course, possible to recouple so that only density operators separately conserving neutron and proton numbers ($\hat{\rho}_{KM}(a_p, b_p)$ and $\hat{\rho}_{KM}(a_n, b_n)$) are present. To do so, we write the two-body Hamiltonian in a manifestly isospin-invariant form,

$$\hat{H}_2 = \frac{1}{4} \sum_{abcd} \sum_{J} [(1+\delta_{ab})(1+\delta_{cd})]^{1/2} V^N_{JT}(ab,cd) A^\dagger_{JT;MT_z}(ab) A_{JT;MT_z}(cd) \,, \qquad (3.22)$$

where, similar to the previous definition (3.6), the pair operator is

$$A^\dagger_{JT;MT_z}(ab) = \sum_{m_a, m_b} (j_a m_a, j_b m_b | JM)(\frac{1}{2} t_a, \frac{1}{2} t_b | TT_z) a^\dagger_{j_b m_b t_b} a^\dagger_{j_a m_a t_a} \,. \qquad (3.23)$$

Here $(\frac{1}{2}, t_a)$, etc. are the isospin indices with $t_a = -\frac{1}{2}$ for proton states and $t_a = \frac{1}{2}$ for neutron states, and (TT_z) is the coupled isospin quantum number. The two-body Hamiltonian can now be written solely in terms of density operators that conserve the proton and neutron numbers. Namely,

$$\hat{H}_2 = \hat{H}'_1 + \hat{H}'_2 \,, \qquad (3.24)$$

where

$$\hat{H}'_1 = \sum_{ad} \sum_{t=p,n} \epsilon'_{ad} \rho_{00,t}(a,d) \,, \qquad (3.25)$$

with

$$\epsilon'_{ad} = -\frac{1}{4} \sum_b \sum_J (-1)^{J+j_a+j_b} (2J+1) \frac{1}{\sqrt{2j_a+1}} V^N_{J,T=1}(ab,bd) \sqrt{(1+\delta_{ab})(1+\delta_{cd})} \,, \qquad (3.26)$$

and

$$\hat{H}_2' = \frac{1}{2}\sum_{abcd}\sum_{K,T=0,1} E_{KT}(ac,bd)[\hat{\rho}_{K,T}(i)\times\hat{\rho}_{K,T}(j)]^{J=0} . \tag{3.27}$$

We define $\hat{\rho}_{KM,T}$ as

$$\hat{\rho}_{K\,M,T} = \hat{\rho}_{K\,M,p} + (-1)^T\hat{\rho}_{K\,M,n} , \tag{3.28}$$

and the $E_{K,T}$ are given by

$$E_{K,T=0}(ac,bd) = (-1)^{j_b+j_c}\sum_J(-1)^J(2J+1)\begin{Bmatrix} j_a & j_b & J \\ j_d & j_c & K \end{Bmatrix}\sqrt{(1+\delta_{ab})(1+\delta_{cd})}$$
$$\times\frac{1}{2}\left[V^N_{J,T=1}(ab,cd) + \frac{1}{2}(V^A_{J,T=0}(ab,cd) - V^S_{J,T=1}(ab,cd))\right] , \tag{3.29}$$

$$E_{K,T=1}(ac,bd) = -(-1)^{j_b+j_c}\sum_J(-1)^J(2J+1)\begin{Bmatrix} j_a & j_b & J \\ j_d & j_c & K \end{Bmatrix}\sqrt{(1+\delta_{ab})(1+\delta_{cd})}$$
$$\times\frac{1}{4}\left(V^A_{J,T=0}(ab,cd) - V^S_{J,T=1}(ab,cd)\right) . \tag{3.30}$$

In this isospin formalism, since $A_{JT;MT_z}(ab) = (-1)^{j_a+j_b-J+T}A_{JT;MT_z}(ba)$, the definition of symmetric and antisymmetric parts of $V^N_{JT}(ab,cd)$, $V^S_{JT}(ab,cd)$, and $V^A_{JT}(ab,cd)$ become

$$V^{S/A}_{JT}(ab,cd) \equiv \frac{1}{2}\left[V^N_{JT}(ab,cd) \pm (-1)^{J+j_a+j_b+T-1}V^N_{JT}(ba,cd)\right] . \tag{3.31}$$

Note that in these expressions, there is less freedom in manipulating the decomposition since we have to couple proton with proton and neutron with neutron in forming the density operators. Also, note that $E_{K,T=0}(ac,bd) - E_{K,T=1}(ac,bd)$ is an invariant related only to the physical part of the interactions, $(V^A_{J,T=1} + V^A_{J,T=0})$. We can choose all $E_{K,T=1}$ to be zero in the above (by setting $V^S_{J,T=1} = V^A_{J,T=0}$) leaving $E_{K,T=0}$ completely determined by the physical matrix elements. In that case, we can halve the number of fields to be integrated. However, while introducing the isovector densities requires more fields, it also gives more freedom in choosing the unphysical matrix elements to optimize the calculation.

If we now diagonalize the $E_{KT}(i,j)$ as before and form the operators

$$\hat{Q}_{KM,T}(\alpha) \equiv \frac{1}{\sqrt{2(1+\delta_{M,0})}}(\hat{\rho}_{KM,T}(\alpha) + (-1)^M \hat{\rho}_{K-M,T}(\alpha)) \,, \tag{3.32}$$

$$\hat{P}_{KM,T}(\alpha) \equiv -\frac{i}{\sqrt{2(1+\delta_{M,0})}}(\hat{\rho}_{KM,T}(\alpha) - (-1)^M \hat{\rho}_{K-M,T}(\alpha)) \,, \tag{3.33}$$

the two-body part of the Hamiltonian can finally be written as

$$\hat{H}_2' = \frac{1}{2}\sum_{KT}\sum_{\alpha}\lambda_{KT}(\alpha)\sum_{M\geq 0}\left(\hat{Q}^2_{K\,M,T}(\alpha) + \hat{P}^2_{K\,M,T}(\alpha)\right) \,. \tag{3.34}$$

In this decomposition, the one-body Hamiltonian $\hat{h}_\sigma$ of the HS transformation does not mix protons and neutrons. We can then represent the proton and neutron wavefunctions by separate determinants, and the number of neutrons and protons will be conserved rigorously during each Monte Carlo sample. For general interactions, even if we choose nonzero $E_{K,T=1}$ matrix elements, the number of fields involved are half that for the neutron-proton mixing decomposition. Also the matrix dimension is halved due to the separation of neutron and proton wavefunctions. These two factors add together to speed up significantly the computation. In this sense, this formalism is more favorable. There is, however, a reduction in the degrees of freedom regarding the symmetric matrix elements V_J^S as compared to those decompositions that mix protons and neutrons.

B. Pairing decomposition

In nuclei where the pairing interaction is important, it is natural to cast at least part of the two-body interaction as quadratic forms in pair creation and annihilation operators. We demonstrate this for the case where the Hamiltonian is written in the isospin formalism. Upon diagonalizing $V^A_{JT}(ab,cd)$ in Eq. (3.22), we can write

$$\hat{H}_2 = \sum_{JT\alpha}\lambda_{JT}(\alpha)\sum_{MT_z} A^\dagger_{JT;MT_z}(\alpha)A_{JT;MT_z}(\alpha) \,, \tag{3.35}$$

where

$$A^{\dagger}_{JT;MT_z}(\alpha) = \sum_i v_{JT\alpha}(i) A^{\dagger}_{JT,MT_z}(i) \; . \tag{3.36}$$

Separating $A^{\dagger}A$ into commutator and anticommutator terms, we have

$$\hat{H}_2 = \hat{H}'_2 + \hat{H}'_1 \tag{3.37}$$

$$\hat{H}'_1 = \frac{1}{2} \sum_{JT\alpha} \lambda_{JT}(\alpha) \sum_{MT_z} \left[A^{\dagger}_{JT;MT_z}(\alpha), A_{JT;MT_z}(\alpha) \right] \; ; \tag{3.38}$$

$$\hat{H}'_2 = \frac{1}{2} \sum_{JT\alpha} \lambda_{JT}(\alpha) \sum_{MT_z} \left\{ A_{jT;MT_z}(\alpha)^{\dagger}, A_{JT;MT_z}(\alpha) \right\} \; . \tag{3.39}$$

$\hat{H}'_1$ is a one-body operator that can be put in $\hat{H}_1$. The remaining two-body term can be written as a sum of squares by defining

$$Q_{JT;MT_z}(\alpha) \equiv \frac{1}{\sqrt{2}} \left(A^{\dagger}_{JT;MT_z}(\alpha) + A_{JT;MT_z}(\alpha) \right) \; ; \tag{3.40a}$$

$$P_{JT;MT_z}(\alpha) \equiv -\frac{i}{\sqrt{2}} \left(A^{\dagger}_{JT;MT_z}(\alpha) - A_{JT;MT_z}(\alpha) \right) \; , \tag{3.40b}$$

so that

$$\hat{H}'_2 = \frac{1}{2} \sum_{JT} \lambda_{JT}(\alpha) \sum_{MT_z} \left(Q^2_{JT;MT_z}(\alpha) + P^2_{JT;MT_z}(\alpha) \right) \; . \tag{3.41}$$

As in the density decomposition, we can then couple the σ and τ fields to Q and P, respectively.

Note that in the pairing decomposition, the one-body Hamiltonian $h(\tau)$ used in the path integral is a generalized one-body operator that includes density, pair-creation and pair-annihilation operators. The wavefunction is then propagated as a Hartree-Fock Bogoliubov state, rather than a simple Slater determinant.

In this decomposition, neutrons and protons are inevitably mixed together in the one-body Hamiltonian $\hat{h}_\sigma$ (consider the Q,P terms for $T = 0$). In fact, $\hat{h}_\sigma$ also does

not conserve the total number of nucleons; rather the conservation is only statistical after a large number of Monte Carlo samples.

For simplicity, we have described how to decompose the Hamiltonian solely in density operators or solely in pair operators. However, it is straightforward to mix the two decompositions with the choice depending on the type of interactions involved. Consider the 'Pairing plus Quadrupole' model, namely

$$\hat{H}_2 = -gP^\dagger P - \frac{1}{2}\chi Q \cdot Q \,, \tag{3.42}$$

where $P^\dagger, P$ are the monopole pair creation and annihilation operator and Q is the quadrupole-moment operator,

$$P^\dagger = \sum_\alpha a^\dagger_\alpha \tilde{a}^\dagger_\alpha \,, \tag{3.43}$$

$$Q_\mu = \sum_{\alpha\beta} \langle\alpha|Q_\mu|\beta\rangle \, a^\dagger_\alpha a_\beta \,. \tag{3.44}$$

Naively, it would be most convenient to use pairing decomposition for the pairing interaction and the density decomposition for the quadrupole interaction. This would require only 8 fields for each time slice in the HS transformation. The pure pairing or pure density decompositions would be much more complicated, as the former would require rewriting the quadrupole interactions in terms of pair operators and the latter would require rewriting the pairing interaction in terms of density operators. The numerical examples given in Section VI below will illustrate the behavior of such forces under different decompositions.

IV. CALCULATION OF STATIC OBSERVABLES

In the previous sections, we expressed the evolution operator for a two-body Hamiltonian as a path integral over auxiliary fields in which the action involves only density and pair operators. In this and the following section, we show how to extract observables from this path integral. The merit of this method will be clear from the compact formulae involved, which require handling only relatively small matrices of dimension N_s or $2N_s$, depending on the type of decomposition used. We derive formulae for three different approaches that use the evolution operator to obtain information about the system: the zero-temperature formalism, the grand-canonical ensemble, and the canonical ensemble. The zero-temperature and grand-canonical ensemble methods have been applied, with the density decomposition, to other physical systems such as the Hubbard Model [17]. However, we believe that the canonical ensemble treatment presented here is novel.

The zero-temperature approach can be used only to extract ground-state information. On the other hand, the grand-canonical ensemble allows finite-temperature calculations, but fluctuations in particle number can be very significant in a system with a small number of single-particle states. Thus, the canonical ensemble is particularly important in nuclear systems, where the particle number is small and shell structure is prominent. The grand-canonical ensemble yields information averaged over neighboring nuclei, which can have very different properties.

The canonical ensemble is more difficult than the other two approaches in two respects. First, the canonical (fixed-number) trace of U_σ is more difficult to compute than the wavefunction overlap of the zero-temperature formalism or the grand-canonical trace. Second, observables are more difficult to extract since Wick's theorem does not apply. We suggest three different methods to handle the canonical ensemble: the fugacity expansion, the Fourier extraction and the integration over real coherent

states. The coherent-state integration method can be applied to calculate canonical trace of any particle number involving only a negligible increase in computation time relative to the zero-temperature and grand-canonical approaches. Unfortunately, its utility is hampered by the sign problem. On the other hand, the fugacity expansion which is suited to calculating nuclei with a small number of valence particles or holes, where the calculation is numerically stable, is less susceptible to the sign problem. The Fourier extraction also shows good "sign" statistics and is numerically stable around mid-shell calculations, and therefore suitable for the region where the fugacity expansion fails.

For each approach, we also derive the general formulae when pair operators (as well as density operators) are present in the single-particle Hamiltonian; i.e., when a pairing decomposition is used for some or all of the interaction terms. As far as we know, there is no known general formulae for the pairing decomposition formalism. Using the fermion coherent state formalism [21], we derive in Appendix A a set of formulae for the calculation of observables that are similar to the well-known formulae for a pure density decomposition. Thus, our methods can be extended to calculations using general one-body operators in the HS transformation. This only doubles the dimension of the matrices involved.

A. Zero-temperature formalism

We begin with 'zero-temperature' observables. The trial wavefunction ψ_0 in Eq. (2.4) is, in principle, any state not orthogonal to the ground state. In practice, it is most conveniently a Slater-determinant. If we have N_s m-scheme orbitals available and N_v indistinguishable particles, ψ_0 is constructed from N_v single-particle wavefunctions, each of which is a vector with N_s components, and we write ψ_0 as a Slater-determinant of a $N_v \times N_s$ matrix, Ψ_0. In the pure density decomposition,

consider the one-body Hamiltonian $\hat{h} = M_{ij}a_i^\dagger a_j$ (sums over the indices i, j from 1 to N_s are implicit). The evolved wavefunction,

$$|\psi(\Delta\beta)\rangle = \exp\left(-\Delta\beta\hat{h}\right)|\psi_0\rangle \tag{4.1}$$

is then a Thouless transformation of the original determinant, the new state being represented by the matrix $\exp(-\Delta\beta M)\Psi_0$. We can therefore represent the product of evolution operators by $N_s \times N_s$ matrices

$$\exp\left(-\Delta\beta\hat{h}_n\right)...\exp\left(-\Delta\beta\hat{h}_1\right) \rightarrow \exp\left(-\Delta\beta M_n\right)...\exp\left(-\Delta\beta M_1\right) . \tag{4.2}$$

Let us now consider the overlap function in Eq. (2.16). Let $U_\sigma(\tau_2, \tau_1)$ be the matrix representing the evolution operator $\hat{U}_\sigma(\tau_2, \tau_1)$. Choosing some value τ of the imaginary time at which to insert the operator $\hat{O}$, we introduce the right and left wavefunctions $\psi_{R,L}(\tau)$ defined by

$$|\psi_R(\tau)\rangle = \hat{U}_\sigma(\tau, 0)|\psi_0\rangle \ , \tag{4.3a}$$

$$|\psi_L(\tau)\rangle = \hat{U}_\sigma^\dagger(\beta, \tau)|\psi_0\rangle \ . \tag{4.3b}$$

Then the required overlap in Eq. (2.16) is

$$\left\langle\psi_0\left|\hat{U}_\sigma(\beta,0)\right|\psi_0\right\rangle = \langle\psi_L|\psi_R\rangle = \det\left[\Psi_L^\dagger\Psi_R\right] \tag{4.4}$$

where

$$\Psi_R(\tau) \equiv \mathrm{U}_\sigma(\tau,0)\Psi_0, \ \Psi_L(\tau) \equiv \mathrm{U}_\sigma^\dagger(\beta,\tau)\Psi_0 \tag{4.5}$$

are the matrices representing ψ_R and ψ_L. Note that if there are two distinguishable species of particles — protons and neutrons — and we use a decomposition that conserves the numbers of neutrons and protons, then there is a separate determinant for each set of single-particle wavefunctions and the total overlap is the product of the proton and neutron overlaps.

With the basic overlap on hand, we now turn to the expectation value of an operator $\hat{O}$ for a given field configuration (i.e., Eqs. (2.15) and (2.19)). By Wick's theorem, the expectation value of any N-body operator can be expressed as the sum of products of expectation values of one-body operators. Hence, the basic quantity required is

$$\left\langle a_b^\dagger a_a \right\rangle_\sigma = \left[\Psi_R \left(\Psi_L^\dagger \Psi_R \right)^{-1} \Psi_L^\dagger \right]_{ba} . \tag{4.6}$$

(A straightforward derivation of this expansion can be found in [22]). Again, the decomposition separately conserves proton and neutron numbers, the expectation values for proton and neutron operators are given by separate matrices.

These formulae can be extended to the case where pair operators are present in the one-body Hamiltonian; i.e., when $\hat{h}$ is of the form

$$\hat{h} = \sum_{ij=1}^{N_s} (\Theta_{ij} a_i^\dagger a_j + \Delta_{ij} a_i^\dagger a_j^\dagger + \Lambda_{ij} a_i a_j) , \tag{4.7}$$

where Θ, Δ, and Λ are general $N_s \times N_s$ complex matrices. Our first task is to find a simple expression for $\langle \psi_0 | \hat{U}_\sigma(\beta, 0) | \psi_0 \rangle$ where $\hat{U}_\sigma(\beta, 0) = \prod_{n=1}^{N_t} \exp(-\Delta\beta \hat{h}_{\sigma_n})$. Using the fermion coherent state representation and Grassman algebra, we derive the expressions in Appendix A. Here we simply state the results.

If the trial wavefunction ψ_0 is a quasi-particle vacuum, such that $\beta_i | \psi_0 \rangle = 0$ where $\beta_i = \sum_j u_{ij} a_j + v_{ij} a_j^\dagger$, then

$$\begin{aligned} &\langle \psi_0 | \prod_{n=1}^{N_t} \exp\left(-\Delta\beta \hat{h}_n\right) | \psi_0 \rangle \\ &\qquad = \det \left[\begin{pmatrix} v^* & u^* \end{pmatrix} \mathbf{U}_\sigma(\beta, 0) \begin{pmatrix} v^T \\ u^T \end{pmatrix} \right]^{\frac{1}{2}} \exp\left(-\frac{\Delta\beta}{2} \sum_{n=1}^{N_t} \mathrm{Tr}[\Theta_n] \right) , \end{aligned} \tag{4.8}$$

where

$$\mathbf{U}_\sigma(\beta, 0) = \exp(-\Delta\beta M_{N_t}) \ldots \exp(-\Delta\beta M_1) , \tag{4.9}$$

is the matrix representing the evolution operator $\hat{U}_\sigma(\beta, 0)$, and M_n is the $2N_s \times 2N_s$ matrix representing $\hat{h}_n$:

$$M_n = \begin{pmatrix} \Theta_n & \Delta_n - \Delta_n^T \\ \Lambda_n - \Lambda_n^T & -\Theta_n^T \end{pmatrix} . \tag{4.10}$$

Here, the evolution operator $\hat{U}_\sigma(\tau_2, \tau_1)$ is represented by a $2N_s \times 2N_s$ matrix and the many-body wavefunction is represented by a $2N_s \times N_s$ matrix independent of the number of particles present. In analogy to Eqs. (4.3–4.6), we can write

$$\left\langle \psi_0 \left| \hat{U}_\sigma(\beta, 0) \right| \psi_0 \right\rangle = \langle \psi_L | \psi_R \rangle = \det \left[\Psi_L^\dagger \Psi_R \right]^{\frac{1}{2}} \exp \left(-\frac{\Delta\beta}{2} \sum_{n=1}^{N_t} \mathrm{Tr}[\Theta_n] \right) \tag{4.11}$$

where

$$\Psi_R \equiv \mathbf{U}_\sigma(\tau, 0) \begin{pmatrix} v^T \\ u^T \end{pmatrix}, \Psi_L \equiv \mathbf{U}_\sigma^\dagger(\beta, \tau) \begin{pmatrix} v^T \\ u^T \end{pmatrix} . \tag{4.12}$$

To calculate the expectation value of a generalized one-body operator, we proceed as in the pure density case. Let

$$\alpha_i = a_i, \quad i = 1, ..., N_s \tag{4.13a}$$

$$\alpha_{i+N_s} = a_i^\dagger, \quad i = 1, ..., N_s . \tag{4.13b}$$

Then the one-quasiparticle density matrix is

$$\begin{aligned} \left\langle \alpha_a^\dagger \alpha_b \right\rangle_\sigma &= \frac{\langle \psi_L | \hat{\rho}_{ab} | \psi_R \rangle}{\langle \psi_L | \psi_R \rangle} \\ &= \frac{1}{2} \left[\Psi_{\mathbf{R}} (\Psi_{\mathbf{L}}{}^\dagger \Psi_{\mathbf{R}})^{-1} \Psi_{\mathbf{L}}{}^\dagger \right]_{ba} \\ &\quad - \frac{1}{2} \left[\begin{pmatrix} 0 & 1 \\ 1 & 0 \end{pmatrix} \Psi_{\mathbf{R}} (\Psi_{\mathbf{L}}{}^\dagger \Psi_{\mathbf{R}})^{-1} \Psi_{\mathbf{L}}{}^\dagger \begin{pmatrix} 0 & 1 \\ 1 & 0 \end{pmatrix} \right]_{ab} + \delta_{ab} \\ &= \left[\Psi_R (\Psi_L^\dagger \Psi_R)^{-1} \Psi_L^\dagger \right]_{ba} . \end{aligned} \tag{4.14}$$

The final step follows from the properties of U in Eq. (A20). Note that both the overlap and the Green's function are similar to those of the density decomposition. However, the enlarged dimension of the representation matrices causes the overlap to be the square-root of a determinant rather than just a determinant. We know

of no simple way to determine the sign of the square root. Computationally, it can be traced by watching the evolution of $\langle\psi_0|\hat{U}_\sigma(\tau,0)|\psi_0\rangle$ as $\hat{U}_\sigma$ is built up from 0 to β (Appendix B), although at the expense of more computation time. Also, the linear dimension of the matrix used in the calculation is twice that for the pure density decomposition case. Therefore, the introduction of the pairing decomposition is costly. However, there lies the potential for more effective sampling in the Monte-Carlo calculation when the interaction has a strong pairing character. It also offers greater freedom in the decomposition, which might be used to mitigate the sign problem.

B. Grand-canonical ensemble

For the grand-canonical ensemble, the trace in Eq. (2.18) is a sum over all possible many-body states with all possible nucleon numbers, and a chemical potential in $\hat{H}$ is required. For the pure density decomposition, the many-body trace is given by

$$\zeta(\sigma) = \hat{\mathrm{Tr}}\,\hat{U}_\sigma(\beta,0) = \det\left(1 + \mathbf{U}_\sigma(\beta,0)\right) , \tag{4.15}$$

which can be proved by expanding the determinant [22].

For the expectation value of a one-body operator, one can recapitulate exactly the argument of the zero-temperature development and obtain

$$\left\langle a_a^\dagger a_b \right\rangle_\sigma = \left[\left(1 + \mathbf{U}_\sigma(\beta,0)\right)^{-1} \mathbf{U}_\sigma(\beta,0)\right]_{ba} . \tag{4.16}$$

We have extended these formulae to decompositions that involve pairing operators (Appendix A). The results are given in terms of the $2N_s \times 2N_s$ matrices $\mathbf{M}_n, \mathbf{U}(\beta,0)$ (4.9, 4.10), representing the Hamiltonians $\hat{h}_n$ and the evolution operator $U(\hat{\beta},0)$, namely

$$\hat{\mathrm{Tr}}\left[\hat{U}(\beta,0)\right] = \det\left[1 + \mathbf{U}(\beta,0)\right]^{\frac{1}{2}} \exp\left(-\frac{\Delta\beta}{2}\mathrm{Tr}[\Theta_n]\right) . \tag{4.17}$$

To motivate this formula, consider the simplest case of one time slice where $\hat{U} = \exp(-\hat{h})$ and $\hat{h}$ is Hermitian and in the form (4.7). Then, $\hat{h}$ can be diagonalized by a HFB transformation

$$\hat{h} = \frac{1}{2}\begin{pmatrix} a^\dagger & a \end{pmatrix}\begin{pmatrix} \Theta & \Delta - \Delta^T \\ \Lambda - \Lambda^T & -\Theta^T \end{pmatrix}\begin{pmatrix} a & a^\dagger \end{pmatrix} + \frac{1}{2}\mathrm{Tr}[\Theta] \tag{4.18a}$$

$$= \sum_i e_i \beta_i^\dagger \beta_i - \frac{1}{2}e_i + \frac{1}{2}\mathrm{Tr}[\Theta] \tag{4.18b}$$

where

$$\begin{pmatrix} \beta \\ \beta^\dagger \end{pmatrix} = \begin{pmatrix} u & v^* \\ v & u^* \end{pmatrix}\begin{pmatrix} a \\ a^\dagger \end{pmatrix} \tag{4.19}$$

and

$$\begin{pmatrix} u & v^* \\ v & u^* \end{pmatrix}\begin{pmatrix} \Theta & \Delta - \Delta^T \\ \Lambda - \Lambda^T & -\Theta^T \end{pmatrix}\begin{pmatrix} u^\dagger & v^\dagger \\ v^T & u^T \end{pmatrix} = \begin{pmatrix} \epsilon_1 & 0 & \dots & 0 & 0 & \dots \\ 0 & \epsilon_2 & \dots & 0 & 0 & \dots \\ \vdots & \vdots & \ddots & \vdots & \vdots & \ddots \\ 0 & 0 & \dots & -\epsilon_1 & 0 & \dots \\ 0 & 0 & \dots & 0 & -\epsilon_2 & \dots \\ \vdots & \vdots & \ddots & \vdots & \vdots & \ddots \end{pmatrix}. \tag{4.20}$$

In the diagonal form, $\hat{\mathrm{Tr}}[\exp(-\hat{h})]$ can be easily identified as

$$\begin{aligned} \prod_i [(1+e^{-\epsilon_i})e^{\frac{1}{2}\epsilon_i}]e^{-\frac{1}{2}\mathrm{Tr}[\Theta]} &= \prod_i \sqrt{(1+e^{-\epsilon_i})(1+e^{\epsilon_i})}e^{-\frac{1}{2}\mathrm{Tr}[\Theta]} \\ &= \det[(1+e^{-M})^{\frac{1}{2}}]e^{-\frac{1}{2}\mathrm{Tr}[\Theta]}, \end{aligned} \tag{4.21}$$

due to the invariance of the determinant with respect to similarity transformations. Here, as in the overlap formulae for zero-temperature approach, the grand-canonical trace is given as the square root of a determinant, so that the evolution of the sign is important (Appendix B). The formula for the observables can be calculated from

$$\begin{aligned}\left\langle \alpha_a^\dagger \alpha_b \right\rangle_\sigma &= \frac{1}{2}\left[(1+\mathbf{U}(\beta,0))^{-1}\,\mathbf{U}(\beta,0)\right]_{ba} \\ &\quad -\frac{1}{2}\left[\begin{pmatrix} 0 & 1 \\ 1 & 0 \end{pmatrix}(1+\mathbf{U}(\beta,0))^{-1}\mathbf{U}(\beta,0)\begin{pmatrix} 0 & 1 \\ 1 & 0 \end{pmatrix}\right]_{ab} + \frac{1}{2}\delta_{ab} \\ &= \left[(1+\mathbf{U}(\beta,0))^{-1}\,\mathbf{U}(\beta,0)\right]_{ba} . \end{aligned} \tag{4.22}$$

C. Fugacity expansion for the canonical ensemble

As mentioned in the beginning of this section, the grand-canonical ensemble may lead to large fluctuations in the particle number for systems with few particles. It is particularly undesirable for nuclear systems exhibiting shell structure. While the particle number does not fluctuate in the zero-temperature approach, that formalism can only give ground-state results. Therefore, the canonical ensemble is important for studying thermal behavior.

In the canonical ensemble, we have to find the trace of $\hat{U}_\sigma(\beta,0)$ over all states with a fixed particle number N_v (actually fixed proton and neutron numbers). We discuss two methods of achieving this: the fugacity expansion presented here and the integration over real coherent states presented in the following subsection.

Consider first the case when only density operators are present in the one-body Hamiltonian $\hat{h}$. From the grand-canonical ensemble formulae (4.16), we can see that the canonical trace is just the sum of all the $N_v \times N_v$ sub-determinants. More explicitly, we consider the *fugacity expansion*: for some parameter λ, let

$$Z(\beta,\lambda) = \hat{\mathrm{Tr}}\lambda^{\hat{N}_v} e^{-\beta\hat{H}} = \sum_{N_v} \lambda^{N_v}\, Z_{N_v}(\beta) . \tag{4.23}$$

In our matrix representation,

$$\hat{\mathrm{Tr}}\,\lambda^{\hat{N}}\hat{U}_\sigma(\beta,0) = \det(\mathbf{1}+\lambda\mathbf{U}) . \tag{4.24}$$

Consider the expansion of Eq. (4.24) in powers of λ: The coefficient of λ^{N_v} is just the

canonical trace of $\hat{U}_\sigma(\beta,0)$ over N_v particles. Therefore, $\det(1+\lambda U)$ is the generating function for the canonical trace. Thus,

$$Z_{N_v}(\beta) = \int \mathcal{D}[\sigma] G(\sigma) \zeta_{N_v}(\sigma) \,, \tag{4.25}$$

where

$$\det\left(1 + \lambda \mathbf{U}_\sigma(\beta,0)\right) = \sum_{N_v} \lambda^{N_v} \zeta_{N_v}(\sigma) \,. \tag{4.26}$$

The trick now is to find simpler expressions for ζ_{N_v}, instead of doing the explicit sum over the determinants. To do this, write

$$\det(1+\lambda \mathbf{U}) = \exp \mathrm{Tr} \ln(1+\lambda \mathbf{U}) = \exp\left(\sum_{n=1}^{\infty} \frac{(-1)^{n-1}}{n} \lambda^n \mathrm{Tr}\left[\mathbf{U}^n\right]\right) \,. \tag{4.27}$$

This expansion converges to the generating function because $Z(\beta,\lambda)$ is a polynomial in λ of finite order. The coefficient of λ^n in the exponential is readily found. For a given particle number N_v, we only need to calculate up to the value of $\mathrm{Tr}[\mathbf{U}^{N_v}]$ and the coefficient of λ^{N_v} can be extracted accordingly.

For one-body expectation values, using again the grand-canonical trace as the generating function for calculating observables and collecting all terms with coefficient λ^{N_v}, we arrive at

$$\left\langle a_a^\dagger a_b \right\rangle_{\sigma,N_v} = \sum_{n=1}^{N_v} (-1)^{n-1} \left(\mathbf{U}^n\right)_{ba} \zeta_{N_v-n}(\sigma)/\zeta_{N_v}(\sigma) \,. \tag{4.28}$$

The expectation value of two-body operators, $\langle \rho_{ab}\rho_{cd}(\sigma)\rangle_{N_v}$, is nontrivial as Wick's theorem must be modified; but again one must simply collect the terms with coefficient λ^{N_v} and obtain

$$\begin{aligned}\left\langle a_a^\dagger a_b a_c^\dagger a_d \right\rangle_{\sigma,N_v} = \sum_{n=1}^{N_v} \Bigg\{ \sum_{m=1}^{N_v-n} \left[(-1)^{m+n} \left(\mathbf{U}^n_{ba}\mathbf{U}^m_{dc} - \mathbf{U}^n_{da}\mathbf{U}^m_{bc}\right) \zeta_{N_v-m-n}(\sigma)/\zeta_{N_v}(\sigma)\right] \\ + \delta_{bc}(-1)^{n-1} \mathbf{U}^n_{da} \zeta_{N_v-n}(\sigma)/\zeta_{N_v}(\sigma) \Bigg\} \,.\end{aligned} \tag{4.29}$$

This form of the fugacity expansion works best for $N_v \leq N_s/2$ (mostly empty model spaces). When $N_v > N_s/2$ (mostly filled spaces), it is more efficient to expand in the fugacity of the hole states. In this case, we define

$$Z_\sigma(\beta,\lambda) = \hat{\mathrm{Tr}}[\lambda^{N_s-\hat{N}} e^{-\beta\hat{H}}] \,, \tag{4.30}$$

and as in Eq. (4.24),

$$\hat{\mathrm{Tr}}[\lambda^{N_s-\hat{N}}\hat{U}(\beta,0;\sigma)] = \det[\lambda+\mathbf{U}] \,. \tag{4.31}$$

The coefficient of λ^N is the partition function for N holes,

$$\det[\lambda+\mathbf{U}] = \det[\mathbf{U}]\exp(\sum_{n\geq 1}\frac{1}{n}(-1)^{n-1}\lambda^n Tr[\mathbf{U}^{-n}]) \equiv \sum_N \lambda^N \zeta'_N \,, \tag{4.32}$$

where the expectation value of a one-body operator is

$$\langle\rho_{ij}\rangle_{N\text{ holes}} = \sum_{n=0}^{N}(-1)^n \mathbf{U}^{-n}_{ji}\zeta'_{N-n}/\zeta'_N \,, \tag{4.33}$$

and the expectation of a two-body operator is

$$\begin{aligned}\langle\rho_{ij}\rho_{kl}\rangle_{N\text{ holes}} = &\sum_{n=0}^{N}\delta_{jk}(-1)^n\mathbf{U}^{-n}_{li}\zeta'_{N-n}/\zeta'_N) \\ &+(\sum_{m=0}^{N-n}(-1)^{m+n}(\mathbf{U}^{-n}_{ji}\mathbf{U}^{-m}_{lk} - \mathbf{U}^{-n}_{li}\mathbf{U}^{-m}_{jk})\zeta'_{N-m-n}/\zeta'_N \,.\end{aligned} \tag{4.34}$$

When pairing operators are involved, we use Eq. (4.17) for the grand-canonical trace, which becomes the generating function for the corresponding canonical trace. As an illustration, we display the formula for the expansion in particle fugacity,

$$\begin{aligned}\hat{\mathrm{Tr}}\left[\lambda^{\hat{N}}\hat{U}\right] &= \det\left[\begin{pmatrix}1 & 0\\ 0 & 1\end{pmatrix} + \begin{pmatrix}\lambda 1 & 0\\ 0 & \frac{1}{\lambda}1\end{pmatrix}\mathbf{U}\right]^{\frac{1}{2}}\lambda^{\frac{N_s}{2}} \\ &= \det\left[\begin{pmatrix}1 & 0\\ 0 & 1\end{pmatrix} + \begin{pmatrix}\lambda 1 & 0\\ 0 & \frac{1}{\lambda}1\end{pmatrix}\begin{pmatrix}\mathbf{S}^{11} & \mathbf{S}^{12}\\ \mathbf{S}^{21} & \mathbf{S}^{22}\end{pmatrix}\right]^{\frac{1}{2}}\lambda^{\frac{N_s}{2}} \\ &= \det\left[\begin{pmatrix}1 & \mathbf{S}^{12}\\ 0 & \mathbf{S}^{22}\end{pmatrix}\right]^{\frac{1}{2}}\det\left[\begin{pmatrix}1 & 0\\ 0 & 1\end{pmatrix} + \lambda\begin{pmatrix}1 & \mathbf{S}^{12}\\ 0 & \mathbf{S}^{22}\end{pmatrix}^{-1}\begin{pmatrix}\mathbf{S}^{11} & 0\\ \mathbf{S}^{21} & 1\end{pmatrix}\right]^{\frac{1}{2}}\end{aligned}$$

$$= \det\left[\begin{pmatrix} 1 & \mathbf{S^{12}} \\ 0 & \mathbf{S^{22}} \end{pmatrix}\right]^{\frac{1}{2}} \exp\left(\frac{1}{2}\mathrm{Tr}\left[\ln\left(\begin{pmatrix} 1 & 0 \\ 0 & 1 \end{pmatrix} + \lambda \mathbf{Y}\right)\right]\right)$$

$$= \det\left[\mathbf{S^{22}}\right]^{\frac{1}{2}} \exp\left(\frac{1}{2}\sum_n \mathrm{Tr}\left[\mathbf{Y}^n\right](-1)^{n-1}\frac{\lambda^n}{n}\right), \tag{4.35}$$

where the definitions of $\mathbf{S^{11}}, \mathbf{S^{12}}, \mathbf{S^{21}}, \mathbf{S^{22}}$ are obvious, and

$$\mathbf{Y} \equiv \begin{pmatrix} 1 & \mathbf{S^{12}} \\ 0 & \mathbf{S^{22}} \end{pmatrix}^{-1} \begin{pmatrix} \mathbf{S^{11}} & 0 \\ \mathbf{S^{21}} & 1 \end{pmatrix}. \tag{4.36}$$

The expectation values of one- and two-body operators can then be derived as in the pure density decomposition.

D. Fourier extraction of canonical ensemble

The fugacity expansion is found to work well for nuclei where the number of holes or number of particles is less than 5 in the *sd* and *fp* shell; but near mid-shells, the calculation suffers from numerical instability. The fugacity expansion there involves small differences resulting from the cancellation of large numbers, that are near or above the floating point accuracy of a 64-bit machine. We therefore investigated the Fourier method, which is suited to mid-shell nuclei.

Recall that the grand canonical overlap function of (4.27) Let us define $\phi_m = 2\pi m/N_s$. Then we may write

$$\eta_m(\sigma) \equiv \det[1 + e^{i\phi_m}\mathbf{U}(\sigma)] = \sum_{N=0}^{N_s} e^{i\phi_m N}\zeta_N(\sigma). \tag{4.37}$$

Using the fact that

$$\frac{1}{N_s}\sum_{m=1}^{N_s} e^{i\phi_m K} = \delta_{K0}, \tag{4.38}$$

we see that for $0 < A < N_s$,

$$\zeta_A(\sigma) = \frac{1}{N_s}\sum_{m=1}^{N_s} e^{-i\phi_m A}\det[1 + e^{i\phi_m}\mathbf{U}(\sigma)]. \tag{4.39}$$

We also find expection values of the density operators in the same manner. For the one body densities we obtain

$$\langle \rho_{ab}(\sigma) \rangle_A = \frac{1}{N_s \zeta_A(\sigma)} \sum_{m=1}^{N_s} e^{-iA\phi_m} \eta_m(\sigma) \gamma_{ab}^m(\sigma), \tag{4.40}$$

and for the two body density operators

$$\langle \rho_{ab}(\sigma)\rho_{cd}(\sigma) \rangle_A = \frac{1}{N_s \zeta_A(\sigma)} \sum_{m=1}^{N_s} e^{-iA\phi_m} \eta_m(\sigma)$$
$$\times [\gamma_{ab}^m(\sigma)\gamma_{cd}^m(\sigma) - \gamma_{ad}^m(\sigma)\gamma_{cb}^m(\sigma) + \delta_{bc}\gamma_{ad}^m(\sigma)], \tag{4.41}$$

where

$$\gamma_{ab}^m(\sigma) = [(1 + e^{i\phi_m}\mathbf{U}(\sigma))^{-1} e^{i\phi_m}\mathbf{U}(\sigma)]_{ba}. \tag{4.42}$$

A direct calculation of the determinants in Eqn. (4.39) is an N_s^4 process due to the N_s ϕ_m's present. However, we can choose to first diagonalize U to give eigenvalues ξ_i; the diagonalization is a N_s^3 process. Then $\eta_m(\sigma)$ can be writen as a direct product

$$\eta_m(\sigma) = \prod_i (1 + \xi_i e^{i\phi_m}). \tag{4.43}$$

Similarly the density operator can be written in terms of the transformation matrix,

$$\gamma_{ab}^m = \sum_k \mathbf{S}_{bk}(1 + e^{i\phi_m}\xi_k)^{-1} e^{i\phi_m}\xi_k \mathbf{S}_{ka}^{-1} \tag{4.44}$$

where

$$\mathbf{S}\mathrm{diag}(\xi_1, \xi_2, ...)\mathbf{S}^{-1} = \mathbf{U}. \tag{4.45}$$

We have performed canonical calculations of mid-*sd* shell using the Fourier extraction method, and we have also performed preliminary canonical calculations in the mid-*fp* shell; these indicate that the extraction method works there as well. The method fails at small number of particle or holes; i.e., those nuclei where the fugacity expansion works well. This can be understood from Eqn. (4.24). The dominant

contributions in the sum comes from mid-shell overlap functions, due to the large number of contributing configurations there. It is very difficult to extract relatively small overlap functions for nuclei at the beginning or the end of the shell. The fugacity and the Fourier expansion are thus complementary to each other in the shell model space. For *sd* and *fp* shell nuclei, we have found that for the number of particles or holes for individual kind of nucleons great than five, the Fourier expansion works well.

E. Canonical ensemble via coherent states

We make use of the operator

$$\hat{J} = C \int \prod_{ph} dX_{ph} \frac{|X\rangle\langle X|}{\det(1 + X^T X)^{\frac{N_s}{2}+1}} , \tag{4.46}$$

which can be shown [23] to be a resolution of unity in the Hilbert space of N_v fermions occupying N_s levels. Here, X_{ph} are the real integration variables, $|X\rangle$ are the real coherent states

$$|X\rangle = \exp(\sum_{hp} X_{ph} a_p^\dagger a_h)|0\rangle, \quad h = 1, ..., N_v; \; p = N_v + 1, ..., N_s , \tag{4.47}$$

$|0\rangle$ is the N_v-fermion state with the levels $1, ..., N_v$ occupied and C is a normalization constant,

$$C = \prod_{p=N_v+1}^{N_s} C_p, \quad C_p = \pi^{-N_s/2} \Gamma\left(\frac{p}{2} + 1\right) / \Gamma\left(\frac{p - N_v}{2} + 1\right) . \tag{4.48}$$

The canonical trace can then be cast in a form of expectation with integration over the variables X_{ph}. For any operator $\hat{O}$,

$$\hat{\mathrm{Tr}}[\hat{O}] = C \int dX \frac{\langle X|\hat{O}|X\rangle}{\det(1 + X^T X)^{\frac{N_s}{2}+1}} \tag{4.49}$$

where $dX = \prod_{ph} dX_{ph}$. The thermal canonical expectation is then

$$\langle \hat{O} \rangle = \frac{\hat{\mathrm{Tr}}[\hat{O}e^{-\beta\hat{H}}]}{\hat{\mathrm{Tr}}[e^{-\beta\hat{H}}]}$$
$$= \frac{\int \mathcal{D}[\sigma] G(\sigma) dX \langle X|\hat{U}_\sigma(\beta,0)\hat{O}|X\rangle / \det(1+X^TX)^{N_s/2+1}}{\int \mathcal{D}[\sigma] G(\sigma) dX \langle X|\hat{U}_\sigma(\beta,0)|X\rangle / \det(1+X^TX)^{N_s/2+1}} . \quad (4.50)$$

We can use the formulae for the overlap and the expectation of observables in the zero-temperature formalism, except that we also have to do the integration over the fields X_{ph} with Monte Carlo sampling. But the number of fields X_{ph} only goes as N_s^2 which is about the same as the number of σ fields in one time slice. Therefore, introducing the coherent-state integration is not much more computationally expensive than the zero-temperature formalism. The advantage of coherent states is that we do not have to find $\mathrm{Tr}[\mathrm{U}(\beta,0)^n]$, which can be numerically unstable when the number of particles present is large. However, the integration of the coherent states may aggravate the sign problem as will be discussed in Sections VI and VII.

V. DYNAMICAL CORRELATIONS

In the previous section, we discussed how to extract the expectation value of one-body operators $\langle O \rangle$ and, by use of Wick's theorem and its extension to the canonical case, equal-time two-body operators $\langle \hat{A}\hat{B} \rangle$, etc. A great deal of the interesting physics, however, is contained in the dynamical response function $\langle \hat{O}^\dagger(t)\hat{O}(0) \rangle$ where $\hat{O}(t) = e^{-i\hat{H}t}\hat{O}e^{i\hat{H}t}$. In our framework, we evaluate the imaginary-time response function $\langle \hat{O}^\dagger(i\tau)\hat{O}(0) \rangle$ and deduce the associated strength function $f_{\hat{O}}(E)$.

In the zero temperature formalism, the strength function is

$$f_{\hat{O}}(E) \equiv \sum_f \delta(E - E_f + E_i)|\langle f|\hat{O}|i\rangle|^2 \,, \tag{5.1}$$

where i is the ground state, while in the canonical or grand-canonical ensemble,

$$f_{\hat{O}}(E) \equiv \frac{1}{Z}\sum_{i,f} \delta(E - E_f + E_i)e^{-\beta E_i}|\langle f|\hat{O}|i\rangle|^2 \,. \tag{5.2}$$

Thus, the imaginary-time response function is related to the strength function by a Laplace transform,

$$R(\tau) \equiv \langle \hat{O}^\dagger(i\tau)\hat{O}(0) \rangle = \int_{-\infty}^{\infty} f_{\hat{O}}(E)e^{-\tau E}dE \,. \tag{5.3}$$

Recovering the strength function, through inversion of the Laplace transform, is an ill-posed numerical problem. Different methods have been proposed to tackle this problem [24,20]. We resort to making the best "guess" for the strength function via the Classic Maximum Entropy (MaxEnt) method [18,19], which was first introduced to recover strength functions in Monte Carlo calculations by Silver *et al.* [20] and then widely used in similar condensed matter simulations. It is in essence a least-squares fit biased by a measure of the phase space of the strength function. In MaxEnt methods, the function to be minimized is $\frac{1}{2}\chi^2 - \alpha S$, where χ^2 is the usual difference squared, S is the entropy of the phase space (not to be confused with the action in the auxiliary fields Monte Carlo), and α is a Lagrange multiplier. In Classic MaxEnt α is

determined self-consistently. The method, described briefly in Appendix C, also can yield error estimates for the extracted strength function. Considering $\left\langle \hat{A}(i\tau)\hat{B}(0)\right\rangle$, we write the thermal expectation as a path integral

$$\begin{aligned}\langle \hat{A}(i\tau)\hat{B}(0)\rangle &= \frac{\hat{\mathrm{Tr}}[e^{-(\beta-\tau)\hat{H}}\hat{A}e^{-\tau\hat{H}}\hat{B}]}{\hat{\mathrm{Tr}}[e^{-\beta\hat{H}}]} \\ &= \frac{\int \mathcal{D}[\sigma]G(\sigma)\hat{\mathrm{Tr}}[\hat{U}_\sigma(\beta,0)]\frac{\hat{\mathrm{Tr}}[\hat{U}_\sigma(\beta,\tau)\hat{A}\hat{U}_\sigma(\tau,0)\hat{B}]}{\hat{\mathrm{Tr}}[\hat{U}_\sigma(\beta,0)]}}{\int \mathcal{D}[\sigma]G(\sigma)\hat{\mathrm{Tr}}[\hat{U}_\sigma(\beta,0)]}\,, \end{aligned} \tag{5.4}$$

and define

$$\hat{O}_\sigma(\tau) \equiv \hat{U}_\sigma(\tau,0)^{-1}\hat{O}\hat{U}_\sigma(\tau,0) \tag{5.5}$$

so that

$$\langle \hat{A}(i\tau)\hat{B}(0)\rangle = \frac{\int \mathcal{D}[\sigma]G(\sigma)\hat{\mathrm{Tr}}[\hat{U}_\sigma(\beta,0)]\frac{\hat{\mathrm{Tr}}[\hat{U}_\sigma(\beta,0)\hat{A}_\sigma(\tau)\hat{B}_\sigma(0)]}{\hat{\mathrm{Tr}}[\hat{U}_\sigma(\beta,0)]}}{\int \mathcal{D}[\sigma]G(\sigma)\hat{\mathrm{Tr}}[\hat{U}_\sigma(\beta,0)]} \tag{5.6a}$$

$$= \frac{\int \mathcal{D}[\sigma]e^{-\mathcal{S}(\sigma)}\langle \hat{A}_\sigma(\tau)\hat{B}_\sigma(0)\rangle}{\int \mathcal{D}[\sigma]e^{-\mathcal{S}(\sigma)}}\,. \tag{5.6b}$$

We now proceed to find $\hat{O}_\sigma(\tau)$. For the purpose of illustration, we show the formulae for the pure density decomposition; formulae for the general case can be derived similarly. For the simplest case when $\hat{O} = a_i^\dagger$ or $\hat{O} = a_i$, it can be shown that [22]

$$a^\dagger_{i\sigma}(n\Delta\beta) = \sum_j [\mathrm{U}_\sigma(n\Delta\beta,0)^{-1}]^T_{ij}a^\dagger_j \tag{5.7a}$$

$$a_{i\sigma}(n\Delta\beta) = \sum_j \mathrm{U}_\sigma(n\Delta\beta,0)_{ij}a_j\,. \tag{5.7b}$$

In this way, the creation and annihilation operators can be 'propagated' back to $\tau = 0$. Any operator $\hat{O}_\sigma(\tau)$ can be first expressed in $a_\sigma(\tau)$ and $a^\dagger{}_\sigma(\tau)$ and therefore can be propagated back and expressed in a and $a^\dagger$. For example, suppose $\hat{O} = C_{ij}a_i^\dagger a_j$ is a one-body operator. Then

$$\hat{O}_\sigma(\tau) = \hat{U}_\sigma(\tau,0)^{-1}\hat{O}\hat{U}_\sigma(\tau,0) \tag{5.8}$$

$$= [\mathbf{U}_\sigma(\tau,0)^{-1}\mathbf{C}\mathbf{U}_\sigma(\tau,0)]_{ij}a_i^\dagger a_j \; . \tag{5.9}$$

Thus, the response function can be measured in the same way as the static observables.

VI. COMPUTATIONAL DETAILS AND ILLUSTRATIONS

A. Monte Carlo methods

Monte Carlo evaluation of the path integral requires a weight function. We have tried two different choices for the weight function, each with advantages and disadvantages.

One choice for the weight function is a Gaussian, with the the static mean-field solution as the centroid, and the widths given by the RPA frequencies. Thus, much of the known physics is embodied in the weight and the Monte Carlo evaluates corrections to mean-field +RPA. Further, it is simple to efficiently generate random field configurations with a Gaussian distribution. However, Gaussian sampling has several disadvantages. First, finding the RPA frequencies can be extremely time consuming since we have to calculate and diagonalize the curvature matrix $\frac{\partial^2}{\partial\sigma_{\alpha,i}\partial\sigma_{\gamma,j}}\mathcal{S}$ at the mean-field solution where α, γ run through the number of quadratic terms in the Hamiltonian and i,j run through the number of time slices. For any general interaction, the curvature matrix is of the dimension $N_s^2 N_t$. Second, the Gaussian has to be modified when there is spontaneous symmetry breaking in the mean fields (such as quadrupole deformations), otherwise the Goldstone modes in the the RPA frequencies (e.g., zero eigenvalues corresponding to shape rotations) will destroy the normalizability of the weight function. Finally, multiple mean-field solutions well separated from each other can also pose a problem, in which case multiple Gaussians may be needed.

A more satisfactory route is to choose $|\exp(-\mathcal{S})| = G(\sigma)|\zeta(\hat{U}_\sigma(\beta,0)|$ as the weight function and to use a stochastic random walk such as the Metropolis algorithm to generate the fields. The expectation of an observable is then given by Eq. (2.21) where

$$\Phi_i = \exp[-i\mathrm{Im}(\mathcal{S}_i)] \,. \tag{6.1}$$

The Metropolis algorithm is free of the disadvantages for the Gaussian weight function, in that it will eventually sample the entire space where $|\exp(-\mathcal{S})|$ is significant. The main disadvantage of Metropolis is its inefficiency as currently implemented and the "sign problem." Let us define the denominator of Eq. (2.21) by $\langle\Phi\rangle$, therefore

$$\langle\Phi\rangle \equiv \frac{1}{N}\sum_i \exp[-i\mathrm{Im}(\mathcal{S}_i)] \,. \tag{6.2}$$

If $\langle\Phi\rangle \ll 1$, the large fluctuations swamp the results with noise. This 'sign problem' will be addressed in detail in the examples illustrated below.

For the Metropolis algorithm, we take random steps in the fields time-slice by time-slice, following a sweeping procedure introduced by Sugiyama and Koonin [5]. For the Monte Carlo results to be valid, one requires that the points in the random walk are both distributed as the weight function and are statistically independent. The first requirement translates into starting the fields in a region of statistically significant weight; if the initial configuration is far from there, a number of initial thermalization sweeps are usually needed to relax the fields to this region. The second requirement means that between samples, the walker must sweep through the fields many times to de-correlate the samples. The number of thermalization sweeps and decorrelation sweeps increases with system size. The choice of random walk procedure greatly affects the sampling efficiency. In the early stage of investigation, we allowed the fields σ_α at a time-slice to change with equal probability within a certain step size. The acceptance probability is then given by the ratio of the weight $|\exp(-\mathcal{S})|$ of the old and new configurations. The step size is chosen to produce average acceptance probability of 0.5. In the calculation of *sd*-shell nuclei described below, it needs approximately 2000 thermalization sweeps and up to 200 decorrelation sweeps between samples. Lately, we use another random walk, the hybrid-Gaussian walk, in which a fixed number of fields are randomly chosen for updating. The ones

chosen are generated from the Gaussian distribution in Eq. (2.9b) while the remaining ones are kept at the previous values. The acceptance probability is then given by the ratio of ζ in the new and old configurations. This random walk needs only around 200 thermalization sweeps and 10 decorrelation sweeps, a factor of 10 more efficient than the previous method. In addition, the existence of boundaries, where $|\exp(-\mathcal{S})| = 0$, can prevent the first random walk to cross while it does not pose any barrier to the second one. The auto-correlations for various observables in consecutive sweeps in the random walk is shown in Fig. 2 for the different sampling schemes, for a calculation on Mg^{24} with the Hamiltonian (6.7). The calculation was done for $\beta = 3$ with 24 time slices, in the zero-temperature formalism. Note that scalar observables $\langle H \rangle, \langle J^2 \rangle$, and $\langle Q^2 \rangle$ decorrelates much faster than observable $\langle Q_z \rangle$.

The walker can thermalize faster if it starts from a configuration where the weight $W(\sigma)$ is large. Usually we choose the static mean fields for the starting point. These are given by

$$\sigma_{\alpha,n} = \bar{\sigma}_\alpha, \quad n = 1, N_t \tag{6.3a}$$

$$\bar{\sigma}_\alpha = -s_\alpha \text{sign}(V_\alpha) \langle \hat{O}_\alpha \rangle_{\bar{\sigma}} \, . \tag{6.3b}$$

One can show that for canonical and grand-canonical calculations, the static mean field $\bar{\sigma}_\alpha$ is a saddle point of the weight function,

$$\frac{\partial [G(\sigma)\zeta(\bar{\sigma})]}{\partial \sigma_{\alpha,i}}|_{\bar{\sigma}} = 0 \, . \tag{6.4}$$

For the zero-temperature approach, we also choose the self-consistent field solution $\bar{\sigma}_\alpha$ although Eq. (6.4) is not rigorously satisfied. This is preferable to starting the fields at zero, which may be far from configurations of significant weight.

The mean field solution (6.3) can be found iteratively

$$\{\bar{\sigma}_\alpha\}_{i+1} = -s_\alpha \text{sign}(V_\alpha) \langle \hat{\mathcal{O}}_\alpha \rangle_{\bar{\sigma}_i} \, . \tag{6.5}$$

For the systems we have tested, Eq. (6.5) usually converges within 100 interactions starting from $\bar{\sigma}_\sigma = 0$. For larger systems and at lower temperature, convergence is slow and sometimes unstable or barely stable. In that case taking

$$\sigma_{\alpha,i} = -s_\alpha \text{sign}(V_\alpha)\langle \hat{O}_\alpha \rangle_{\sigma=0} \tag{6.6}$$

for a starting configuration also leads to a shorter thermalization time than the choice of $\sigma = 0$.

B. Comparison of continuous and discrete HS transformation

The discrete HS transformation mentioned in Section II has also been carried out. In the trial step, a fixed number of fields are randomly chosen for updating with the new discrete value generated according to the function $f(\sigma)$ in (2.28). The acceptance probability is then given by the ratio of ζ in the new and old configuration. We have tried the discrete transformations of (2.30) and (2.31), which give rise to approximation to order $\Delta\beta$ and $(\Delta\beta)^2$ respectively, in calculations of ^{24}Mg and ^{20}Ne. As can be seen from Fig. 2, both methods are found to have short thermalization and decorrelation lengths similary to the continuous transformation in the hybrid-Gaussian random walk. We conclude that the continous transformation performs as efficiently as the discrete transformation in the cases studied. The previous conclusion from the Hubbard model calculations that the discrete transformation is superior may be due to the inefficient random walk used in the continuous transformation studies.

The convergence in $\Delta\beta$ also depends on the transformation scheme due to the different levels of approximation to the many-body evolution operator. The two-value transformation is found to converge slower in $\Delta\beta$ to the exact result, while the three-value transformation converges as well as the continuous transformation. An example of the convergence behavior of different schemes is shown in Fig. 3, in calculations of Mg^{24} in the zero-temperature formalism at $\beta = 3$.

C. Examples

We now describe several examples to demonstrate the method in calculating properties of nuclei. Two major considerations arise in the implementation, namely the choice of decomposition scheme and the choice of ensemble. Different decomposition schemes involve different dimensions of matrices and numbers of fields, which control the computational speed. Also, the rates of convergence as $\Delta\beta \rightarrow 0$ are different and determine the number of time slices to be used. Last, but not least, the choice also affects the "sign problem" associated with the statistical stability of the calculation. Comparison of different decomposition schemes will be made in examples 1 and 2 below. The choice of ensemble among zero-temperature, canonical, and grand canonical ensembles usually do not affect the above issues. Instead, it depends on the kind of properties to be calculated. The zero-temperature formalism with a good trial wavefunction is effective in projecting out the ground state and is suitable for calculating ground-state static observables. For calculating finite temperature properties, the canonical ensemble is physically most relevant but also is most difficult to implement. Examples 1, 2, and 3 use grand canonical, zero-temperature, and canonical ensemble, respectively, for demonstration.

Finally, we choose a particular nucleus ^{20}Ne to demonstrate the calculation of dynamical responses of different operators and recover the strength function by the MaxEnt Method. The examples shown below were done with 3000 to 6000 samples on the Touchstone Gamma and Delta systems at Caltech.

Example 1: Monopole pairing interaction in the *sd* shell

We have described the considerable flexibility in writing the two-body interaction in quadratic form; e.g., density versus pairing decomposition and direct versus exchange decomposition. To illustrate this flexibility, we consider protons only in the

sd-shell, and keep only the $J = 0$ terms in Eq. (3.5); the values of $V_{J=0}$ and single particle energies are taken from the Wildenthal interaction [10]. First, we recouple the Hamiltonian into a quadratic form in the density operators in Eq. (3.21); because all possible density operators are required, there are 144 fields for each time slice. Second, we use the pairing decomposition in Eq. (3.41); after diagonalization only 6 fields are required. Finally, we write the two-body interaction as $\hat{H}_2 = \frac{1}{2}\hat{H}_2 + \frac{1}{2}\hat{H}_2$ and decompose the first half using densities and the second half using pairs; the total number of fields in this case is 150. It turns out that for protons only, this system is 99% free of the sign problem (i.e., Real $(\Phi_i) > 0$, 99% of the time), independent of the decomposition. All three calculations were performed in the grand-canonical ensemble using a Gaussian weight function around the static mean field, at an inverse temperature of $\beta = 1$ (here and henceforth, we measure all physical energies in MeV) and fixed chemical potential. The expectation value of the proton number, energy, and J^2 are given in Fig. 4 as a function of $\Delta\beta$. As the number of time slices increases towards infinity (i.e., $\Delta\beta \to 0$), all three decompositions converge to the exact answer, demonstrating their mutual equivalence in the continuum limit. Note, however, the different rates of convergence.

Example 2: ^{24}Mg with schematic forces

Next we consider *sd*-shell nuclei with a schematic Pairing + Multipole density interaction, where the multipole force is separable. It is the same interaction used in [25]. Therefore

$$\hat{H} = -g \sum_{T_z=-1,0,1} P^\dagger_{T_z} P_{T_z} - \frac{1}{2}\chi_0 \bar{\rho}_{0,0}\bar{\rho}_{0,0} - \frac{1}{2}\chi_2 \sum_M \bar{\rho}_{2,M}\bar{\rho}_{2,-M}(-1)^M - \frac{1}{2}\chi_4 \sum_M \bar{\rho}_{4,M}\bar{\rho}_{4,-M}(-1)^M \tag{6.7}$$

where

$$P_{T_z} = \sum_{jmt_1t_2} (\frac{1}{2}t_1\frac{1}{2}t_2|1T_z)a_{jmt_1}\tilde{a}_{jmt_2} \tag{6.8}$$

and

$$\bar{\rho}_{K,M} = \sum \tilde{u}_K(j_1j_2)\rho_{K,M,T=0}(j_1,j_2)\,. \tag{6.9}$$

This Hamiltonian was also decomposed in several ways. We first decomposed the pairing interaction as pair operators and the multipole force as density operators. In this way, the number of fields is kept to a minimum, only 21 fields per time slice. The pair-operator $P_{T_z=0}$ mixes protons and neutrons and therefore one matrix representing the mixed neutrons and protons wavefunction is needed. Also, the pairing breakup approach needs a matrix representation whose dimension is $2Ns$. Therefore, the matrix involved in this decomposition is 48×48. We calculated ^{24}Mg (4 valence protons and 4 valence neutrons in *sd*-shell) in the zero-temperature formalism; i.e., using the evolution operator at large β to project out the ground state from a trial state ψ_0. Since $\hat{h}$ is Hermitian (here $\bar{\rho}$ has the property $\bar{\rho}^\dagger_{K,M} = \bar{\rho}_{K,-M}(-1)^M$), in the static path $\zeta = \langle\psi_0|\exp(-\beta\hat{h})|\psi_0\rangle$ is always positive definite and $\Phi_i = 1$. However, for calculations with more than one time slice $\langle\Phi\rangle$ becomes very small. Therefore, we can only obtain sensible results in the SPA. These results turned out to be extremely good, relaxing to the right energy and angular momentum (Fig. 5). However, the success of the static path is case-specific and not well understood. We have also tried using just the monopole, quadrupole, and hexadecupole interactions in the case with only 4 protons in the *sd*-shell (^{20}Mg), in which the static path relaxes to an energy 2 MeV higher than the ground state, showing that the static path is not as satisfactory in this case.

In a second scheme, we transformed the pairing part of the interaction (6.7) into a quadratic form in the density operators. In the transformation, we use only density operators that conserve proton and neutron numbers (3.24–3.34), and we choose all

$E_{K,T=1}$ elements in Eq. (3.27) to be zero so that only isoscalar density operators are present in the quadratic form.

Now the interactions are in a much more complicated form due to the Pandya transformation of the pairing interaction. One needs 144 fields in the pure density decomposition as compared to 21 fields needed in the first decomposition. However, an advantage lies in the separation of the Slater-determinants for protons and neutrons since only density operators that separately conserve neutron and proton numbers are present. In the *sd*-shell, the dimension of matrix involved is only 12×12. For this particular interaction, an even more desirable property of the second scheme is that the eigenvalues $\lambda_{K,\alpha}$in Eq. (3.34) found by diagonalizing E_K in Eq. (3.27) has the property $\text{sign}(\lambda_K) = (-1)^{K+1}$. We prove in the next section that this property guarantees $\zeta(\sigma)$ to be positive definite for even-even nuclei if a suitable trial state is chosen. This allows the calculations to be carried out with any number of time slices without any sign problem.

We performed the calculation using the zero-temperature formalism at different β and $\Delta\beta$ values, choosing first the Hartree Slater-determinant as the trial wavefunction. The SPA calculation and the one with $\Delta\beta = 0.125$ are shown in Fig. 6. We have also performed calculations at $\Delta\beta = 0.5$ and $\Delta\beta = 0.25$. They are not shown but they lie between the SPA and the $\Delta\beta = 0.125$ results, and show a convergence to the result at $\Delta\beta = 0.125$. At $\Delta\beta = 0.125$, the energy relaxes to the right energy whereas the SPA also relaxes but to a much higher energy.

Next we tried a different trial wavefunction ψ_0, with the orbital $(j,m) = (\frac{5}{2},\pm\frac{1}{2}),(\frac{5}{2},\pm\frac{3}{2})$ occupied. A different relaxation curve is traced out by the calculations at $\Delta\beta = 0.125$, converging to the same exact result. Therefore, in using the zero-temperature approach to project out the ground state, the choice of the trial state is important for determining the rate of relaxation, although the final result is independent of the trial state as expected. In this case, although the Hartree state is

lower in energy than the maximal prolate state (compare $\langle H \rangle$ at $\beta = 0$), it contains some high angular momentum components (compare $\langle J^2 \rangle$ at $\beta = 0$), so that it relaxes more slowly and reaches the ground state at a larger value of β.

Example 3: Canonical calculations on ^{20}Ne and ^{24}Mg

Next, we demonstrate the canonical ensemble for the same interaction (6.7) using the pure density breakup as described in Example 2. We calculate ^{20}Ne because it is small enough to allow for an exact diagonalization to give all the states of $\hat{H}$, since we are concerned with both the ground-state and thermal properties. The canonical trace for this path-integral in also positive definite (see Section VII), allowing the calculations to be done using many time slices without any sign problem.

The results for calculations with $\Delta\beta = 0.25, 0.125$, and 0.0625 are shown in Fig. 6. The convergence as a function of $\Delta\beta$ is also apparent. Note that particular attention should be given to the extrapolation at high temperature. However, it is not hard to increase the number of time slices to improve the $\Delta\beta$ effect at high temperature. For example, for $\beta = 0.5, \Delta\beta = 0.0625$ amounts to only 8 time slices. Similar results on ^{24}Mg in the canonical ensemble are shown in Fig. 7. The relaxation to the ground state can be compared with the zero-temperature result in Fig. 5, however, now the results at small values of β are also physically significant.

In the calculation of ^{20}Ne, the fugacity expansion method is numerically stable. However, instabilities appear for *sd*-nuclei when the number of proton or neutron valence particles (or holes) is greater than 4. The instability is signalled by the deviation of $\langle N_p \rangle$ and $\langle N_n \rangle$ from the exact integers. In those cases, the expansion in Eq. (4.27) or (4.35) gives the canonical trace as the small difference between very large numbers. Therefore, the mid-shell nuclei cannot be calculated directly by those equations. We have tried the Fourier expansion technique to extract the canonical trace that gives satisfactory preliminary results [26]. The real coherent-state method

for the canonical trace for ^{24}Mg gives the same results as the fugacity expansion approach. However, $\langle\Phi_i\rangle$ is not always unity due to the coupling to the field X_{ph} for integration of the coherent states in Eq. (4.49) (as will be explained in the next section). It changes from 0.70 to 0.23 for β changing from 0.5 to 1.0 at $\Delta\beta = 0.25$. In the canonical ensemble, we can also study rotating nuclei by adding a Lagrange multiplier to the Hamiltonian, $\hat{H}' = \hat{H} - \omega\hat{J}_z$, where $\hat{J}_z$ is the z component of the angular momentum. The calculations at $\beta = 1$ for ^{20}Ne with $\Delta\beta = 0.125, 0.0625,$ and 0.03125 are shown in Fig. 8, where the convergence to the exact results can be seen. The moment of inertia fitted from the three sets of data are 5.10, 5.30, and 4.95, compared to 4.74, which is the value from the exact curve. In adding the term linear in J_z, we break the time reversal symmetry of $\hat{h}(\sigma)$, which is related to the sign properties of the weight function $\zeta(\sigma)$. $\langle\Phi\rangle$ decreases from 1 to 0.55 when ω is increased from 0 to 1.5 at $\Delta\beta = 0.125$ while it decreases from 1 to 0.52 at $\Delta\beta = 0.03125$.

Example 4: Response and strength functions for ^{20}Ne

Finally, we would like to obtain the imaginary-time response function and then reconstruct the strength functions. The calculation for ^{20}Ne is expansion method. The canonical ensemble is more suitable than the zero temperature formalism for measuring the dynamical response, because in the latter case many boundary time slices are needed to project out the ground state on both the left and the right, and extra time slices would have to be introduced in the middle to measure the response. In contrast, in the canonical ensemble, full use can be made of every time slice. We choose $\beta = 2.5$; from Fig. 6, the system has already reached the ground state at this low temperature. We calculate the response function at $\Delta\beta = 0.125$ and $\Delta\beta = 0.0625$ for the one-body operators, namely the isovector- and the isoscalar-quadrupole operator $Q_v = Q_p - Q_n, Q_s = Q_p + Q_n$, and the isovector and isoscalar

angular momentum operator $J_v = J_p - J_n, J_s = J_p + J_n$. We choose this particular 1^+ operator purely out of convenience. J_s is just the total angular momentum, which we verified to produce a constant zero response. The response functions are shown in a semi-log plot in Fig. 9(a,c,e). The response functions for these Hermitian operators are symmetric about $\tau = \beta/2$, so it is shown only up to $\tau = \beta/2$. The slope of the plot is approximately the energy of the dominant strength. The J_v and Q_v response relax more rapidly than the Q_s response, indicating that the two isovector operators connect to states with higher excitation energy than does the Q_s operator. Since ^{20}Ne has a $J = 0$, $T = 0$ ground state, the excited states connected by an operator will carry the same J and T quantum numbers as the operator. The plots are consistent with the fact that there is a low lying 2^+ state.

The MaxEnt reconstructions of the most probable strength function for the different one-body operators are shown in Fig. 9(b,d,e). The reconstruction is performed for each set of response functions measured at individual $\Delta\beta$ values. The figures show the convergence in $\Delta\beta$ of the resulting strength functions to the exact strength function. Note the movement of the peaks towards the exact position and also the decrease in the widths as $\Delta\beta$ decreases. The average n^{th} moments are found in the Monte Carlo integration of all the possible distributions of f_i. The n^{th}-moment of the strength function is defined by

$$M_n \equiv \sum_i \omega_i^n f(w_i) \,. \tag{6.10}$$

The errors are also determined in the Monte Carlo integration. The 1^{st} and 2^{2n} moment $\langle M_1 \rangle$ of the strength functions are listed in Table 1 for different operators and different $\Delta\beta$. The extrapolated moments ($\Delta\beta \to 0$) and the exact results for the ground state transitions are also shown.

The single-particle pick-up and stripping response functions for different orbitals are given in a semi-log plot in Fig. 10(a,c,e) and Fig. 11. The strength functions

extracted from these responses are related to the excitation spectrum in the neighboring nucleus with particle numbers differing from the original nucleus by one. The strength function is just the probability to find the nuclei at a certain final energy when the specified particle is added to or removed from the nucleus. The ground state of ^{20}Ne is isoscalar, therefore the stripping and pick-up responses are the same for protons and neutrons. The final states carry the same angular momentum as the single particle that is added or removed. We see from Fig. 10 that the pick-up and stripping responses for the $j = \frac{5}{2}$ orbital and also the pick-up response for the $j = \frac{1}{2}$ orbital converge to the exact results as $\Delta\beta$ tends to zero. The MaxEnt reconstruction of the corresponding strength functions in Fig. 10(b,d,e) also show a convergence to the exact results. The extracted moments are also listed in Table 1. The responses for the $j = \frac{3}{2}$ orbital show an anomalous behavior, starting close to the exact result at $\tau = 0$, and then, with a sudden change in slope, follow the responses of the $j = \frac{5}{2}$ orbital. A possible reason is that angular momentum is not strictly conserved in the calculation (not conserved in every sample). The $J = \frac{5}{2}$ states for ^{19}Ne and ^{20}Ne nuclei are much lower in energy than the $J = \frac{3}{2}$ states (because the $j = \frac{5}{2}$ orbital is lower than the $j = \frac{3}{2}$ orbital by 5.6 MeV). Therefore, if a small admixture of the $J = \frac{5}{2}$ states "leaks" into the intermediate states for the $j = 3/2$ response, it will dominate with an exponentially growing correlation function. (The $j = \frac{1}{2}$ orbital is much closer to the $j = \frac{5}{2}$ orbital in comparison, only higher by 0.8 MeV).

VII. THE SIGN PROBLEM AND FUTURE DEVELOPMENTS

We have seen in the examples above that the sign properties for the function $G(\sigma)\zeta(\sigma)$ are extremely important for the stability of the calculation, and may frustrate attempts to apply the Monte Carlo path integral to any general two-body interaction. In general, if we choose an arbitrary two-body interaction and arbitrarily decompose it via pair or density operators, $\langle\Phi\rangle \rightarrow 0$ quickly as β increases or as the number of time slices N_t increases at a fixed value of β. For example, with the Wildenthal interaction and for any calculation for $\beta > 1$ with more than three time slices, the noise due to the sign completely swamps the signal. This "sign-problem" is a well-known problem existing in auxiliary-field path-integral calculations [27] and quantum Monte Carlo for fermions in general. Generally, if there is no explicit symmetry to enforce the positivity of ζ_σ, $\langle\Phi\rangle$ decays exponentially as a function of β. The problem is more severe when using a finer resolution for $\Delta\beta$. Therefore, it is very difficult to calculate low-temperature properties. Only a handful of interacting fermion systems are known to give rise to positive definite path-integral: the one-dimensional Hubbard Model, the half-filled Hubbard Model, and the attractive Hubbard Model at any dimension and filling [3]. We will show in the following that an important class of interactions for the nuclear shell model has positive definite path-integral representation for even-even nuclei. This may serve as a starting point in understanding and controlling the 'sign problem'. It makes use of the symmetry between time-reversed single-particle orbitals to enforce the positivity of the path-integral.

We first introduce the 'time-reversed' partner of an operator. Define the time-reversed partner of the creation and annihilation operator to be

$$\tilde{a}_{j,m} \equiv a_{j,\bar{m}} = (-1)^{j+m} a_{j,-m} \tag{7.1a}$$

$$\tilde{a^\dagger}_{j,m} \equiv a^\dagger_{j,\bar{m}} = (-1)^{j+m} a^\dagger_{j,-m} \,. \tag{7.1b}$$

Note that

$$\tilde{\tilde{a}}_{j,m} = -a_{j,m} \tag{7.2}$$

due to the spin-half statistics.

The class of Hamiltonian found to give rise to positive-definite path integral possesses the form

$$\hat{H} = -\frac{1}{2}\sum_{\alpha} \chi_\alpha \rho_\alpha \tilde{\rho}_\alpha + e_\alpha \rho_\alpha + e^*_\alpha \tilde{\rho}_\alpha \tag{7.3}$$

where $\chi_\alpha > 0$, e_α can be generally complex, and ρ_α is a general density operator of the form

$$\rho_\alpha = \sum_{ij} C_{ij} a^\dagger_i a_j \ . \tag{7.4}$$

Note the requirement of a negative coupling constant for the density operator with its time-reversed partner and the time-reversal invariant form of the remaining one-body part.

For application to the shell model, we refer to Eq. (3.17), so that in the density decomposition,

$$\tilde{\rho}_{KM}(\alpha) = \rho_{K-M}(\alpha)(-1)^{K+M} \ . \tag{7.5}$$

The requirement of a negative coupling constant for the density operators leads to a sign rule for the $\lambda_{K\alpha}$, namely

$$\mathrm{Sign}(\lambda_{K\alpha}) = (-1)^{K+1} \ . \tag{7.6}$$

As we will show below, the Hamiltonian (7.3) gives rise to $\hat{h}(t)$ (in the action of the path-integral) symmetric in time-reversed orbitals. Time-reversed pairs of single-particle orbitals then pick up complex-conjugate phases in the propagation, guaranteering a positive definite overlap function ζ.

After the HS transformation on Eq. (7.3), the linearized Hamiltonian is

$$\hat{h} = \sum_{\alpha} \chi_{\alpha} ((\sigma_{\alpha} + i\tau_{\alpha})\rho_{\alpha} + (\sigma_{\alpha} - i\tau_{\alpha})\tilde{\rho}_{\alpha}) + e_{\alpha}\rho_{\alpha} + e^{*}_{\alpha}\tilde{\rho}_{\alpha} \, . \tag{7.7}$$

Therefore ρ and $\tilde{\rho}$ couple to complex-conjugate fields. (If some part of the coupling does not satisfy (7.6), then there will be terms in $\hat{h}$ that are of the form $i(\sigma_{\alpha}+i\tau_{\alpha})\rho_{\alpha}+ i(\sigma_{\alpha} - i\tau_{\alpha})\tilde{\rho}_{\alpha}$, and the above statement is not true.)

We represent the vector space in the single-particle wavefunction as

$$\begin{pmatrix} jm \\ j\bar{m} \end{pmatrix}, m > 0 \, , \tag{7.8}$$

with states with $m > 0$ in the first half of the vector and their time reversed orbitals in the second half. Due to Eq. (7.3) and the fact that time reversed operators are coupled to complex conjugate fields, the matrix $\mathbf{M}_i$ representing $\hat{h}_i$ has the following structure,

$$\mathbf{M}_i = \begin{pmatrix} \mathbf{A}_i & \mathbf{B}_i \\ -\mathbf{B}^{*}_i & \mathbf{A}^{*}_i \end{pmatrix} \, , \tag{7.9}$$

and one can easily verify that the total evolution matrix

$$\mathbf{U} = \prod_{i=1}^{N_t} \exp(-\mathbf{M}_i \Delta\beta) = \begin{pmatrix} \mathbf{P} & \mathbf{Q} \\ -\mathbf{Q}^{*} & \mathbf{P}^{*} \end{pmatrix} \, , \tag{7.10}$$

possesses the same structure, where $\mathbf{A}, \mathbf{B}, \mathbf{P}, \mathbf{Q}$ are matrices of dimension $N_s/2$. One can show that this matrix has pairs of complex conjugate eigenvalues ϵ, ϵ^{*} with eigenvectors $\begin{pmatrix} u \\ v \end{pmatrix}$ and $\begin{pmatrix} -v^{*} \\ u^{*} \end{pmatrix}$. In the case where ϵ is real, it is a double root since the two eigenvectors are distinct.

For the grand-canonical ensemble, the overlap function is given by

$$\zeta = \det[1 + \begin{pmatrix} \mathbf{P} & \mathbf{Q} \\ -\mathbf{Q}^{*} & \mathbf{P}^{*} \end{pmatrix}] = \prod_{i=1}^{N_s/2} (1 + \epsilon_i)(1 + \epsilon^{*}_i) > 0 \, . \tag{7.11}$$

If only particle-type (neutron-proton) conserving density operators are present in Eq. (7.3), wavefunctions are represented by separate Slater-determinants for the individual type. In this case, the individual matrix possesses the structure (7.9), and therefore $\zeta = \zeta_p \times \zeta_n > 0$, since $\zeta_p > 0$ and $\zeta_n > 0$.

In the zero-temperature formalism, if the trial wavefunction for an even number of particles is chosen to consist of time-reversed pairs of single-particle states,

$$\Psi_0 = \begin{pmatrix} \mathbf{a} & \mathbf{b} \\ -\mathbf{b}^* & \mathbf{a}^* \end{pmatrix} , \tag{7.12}$$

where $\mathbf{a}, \mathbf{b}$ are matrices with dimension $(\frac{N_s}{2} \times \frac{N_v}{2})$, then $\Psi_0^\dagger \mathbf{U} \Psi_0$ is a $N_v \times N_v$ matrix with the structure (7.10). Therefore, the overlap function

$$\zeta = \det[\Psi_0^\dagger \mathbf{U} \Psi_0] > 0 . \tag{7.13}$$

If only particle-type conserving operators are present, then with even-even nuclei, time-reversed pairs of trial wavefunctions can be chosen for both protons and neutrons, giving rise to $\zeta = \zeta_p \times \zeta_n > 0$. Notice that, while the overlap function is positive definite in the grand-canonical ensemble for any chemical potential and thus any average number of particles, it is only true for an even (or even-even if involving type-conserving decomposition) system in the zero-temperature formalism with a suitable trial wavefunction.

In the canonical ensemble for N particles, a fixed number trace is involved and therefore

$$\zeta \left(\prod_i \exp(-\mathbf{M}_i \Delta\beta) \right) = \sum_{i1 \neq i2 \neq \ldots i_N} \epsilon_{i1} \epsilon_{i2} \ldots \epsilon_{i_N} . \tag{7.14}$$

We have found empirically that ζ is positive definite for even-even system, although we lack a rigorous proof. A special case of the Hamiltonian (7.2) exists in which the overlap function is positive definite also for odd-odd $N = Z$ nuclei. The required condition is that only isoscalar-density operators are present in Eq. (7.2). This leads to a further symmetry that protons and neutrons couple to the same field in Eq. (7.7). Therefore, the evolution matrices $\mathbf{U_p} = \mathbf{U_n} \equiv \mathbf{U}$. In the zero-temperature formalism, if we choose the trial wavefunction for proton and neutrons to be time reversed partners of each other, so that

$$\Psi_{0,p} = \begin{pmatrix} \mathbf{a} \\ \mathbf{b} \end{pmatrix}, \Psi_{0,n} = \begin{pmatrix} -\mathbf{b}^* \\ \mathbf{a}^* \end{pmatrix} \tag{7.15}$$

then

$$\begin{aligned} \zeta_p &= \det[\Psi_{0,p}^\dagger \mathbf{U} \Psi_{0,p}] \\ &= \det[\mathbf{a}^\dagger \mathbf{P}\ \mathbf{a} + \mathbf{a}^\dagger \mathbf{Q}\ \mathbf{b} - \mathbf{b}^\dagger \mathbf{Q}^* \mathbf{a} + \mathbf{b}^\dagger \mathbf{P}^* \mathbf{b}] = \zeta_n^* \,. \end{aligned} \tag{7.16}$$

Therefore $\zeta = \zeta_p \times \zeta_n > 0$. On the other hand, for the canonical ensemble, one can prove that Eq. (7.13) is real. Given that $\zeta_n = \zeta_p$, ζ is a square and, therefore, is positive.

For a system with general form (7.3), if we use the integration of real coherent states to sum the canonical trace, then there is an extra operator $\exp(X_{ph} a_p^\dagger a_h)$ multiplying the evolution operator. Time-reversed states couple to different real fields in the extra operator, and a sign problem arises as seen in Example 3.

Cranking also causes the sign to deviate from unity. In cranking, the Lagrange multiplier term ωJ_z is added to $\hat{h}$ in Eq. (7.7), destroying the property that time-reversed operators will be coupled to complex-conjugate numbers (because $\tilde{J}_z = -J_z$). Notice, however, that cranking with an imaginary Lagrange multiplier $i\omega J_z$ observe the time reversed symmetry and will give rise to positive path-integral.

In summary, for system (7.3), the above proof guarantees the overlap function to be positive for any nuclei in the grand canonical ensemble, and for even-even nuclei in either the canonical ensemble or zero-temperature formalism (with suitable trial wavefunction). It also guarantees the positivity for odd-odd $N = Z$ system when only isoscalar density operators are involved.

The Hamiltonian (6.7) satisfies (7.6) upon transformation of the paring interaction to density coupling, and involves only isoscalar operators. Therefore, ζ is positive for even-even and $N = Z$ nuclei. For other systems, $\langle \Phi \rangle$ decreases as a function of β. At $\Delta\beta = 0.0625$, $\langle \Phi \rangle = 0.4$ at $\beta = 1.5$ for ^{24}Na and $\langle \Phi \rangle = 0.2$ at $\beta = 2.0$ for ^{23}Na.

The sign properties of (6.7) even for odd A nuclei are still much better than that of a general interaction violating criteria (7.6). For example, using the Wildenthal interaction, $\langle\Phi\rangle$ drops to several percent at $\beta = 1$ for any nucleus.

Arbitrary two-body interactions do not satisfy the sign rule (7.6). When the rule is violated, $\langle\Phi\rangle$ rapidly decreases as a function of β. Note that monopole pairing plays an important role here. The pairing interaction can be written as

$$-g\sum_{ij} a_i^\dagger a_j \tilde{a}^\dagger{}_i \tilde{a}_j \ . \tag{7.17}$$

It produces a constant shift in every χ_i in Eq. (7.3). It may be seen also from the multipole decomposition of the pairing force, which is

$$-g\sum_{\alpha}(-1)^K \rho_{KM}(\alpha)\rho_{K-M}(\alpha)(-1)^M \ . \tag{7.18}$$

Therefore, if pairing interaction is strong enough compared to the remaining interactions, the sign rule can be satisfied.

VIII. CONCLUSION

We have developed a general framework for carrying out auxiliary-field Monte Carlo calculations on the nuclear shell model. In this framework we evaluate ground state or thermal observables, using pairing or density fields or both.

Although the use of pairing fields naturally encompasses important physics, these calculations are more difficult due to the larger matrix dimension needed and the extra effort to keep track of the sign of the overlap function as the wavefunction is propagated. Furthermore, for calculations with multiple time slices, the Monte Carlo method with pairing fields suffers from severe sign problem. The use of pairing fields is suitable for carrying out static path or two-time-slice calulations where the linearized Hamiltonian is Hermitian, thereby enforcing the positivity of the overlap

function. This can be easily verified by observing that for Hermitian $\hat{h}, \hat{h}_a$, and $\hat{h}_b$, with real eigenvalues E_i, E_{i_a} and E_{i_b},

$$\hat{\mathrm{Tr}}[e^{-\beta\hat{h}}] = \sum_i e^{-\beta E_i} > 0, \tag{8.1}$$

and

$$\hat{\mathrm{Tr}}[e^{-\frac{\beta}{2}\hat{h}_a} e^{-\frac{\beta}{2}\hat{h}_b}] = \sum_{i_a} e^{-\frac{\beta}{2}E_{i_a}} \langle i_a | e^{-\frac{\beta}{2}\hat{h}_b} | i_a \rangle > 0. \tag{8.2}$$

In these cases, there is no sign problem and also there is no need to keep track of the evolution of the sign.

For the density decomposition, we have found a class of interactions which give rise to a positive definite integrand upon the HS transformation. For these interactions, stable calculations can be carried out for many time slices to extrapolate ($\Delta\beta \rightarrow 0$) exact results. This class of interactions includes phenomenological pairing plus multipole interaction which is widely used in studying nuclei. We have carried out calculations with this type of interactions in the *s-d* shell, demonstrating the power of the method in calculating both ground state and finite temperature, and both static and dynamical properties. High-spin nuclei were also studied by cranking. The calculations converge to the exact results (as found by direct diagonalization) with increasing number of time slices. Although the nuclear wavefunction is not explicitly found in these calculations, many nuclear properties can be obtained.

For general interactions in the shell model, it appears that the sign or phase property of the integrand is the major controlling factor to the successful application of the Monte Carlo sampling. Successful calculations are usually confined to high temperature studies. We have demonstrated the freedom one has in the decomposition scheme of the two body interaction and found that the behavior of the sign can be different in the various schemes. The next crucial step is to explore whether we can manipulate these degrees of freedom to enable stable calculations of nuclei using general forces.

APPENDIX A: FORMULAE FOR OVERLAP IN THE PRESENCE OF PAIRING FIELDS

We consider operators of the form

$$\hat{U} = \exp(-\Delta\beta\hat{h}_{N_t})\exp(-\Delta\beta\hat{h}_{N_t-1})...\exp(-\Delta\beta\hat{h}_1) \tag{A1}$$

where each $\hat{h}_t$ is a quadratic operator

$$\hat{h}_t = \sum_{i,j=1}^{N_s} \Theta(t)_{ij}a_i^\dagger a_j + \Delta(t)_{ij}a_i^\dagger a_j^\dagger + \Lambda(t)_{ij}a_i a_j. \tag{A2}$$

Here $a_i, a_i^\dagger$ are the fermion anihilation and creation operators. N_t is the total number of time-slices ($\Delta\beta = \beta/N_t$), and N_s is the total number of (m-scheme) single particle states. Without loss of generality, we choose Δ, Λ to be anti-symmetric ($\Delta = -\Delta^T$ etc.). We follow the development of Berezin [21], who considered the special case $\hat{U} = \exp(-i\hat{h}t)$ with $\hat{h}$ Hermitian; we take the general case.

We calculate the grand-canonical trace

$$\hat{\mathrm{Tr}}\hat{U} = \sum_i \langle i|\hat{U}|i\rangle \tag{A3}$$

(the sum is over all states of all particle number) by using the fermion coherent state (FCS) representation of unity, [28]

$$1 = \int \prod_\alpha d\xi_\alpha d\xi_\alpha^* \exp(-\sum_\alpha \xi_\alpha^*\xi_\alpha)|\xi\rangle\langle\xi|. \tag{A4}$$

Here ξ_α are Grassman varibles and the $|\xi\rangle$ are fermion coherent states. Then

$$\hat{\mathrm{Tr}}\hat{U} = \int \prod_\alpha d\xi_\alpha d\xi_\alpha^* \exp(-\sum_\alpha \xi_\alpha^*\xi_\alpha)\langle\xi|\hat{U}|\xi\rangle. \tag{A5}$$

We need the FCS representation of $\hat{U}$. In what immediately follows we show that if U is the matrix representation of $\hat{U}$, that is

$$\mathbf{U} \equiv \begin{pmatrix} \mathbf{U^{11}} & \mathbf{U^{12}} \\ \mathbf{U^{21}} & \mathbf{U^{22}} \end{pmatrix} \tag{A6a}$$

$$\equiv \exp(-\mathrm{M}(N_t)\Delta\beta)\exp(-\mathrm{M}(N_t-1)\Delta\beta)...\exp(-\mathrm{M}(1)\Delta\beta), \tag{A6b}$$

where

$$\mathrm{M}(t) \equiv \begin{pmatrix} \Theta(t) & 2\Delta(t) \\ 2\Lambda(t) & -\Theta^T(t) \end{pmatrix}, \tag{A7}$$

then

$$\langle\xi|\hat{U}|\xi\rangle = C\exp\left(\frac{1}{2}(\xi \quad \xi^*)\begin{pmatrix} \mathbf{B^{11}} & \mathbf{B^{12}} \\ \mathbf{B^{21}} & \mathbf{B^{22}} \end{pmatrix}\begin{pmatrix} \xi \\ \xi^* \end{pmatrix}\right) \tag{A8}$$

with

$$\mathbf{B^{11}} = \mathbf{U^{22^{-1}}U^{21}}, \quad \mathbf{B^{12}} = -\mathbf{U^{22^{-1}}} \tag{A9a}$$

$$\mathbf{B^{21}} = (\mathbf{U^{22^{-1}}})^T, \quad \mathbf{B^{22}} = \mathbf{U^{12}U^{22^{-1}}} \tag{A9b}$$

and

$$C = \det(\mathbf{U^{22}})^{\frac{1}{2}}\exp(-\frac{\Delta\beta}{2}\sum_{n=1}^{N_t}\mathrm{Tr}\Theta(n)). \tag{A10}$$

In this case the trace becomes a Gaussian integral over Grassman variables; the result is given beginning with equation (A29) below. Before coming to that point we must derive equations (A8-A10).

Towards this end we employ the standard rules for operating on $|\xi\rangle, \langle\xi|$ with $a^\dagger, a$:

$$\langle\xi|\hat{U}\hat{a_\alpha}|\xi\rangle = \langle\xi|\hat{U}|\xi\rangle\xi_\alpha \tag{A11a}$$

$$\langle\xi|\hat{U}a_\alpha^\dagger|\xi\rangle = \langle\xi|\hat{U}|\xi\rangle\frac{\overleftarrow{\partial}}{\partial\xi_\alpha} \tag{A11b}$$

$$\langle\xi|a_\alpha^\dagger\hat{U}|\xi\rangle = \xi_\alpha^*\langle\xi|\hat{U}|\xi\rangle \tag{A11c}$$

$$\langle\xi|a_\alpha\hat{U}|\xi\rangle = \frac{\partial}{\partial\xi^*_\alpha}\langle\xi|\hat{U}|\xi\rangle. \tag{A11d}$$

Next, we derive expressions for $a_\alpha\hat{U}, a^\dagger_\alpha\hat{U}$, as linear combinations of $\hat{U}a_\alpha, \hat{U}a^\dagger_\alpha$. Then, with the ansatz (A8) of $\langle\xi|\hat{U}|\xi\rangle$ as a Gaussian in the Grassman variables ξ, ξ^*, we use (A11) to derive the elements **B** of the Gaussian given in (A9).

To do this, we introduce the operators b, $\bar{b}$ (which are not necessarily Hermitian conjugates)

$$b_\alpha \equiv \hat{U}^{-1}a_\alpha\hat{U}, \quad \bar{b}_\alpha \equiv \hat{U}^{-1}a^\dagger\hat{U}. \tag{A12a}$$

Then

$$a_\alpha\hat{U} = \hat{U}b_\alpha, \quad a^\dagger_\alpha\hat{U} = \hat{U}\bar{b}_\alpha, \tag{A12b}$$

and we want to find $b, \bar{b}$ as linear combinations of $a^\dagger, a$.

Define

$$a_\alpha(\tau) = e^{\hat{h}\tau}a_\alpha e^{-\hat{h}\tau}. \tag{A13}$$

Then

$$\frac{d}{d\tau}a_\alpha(\tau) = [\hat{h}, a_\alpha(\tau)], \tag{A14}$$

and similarly for $a^\dagger_\alpha(\tau)$. Putting all the $a_\alpha(\tau), a^\dagger_\alpha(\tau)$ into a single vector, and using the representaion (A2) for $\hat{h}$, one finds

$$\frac{d}{d\tau}\begin{pmatrix} a(\tau) \\ a^\dagger(\tau) \end{pmatrix} = -\mathbf{M}\begin{pmatrix} a_(\tau) \\ a^\dagger(\tau) \end{pmatrix} \tag{A15}$$

with **M** given by (A7).

Solving the differential equation (A15),

$$\begin{pmatrix} a(\tau) \\ a^\dagger(\tau) \end{pmatrix} = \exp(-\mathbf{M}\tau)\begin{pmatrix} a \\ a^\dagger \end{pmatrix}. \tag{A16}$$

and so in general

$$\begin{aligned}\begin{pmatrix} b \\ \bar{b} \end{pmatrix} &= \exp(\Delta\beta\hat{h}_1)\ldots\exp(\Delta\beta\hat{h}_{N_t})\begin{pmatrix} a \\ a^\dagger \end{pmatrix}\exp(-\Delta\beta\hat{h}_{N_t})\ldots\exp(-\Delta\beta\hat{h}_1) \\ &= \exp(-\Delta\beta\mathbf{M}_1)\ldots\exp(-\Delta\beta\mathbf{M}_{N_t})\begin{pmatrix} a \\ a^\dagger \end{pmatrix} \\ &= \begin{pmatrix} \mathbf{U}^{11} & \mathbf{U}^{12} \\ \mathbf{U}^{21} & \mathbf{U}^{22} \end{pmatrix}\begin{pmatrix} a \\ a^\dagger \end{pmatrix}. \end{aligned} \tag{A17}$$

Then clearly (with implicit summation on γ),

$$b_\alpha = \mathbf{U}^{11}{}_{\alpha\gamma}a_\gamma + \mathbf{U}^{12}{}_{\alpha\gamma}a^\dagger_\gamma \tag{A18a}$$

$$\bar{b}_\alpha = \mathbf{U}^{21}{}_{\alpha\gamma}a_\gamma + \mathbf{U}^{22}{}_{\alpha\gamma}a^\dagger_\gamma. \tag{A18b}$$

Inserting (A18) in (A12b), and using the ansatz (A8), one can straightforwardly derive the **B**'s in terms of the **U**'s as given in (A9).

Although we do not show it in detail, we note that **B** is antisymmetric ($\mathbf{B}^{11^T} = -\mathbf{B}^{11}, \mathbf{B}^{21^T} = -\mathbf{B}^{12}$, etc.); which can be proved using

$$\begin{pmatrix} \mathbf{0} & \mathbf{1} \\ \mathbf{1} & \mathbf{0} \end{pmatrix}\mathbf{M}\begin{pmatrix} \mathbf{0} & \mathbf{1} \\ \mathbf{1} & \mathbf{0} \end{pmatrix} = -\mathbf{M}^T \tag{A19}$$

and

$$\begin{pmatrix} \mathbf{0} & \mathbf{1} \\ \mathbf{1} & \mathbf{0} \end{pmatrix}\mathbf{U}\begin{pmatrix} \mathbf{0} & \mathbf{1} \\ \mathbf{1} & \mathbf{0} \end{pmatrix} = (\mathbf{U}^{-1})^T. \tag{A20}$$

Now we must show the normalization C is of the form (A10). To do this, we find a differential equation for C. Letting

$$\hat{U}_{n+1} = \exp(-\Delta\beta\hat{h}_{n+1})\hat{U}_n \tag{A21}$$

we define

$$\hat{U}_n(t) = \exp(-t\hat{h}_{n+1})\hat{U}_n \tag{A22}$$

(so $\hat{U}_{n+1} = \hat{U}_n(\Delta\beta)$). Taking the expectation value of (A22) between FCS's, invoking (A11) and equating the parts independent of ξ, ξ^*, one obtains,

$$\frac{d}{dt}\ln C_n(t) = -\mathrm{Tr}\left(\Lambda(n+1)\mathbf{B}^{22}{}_n(t)\right). \tag{A23}$$

If one differentiates (A10), one obtains

$$\frac{d}{dt}\ln\text{“}C_n(t)\text{”} = \frac{1}{2}\mathrm{Tr}\frac{d}{dt}\ln\mathbf{U}^{22}{}_n(t) - \frac{1}{2}\mathrm{Tr}\Theta_{n+1}. \tag{A24}$$

Using $\mathbf{U}_n(t) = \exp(-\mathbf{M}_{n+1}t)\mathbf{U}_n$, one arrives at

$$\frac{d}{dt}\mathbf{U}^{22}{}_n = -2\Lambda_{n+1}\mathbf{U}^{12}{}_n + \Theta^T_{n+1}\mathbf{U}^{22} \tag{A25}$$

and (A24) becomes (A23). Thus the expression (A10) satisfies the differential equation for C. The only thing left is the overall normalization. This is found by choosing $\mathbf{M} = 0$ so that $\hat{U} = 1, C = 1$, then

$$\langle\xi|\hat{U}|\xi\rangle = \exp(-\sum_\alpha \xi^*_\alpha\xi_\alpha) \tag{A26}$$

which is $\langle\xi|\xi\rangle$. Thus we have established the form (A8) for $\langle\xi|\hat{U}|\xi\rangle$.

The integral (A5) is straightforward (see Berezin [21]; the magnitude is

$$\hat{\mathrm{T}}\mathrm{r}\hat{U} = C\det\begin{pmatrix} \mathbf{B^{11}} & \mathbf{B^{12}} - \mathbf{1} \\ \mathbf{B^{21}} + \mathbf{1} & \mathbf{B^{22}} \end{pmatrix}^{\frac{1}{2}}. \tag{A27}$$

The phase of $\hat{\mathrm{T}}\mathrm{r}\hat{U}$, though critical, is more difficult to obtain; see Appendix B for details.

One can rewrite (A27) into a compact form. The constant C contains the factor $\det(\mathbf{S^{22}})^{\frac{1}{2}}$, which can be written using

$$\det\mathbf{U^{22}} = \det\begin{pmatrix} \mathbf{U^{22}} & \mathbf{U^{12}} \\ \mathbf{0} & \mathbf{1} \end{pmatrix} = \det\begin{pmatrix} \mathbf{U^{12}}^T & \mathbf{U^{22}}^T \\ \mathbf{1} & \mathbf{0} \end{pmatrix}(-1)^{N_s{}^2}. \tag{A28}$$

Then, introducing (A28), into (A27), after some algebra and using relationships from (A20) one arrives at

$$\hat{\mathrm{T}}\mathrm{r}\hat{U} = \det(1+\mathbf{U})^{\frac{1}{2}} \exp(-\frac{\Delta\beta}{2}\mathrm{Tr}\sum_{n=1}^{N_t}\Theta(n)) \tag{A29}$$

(where, again, U is the matrix in (A6) representing the evolution operator $\hat{U}$).

As for the density case, one can introduce a fugacity expansion to project out exact particle number: take

$$\hat{\mathrm{T}}\mathrm{r}(\lambda^{\hat{N}}\hat{U}) = \det(1+\begin{pmatrix}\lambda & 0\\ 0 & \frac{1}{\lambda}\end{pmatrix}\mathbf{U})^{\frac{1}{2}} \exp\left(-\frac{\Delta\beta}{2}\sum_{n=1}^{N_t}\mathrm{Tr}\Theta(n)\right)\lambda^{N_s/2}. \tag{A30}$$

Because the matrices $\mathbf{1}, \mathbf{U}$ are of dimension $2N_s \times 2N_s$, one can write $\lambda^{N_s/2} = \det\begin{pmatrix}1 & 0\\ 0 & \lambda\end{pmatrix}^{\frac{1}{2}}$ and (A30) becomes

$$\det\left(\begin{pmatrix}1 & 0\\ 0 & \lambda\end{pmatrix} + \begin{pmatrix}\lambda & 0\\ 0 & 1\end{pmatrix}\mathbf{U}\right)^{\frac{1}{2}} \times \exp\left(-\frac{\Delta\beta}{2}\sum_{n=1}^{N_t}\mathrm{Tr}\Theta(n)\right). \tag{A31}$$

This can be expanded into a polynomial in λ, which then gives the canonical ensemble.

Finally, we give the expectation value of $\langle\psi_t|\hat{U}|\psi_t\rangle$. First we note that the vacuum expection value $\langle 0|\hat{U}|0\rangle$ is the term in (A31) independent of λ, which clearly is

$$\begin{aligned}\langle 0|\hat{U}|0\rangle &= \det\begin{pmatrix}1 & 0\\ 0 & \mathbf{U}^{22}\end{pmatrix}^{\frac{1}{2}} \exp\left(-\frac{\Delta\beta}{2}\sum_n \mathrm{Tr}\Theta(n)\right)\\ &= \det\left((0\quad 1)\,\mathbf{U}\begin{pmatrix}0\\ 1\end{pmatrix}\right)^{\frac{1}{2}} \exp\left(-\frac{\Delta\beta}{2}\sum_n \mathrm{Tr}\Theta(n)\right).\end{aligned} \tag{A32}$$

Any quasi-particle excitations can be represented as Hatree-Fock Bogoliubov vacua for properly defined new quasi-particle opertors. That corresponds to doing a similarity transformation on the matrices. If $|\psi_t\rangle$ is the vacuum to the quasi-particle annihilation operator β_i, i.e.,

$$\beta_i|\psi_t\rangle = 0, \quad \beta_i = \mathbf{u}_{ij}a_j + \mathbf{v}_{ij}a_j^\dagger, \tag{A33}$$

then

$$\langle\psi_t|\hat{U}|\psi_t\rangle$$
$$= \det\left(\begin{pmatrix} 0 & 1 \end{pmatrix} \begin{pmatrix} \mathbf{u} & \mathbf{v} \\ \mathbf{v}^* & \mathbf{u}^* \end{pmatrix} \mathbf{U} \begin{pmatrix} \mathbf{u}^\dagger & \mathbf{v}^T \\ \mathbf{v}^\dagger & \mathbf{u}^T \end{pmatrix} \begin{pmatrix} 0 \\ 1 \end{pmatrix} \right) \times \exp\left(-\frac{\Delta\beta}{2} \sum_n \mathrm{Tr}\Theta(n) \right)$$
$$= \det\left(\begin{pmatrix} \mathbf{v}^* & \mathbf{u}^* \end{pmatrix} \mathbf{U} \begin{pmatrix} \mathbf{v}^T \\ \mathbf{u}^T \end{pmatrix} \right)^{\frac{1}{2}} \exp\left(-\frac{\Delta\beta}{2} \sum_n \mathrm{Tr}\Theta(n) \right). \qquad \text{(A34)}$$

APPENDIX B: FINDING THE SIGN OF OVERLAP IN PRESENCE OF PAIRING FIELDS

The formulae for calculating the overlap $\zeta_\sigma(\beta) = \langle\psi_L|\hat{U}(\beta,0;\sigma)|\psi_R\rangle$ in the zero-temperature formalism, $\hat{\mathrm{Tr}}[\hat{U}_\sigma(\beta,0)]$ in the thermal formalisms, all involve the square root of a determinant, leaving the phase of $\zeta_\sigma(\beta)$ undeterminted by a factor of ± 1. This ambiguity is irrelevant for the Monte Carlo random walk inasmuch as we typically take $|\zeta|$ as the weight function, but the phase must be known unambiguously for calculation of observables as important cancellations may result.

We determine the phase by following the evolution of $\zeta_\sigma(\tau)$ and its derviatives with respect to τ as τ goes from 0 to β. For example, if $\zeta_\sigma(\tau)$ were purely real, zero-crossing (with $\zeta'(\tau) \neq 0$) would indicate a change in the phase by -1. The initial phase at $\tau = 0$ is positive and real. Following the evolution is computationally expensive, but as most of the time is spent on the random walk, where the phase is irrelevant, the overall computational time is negligible.

In what follows we give the formulae for up to fourth derivatives for each of the different formalisms.

Grand-canonical ensemble

Define

$$f(t) = \zeta_\sigma(k\Delta\beta + t) = \hat{\mathrm{Tr}}[e^{-h_{k+1}t}\hat{U}_\sigma(k\Delta\beta, 0)], \qquad \text{(B1)}$$

then

$$f(t) = \det[1 + e^{-\mathbf{M}_{k+1}t}\mathbf{U}]^{\frac{1}{2}} \exp(-\frac{\Delta\beta}{2}\sum_{i=1}^{k}\mathrm{Tr}[\Theta_i] - \frac{t}{2}\mathrm{Tr}[\Theta_{k+1}]) \tag{B2}$$

$$\ln(f) = \frac{1}{2}\mathrm{Tr}[\ln(1 + e^{-\mathbf{M}_{k+1}t}\mathbf{U})] - \frac{\Delta\beta}{2}\sum_{i=1}^{k}\mathrm{Tr}[\Theta_i] - \frac{t}{2}\mathrm{Tr}[\Theta_{k+1}]. \tag{B3}$$

Using the abbreviation $\mathbf{M} = \mathbf{M}_{k+1}, \Theta = \Theta_{k+1}$, let

$$\mathbf{G} = (1 + e^{-\mathbf{M}t}\mathbf{U})^{-1}e^{-\mathbf{M}t}\mathbf{U} = 1 - (1 + e^{-\mathbf{M}t}\mathbf{U})^{-1}, \tag{B4}$$

$$\begin{aligned}\frac{\partial \mathbf{G}}{\partial t} &= -[1 + e^{-\mathbf{M}t}\mathbf{U}]^{-1}\mathbf{M}e^{-\mathbf{M}t}\mathbf{U}[1 + e^{-\mathbf{M}t}\mathbf{U}]^{-1} \\ &= -(\mathbf{1} - \mathbf{G})\mathbf{M}\mathbf{G}.\end{aligned} \tag{B5}$$

The derivatives of $\ln(f)$ can be expressed in terms of the matrices $\mathbf{G}$ and $\mathbf{M}$,

$$g_1 = \frac{\partial \ln(f)}{\partial t} = -\frac{1}{2}\mathrm{Tr}[\mathbf{M}\mathbf{G}] - \frac{1}{2}\mathrm{Tr}[\Theta] \tag{B6}$$

$$g_2 = \frac{\partial^2 \ln(f)}{\partial t^2} = \frac{1}{2}\mathrm{Tr}[\mathbf{M}(\mathbf{1} - \mathbf{G})\mathbf{M}\mathbf{G}] \tag{B7}$$

$$g_3 = \frac{\partial^3 \ln(f)}{\partial t^3} == -\frac{1}{2}\mathrm{Tr}[\mathbf{M}\mathbf{G}\mathbf{M}(\mathbf{1} - \mathbf{G})\mathbf{M}(\mathbf{1} - \mathbf{2G})] \tag{B8}$$

$$\begin{aligned}g_4 &= \frac{\partial^4 \ln(f)}{\partial t^4} \\ &= -\frac{1}{2}\mathrm{Tr}[\mathbf{M}(\mathbf{1} - \mathbf{G})\mathbf{M}\mathbf{G}\mathbf{M}(\mathbf{1} - \mathbf{G})\mathbf{M}(\mathbf{1} - \mathbf{2G})] \\ &\quad -\frac{1}{2}\mathrm{Tr}[\mathbf{M}\mathbf{G}\mathbf{M}(\mathbf{1} - \mathbf{G})\mathbf{M}\mathbf{G}\mathbf{M}(\mathbf{1} - \mathbf{2G})] \\ &\quad -\mathrm{Tr}[\mathbf{G}\mathbf{M}(\mathbf{1} - \mathbf{G})\mathbf{M}(\mathbf{1} - \mathbf{G})\mathbf{M}\mathbf{G}\mathbf{M}]\end{aligned} \tag{B9}$$

Then $\zeta_\sigma(k\Delta\beta + t)$ is given by,

$$\zeta_\sigma(k\Delta\beta + t) = f(t) = f(0)\exp\left(g_1 t + g_2\frac{t^2}{2!} + g_3\frac{t^3}{3!} + g_4\frac{t^4}{4!} + \ldots\right). \tag{B10}$$

Zero temperature formalism

In this case

$$f(t) = \zeta_\sigma(k\Delta\beta + t) =< \psi_t|e^{-\hat{h}_{k+1}t}\hat{U}(k\Delta\beta, 0; \sigma)|\psi_t >=< \psi_L|e^{-\hat{h}_{k+1}t}|\psi_R > \quad \text{(B11)}$$

$$f(t) = \det[\Psi_{\mathbf{L}}e^{-\mathbf{M}_{k+1}t}\Psi_{\mathbf{R}}]^{\frac{1}{2}}e^{-\frac{\Delta\beta}{2}\sum_{i=1}^{k}\mathrm{Tr}[\Theta_i]-\frac{t}{2}\mathrm{Tr}[\Theta_{k+1}])} \quad \text{(B12)}$$

$$\ln(f) = \frac{1}{2}\mathrm{Tr}[\ln(\Psi_{\mathbf{L}}e^{-\mathbf{M}_{k+1}t}\Psi_{\mathbf{R}})] - \frac{\Delta\beta}{2}\sum_{i=1}^{k}\mathrm{Tr}[\Theta_i] - \frac{t}{2}\mathrm{Tr}[\Theta_{k+1}] \quad \text{(B13)}$$

So let $\mathbf{M} = \mathbf{M}_{k+1}, \Theta = \Theta_{k+1}$, and let

$$\mathbf{G} = e^{-\mathbf{M}t}\Psi_{\mathbf{R}}[\Psi_{\mathbf{L}}e^{-\mathbf{M}t}\Psi_{\mathbf{R}}]^{-1}\Psi_{\mathbf{L}} \quad \text{(B14)}$$

$$\begin{aligned}\frac{\partial \mathbf{G}}{\partial t} &= e^{-\mathbf{M}t}\Psi_{\mathbf{R}}[\Psi_{\mathbf{L}}e^{-\mathbf{M}t}\Psi_{\mathbf{R}}]^{-1}\Psi_{\mathbf{L}}\mathbf{M}e^{-\mathbf{M}t}\Psi_{\mathbf{R}}[\Psi_{\mathbf{L}}e^{-\mathbf{M}t}\Psi_{\mathbf{R}}]^{-1}\Psi_{\mathbf{L}} \\ &\quad -\mathbf{M}e^{-\mathbf{M}t}\Psi_{\mathbf{R}}[\Psi_{\mathbf{L}}e^{-\mathbf{M}t}\Psi_{\mathbf{R}}]^{-1}\Psi_{\mathbf{L}} \\ &= \mathbf{GMG} - \mathbf{MG} = -(\mathbf{1} - \mathbf{G})\mathbf{MG}. \end{aligned} \quad \text{(B15)}$$

Then

$$g_1 = \frac{\partial \ln(f)}{\partial t} = -\frac{1}{2}\mathrm{Tr}[\mathbf{MG}] - \frac{1}{2}\mathrm{Tr}[\Theta], \quad \text{(B16)}$$

and so on; all formulae are the same as in the grand canonical ensemble (B6-9), except that the matrix **G** now has a different expression. In fact, in both cases **G** can be shown to be the matrix for Green's function, i.e.,

$$\mathbf{G}_{ij} =< \alpha_j^\dagger \alpha_i > \quad \text{(B17)}$$

where

$$\alpha_i = a_i, i = 1, ..., Ns \quad \text{(B18a)}$$

$$\alpha_{i+N_s} = a_i^\dagger, i = 1, ..., Ns. \quad \text{(B18b)}$$

Canonical ensemble

In Eq. (4.35), the undetermined sign only involves the vacuum expectation of the ITEO $< 0|\hat{U}(\beta,0)|0 >$. Once it is determined, the sign for $\hat{\mathrm{Tr}}[\hat{U}(\beta,0)]$ is known. We can use the equations for the zero temperature formalism to obtain the sign of $< 0|\hat{U}(\beta,0)|0 >$.

APPENDIX C: MAXIMUM ENTROPY EXTRACTION OF STRENGTH FUNCTION

We use the Maximum entropy (MaxEnt) method to reconstruct the strength function from the response function. Here we briefly describe the Classic MaxEnt Method; details can be found from the paper by Gull [19].

The MaxEnt method is a Bayesian approach for reconstruction of postive additive images f from noisy data. In our case the image is the strength function $f(\omega)$. The noisy data are the measurement of the response function at discrete imaginary time $D_j = d_j + \eta_j$, where $d_j = R(j\Delta\beta)$ and η_j is the noise in the data. In the absence of any data, the most probable image is chosen to be a default model m. Skilling [18] proved that in the absence of any data, the only consistent choice of probability for image f is determined up to a parameter α,

$$pr(f) = \exp(\alpha S(f,m))/Z(\alpha,m) \tag{C1}$$

where S is the entropy of image f relative to the default model; if the image is discretized to $f_i, i = 1,...,r$,

$$S(f,m) = \sum_j (f_j - m_j - f_j \log(f_j/m_j)) \tag{C2}$$

$$Z_S(\alpha,m) = \int_0^\infty d^r f \prod f^{-\frac{1}{2}} \exp(\alpha S(f)) = \int_{-\infty}^\infty d^r u \ \exp(\alpha S(u^2)). \tag{C3}$$

The last step was obtained by a change of variable $u_i = \sqrt{f_i}$. (Z_S is in no relation to the partition function in the previous sections.)

In the presence of data, we gain some knowlege about the image. Assuming the Gaussian distribution of error in the data D_i, the probability for f is

$$pr(f) = \exp(\alpha S - \frac{1}{2}\chi^2(f))\frac{1}{Z_S}\frac{1}{Z_L} \tag{C4}$$

where

$$\chi^2(f) = \sum(d_i(f) - D_i)(d_j(f) - D_j)G^{-1}_{ij}, \tag{C5}$$

and $G_{ij} =< \eta_i\eta_j >$ is the matrix of correlation of the errors in the data.

$$Z_L = \int d^N D \exp(-\frac{1}{2}\chi^2(f)). \tag{C6}$$

For a given choice of α, the most probable image can be found by maximizing $\alpha S - \frac{1}{2}\chi^2$, giving rise to the term Maximum Entropy method. However, α is not predetermined. Usually, people vary the value of α until the χ^2 found at the maximum of $\alpha S - \frac{1}{2}\chi^2$ is approximately equal to the total number of data D_i. But this assignment of α is adhoc and, according to Gull [19], usually leads to underfitting of the data. In the classic MaxEnt, α is fixed by maximizing probability of α given the data set D_i and the default model m, which is

$$p(\alpha|D, m) \propto Z_Q Z_S^{-1} Z_L^{-1}, \tag{C7}$$

where

$$Z_Q = \int_0^\infty d^r f \prod f^{\frac{1}{2}} \exp(\alpha S - \frac{1}{2}\chi^2) = \int_{-\infty}^\infty d^r u \ \exp(\alpha S - \frac{1}{2}\chi^2). \tag{C8}$$

After α is fixed, we can obtain the most probable f by maximizing $\alpha S - \frac{1}{2}\chi^2$, or we can obtain the average of f by a Monte Carlo sampling of f using the integrand of (C4) as weight function. We can also obtain error information about f by the Monte Carlo

sampling. In our case, we would like to obtain, for example, the error in location of the peaks in f, or the errors in different moments of ω, $M_n = \int \tilde{f}(\omega)\omega^n d\omega / \int \tilde{f}(\omega)d\omega$.

Let us return to our case. First of all, since the imaginary time response function $R(\tau)$ is taken at discrete times, we can only allow a limited amount of parameters in the strength function $\tilde{f}$. We do that by discretizing $\tilde{f}(\omega)$ to f_i at ω_i. To allow for some smoothness, we choose a Gaussian function centered around each ω_i instead of a delta function . After we obtain the imaginary time response function, we determine the relevant range of ω in which the strength function is significant and then choose ω_{min} and ω_{max}. The ω_i are chosen to be evenly distributed between ω_{min} and ω_{max}. The number of f_n, n_ω, should not exceed the number of data D_i we have, which is the total number of time slices, Nt, in breaking up the imaginary time evolution operator. We choose the width in the Gaussian, $\Delta\omega$ to be half of the spacing between the ω_i's. For non-Hermitian operator $\hat{O}$, the strength function $f(\omega)$ is related to f_i by,

$$f(\omega) = \sum_i f_i \frac{1}{\Delta\omega\sqrt{2\pi}} \exp(-\frac{1}{2}(\omega - \omega_i)^2/\Delta\omega^2). \tag{C9}$$

For Hermitian operator $\hat{O}$, we have the property $f(-\omega) = e^{-\beta\omega} f(\omega)$ in the canonical ensemble. In that case we choose

$$f(\omega) = \sum_i f_i \exp(\frac{\beta}{2}(\omega - \omega_i)) \frac{1}{\Delta\omega\sqrt{2\pi}}$$
$$(\exp(-\frac{1}{2}(w - w_i)^2/\Delta\omega^2) + \exp(-\frac{1}{2}(\omega + \omega_i)^2/\Delta\omega^2)). \tag{C10}$$

The response $R(\tau)$ generated by $f(\omega)$ is,

for non-Hermitian operators,

$$R(\tau) = \sum_i f_i \exp(-\omega_i\tau + \frac{1}{2}\tau^2\Delta\omega^2) \tag{C11}$$

for Hermitian operators

$$R(\tau) = \sum_i f_i(\exp(-\tau\omega_i) + \exp(-(\beta - \tau)\omega_i)) \exp(\frac{1}{2}(\frac{\beta}{2} - \tau)^2\Delta\omega^2). \tag{C12}$$

We choose the default model m_i, $i = 1, ..., n_\omega$ to be constant . The normalization is fixed by fitting to the measured response function at zero time $R(0)$ which is related to the total strength. The data D_j is the value of $R(\tau)$ for $\tau = j\Delta\beta$ measured from the Monte Carlo sampling. The error correlation function can also be obtained.

To carry out the maximizing of function p in (C7) , we have to obtain the dependence of Z_S and Z_Q on α. To simplify the problem a little bit, Z_S is found by the saddle point approximation. $S(u^2, m)$ has the saddle point at $u_i^2 = m_i$ with the second derivatives $\frac{\partial S}{\partial u_i \partial u_j}|_{u_i^2 = m_i} = -4\delta_{ij}$, which leads to the approximate integral of S,

$$\int_{-\infty}^{\infty} d^r u \ \exp(\alpha S) \simeq \int_{-\infty}^{\infty} d^r u \ \exp(-2\alpha \sum_i u_i^2) = (\frac{\pi}{2\alpha})^{r/2} \tag{C13}$$

Therefore the the condition $\frac{\partial p}{\partial \alpha} = 0$ becomes

$$\frac{1}{Z_Q} \int_{-\infty}^{\infty} d^r u \ S \exp(\alpha S - \frac{1}{2}\chi^2) = \frac{1}{Z_S} \frac{\partial Z_S}{\partial \alpha} = -\frac{r}{2\alpha} \tag{C14}$$

where the average distribution f_i is given by,

$$< f_i >= \frac{1}{Z_Q} \int_{-\infty}^{\infty} d^r u \ f_i \exp(\alpha S - \frac{1}{2}\chi^2). \tag{C15}$$

We do these integrals by Monte Carlo sampling of u_i using $\exp(\alpha S - \frac{1}{2}\chi^2)$ as the weight function. The value α is determined by the self-consistent condition $< S >_\alpha = -\frac{r}{2\alpha}$. When α is found, the the average distribution $< f_i >=< u_i^2 >$ and the fluctuation $\delta f_i = \sqrt{< f_i^2 > - < f_i >^2}$ would also be given by the same Monte Carlo as in (C15).

REFERENCES

[1] A. Covello, ed., *Shell Model and Nuclear Structure: Where Do We Stand?*, 2nd International Spring Seminar on Nuclear Physics (World Scientific, 1988)

[2] M. Cyrot, Physica, **91B**, 141 (1977); and references therein

[3] Review article by W. von der Linden, Phys. Rep. **220** , 53(1992) and references therein.

[4] M. H. Kalos, D. Levesque and L. Verlet, Phys. Rev. **A 9**, 2178 (1974); P.A. Whitlock, M. H. Kalos, G. V. Chester and D. M. Ceperley, Phys. Rev. **B 19**, 5598 (1978); D. Ceperley and M. H. Kalo, Quantum Many-Body Physics in *Monte-Carlo Methods in Statistical Physics*, K. Binder, ed. (Springer-Verlag, N.Y. 1979)

[5] S. E. Koonin, G. Sugiyama, and H. Friederich, *Proc. Int. Symp. Bad Honnef* (Springer, Heidelberg, 1982); G. Sugiyama and S. E. Koonin, Annals of Phys. **168**, 1 (1986).

[6] R. D. Lawson, *Theory of the Nuclear Shell Model*, Clarendon Press, Oxford (1980)

[7] T.-S.H. Lee and R. B. Wiringa, ed., *The Nuclear Shell Model*, North Holland (1990)

[8] M. G. Mayer and J. Hans D. Jensen, *Elementary Theory of Nuclear Shell Structure*, John Wiley & Sons, Inc., New York (1955)

[9] F. Iachello and A. Arima, *The Interacting Boson Model*, Cambridge University Press, Cambridge (1987)

[10] B. H. Wildenthal, Prog. Part. Nucl. Phys. **11** (1984)

[11] B. H. Wildenthal, in *Shell Model and Nuclear Structure: Where Do We Stand?*, 2nd International Spring Seminar on Nuclear Physics, edited by A. Covello

(World Scientific, 1988)

[12] J. Hubbard, Phys. Lett. **3**, 77 (1959); R. D. Stratonovich, Dokl. Akad. Nauk., SSSR **115**, 1907 (1957) [transl: Soviet Phys. Kokl. **2**, 416 (1958)].

[13] P. Arve, G. Bertsch, B. Lauritzen, and G. Puddu, Annals of Phys. **183**, 309 (1988); B. Lauritzen and G. Bertsch, Phys. Rev. **C39**, 2412 (1989); B. Lauritzen, P. Arve, and G. F. Bertsch, Phys. Rev. Lett. **61**, 2835 (1988); Y. Alhassid and B. W. Bush, Nucl. Phys. **A549**, 43 (1992).

[14] G. Puddu, P. F. Bortignon, R. A. Broglia, Annals of Phys. **206**, 409 (1991); Phys. Rev. **C42**, R1830 (1990).

[15] D. J. Thouless, *The Quantum Mechanics of Many Body Systems*, Academic Press, New York (1961)

[16] B. A. Brown, A. Etchegoyen, and W. D. M. Rae, MSU-NSCL Report 524, 1985.

[17] J. E. Hirsch, Phys. Rev. **B28**, 4059 (1983)

[18] J. Skilling, in *Maximum Entropy and Bayesian Methods*, edited by J. Skilling, (Klumer Academic Publisher, 1989) p. 45.

[19] S. F. Gull, in *Maximum Entropy and Bayessina Methods*, edited by J. Skilling (Klumer Academic Publisher, 1989) p. 53.

[20] R. N. Silver, J. E. Gubernatis, D.S. Sivia, and M. Jarell, Phys. Rev. Lett. **65**, 496 (1990); R. N. Silver, D. S. Sivia, and J. E. Gubernatis, Phys. Rev. **B41**, 2380 (1990).

[21] F. A. Berezin, *The Method of Second Quantization* (Academic Press, 1966).

[22] E. Y. Loh, Jr., and J. E. Gubernatis, in *Electronic Phase Transitions*, edited by W. Hanke and Yu. V. Kopaev (Elsevier Science Publishers B.V., 1992).

[23] J. Dobaczewski and S. E. Koonin, Caltech Preprint No. MAP-35, 1983 (unpublished).

[24] S. R. White, D. J. Scalapino, R. L. Sugar, and N. E. Bickers, Phys. Rev. Lett. **63**, 14 (1989); S. R. White, Phys. Rev. **B46**, 5678 (1992).

[25] C. W. Johnson, S. E. Koonin, G. H. Lang and W. E. Ormand, Phys. Rev. Lett. **69**, 3157 (1992)

[26] W. E. Ormand, D. J. Dean, C. W. Johnson, G. H. Lang and S. E. Koonin, to be submitted to Phys. Rev. **C**.

[27] E. Y. Loh, Jr., J. E. Gubernatis, R. T. Scalettar, S. R. White, D. J. Scalapino, and R. L. Sugar, Phys. Rev. **B41**, 9301 (1990); S. B. Fahy and D. R. Hamann, *Phys. Rev.* **B43**, *765 (1991).*

[28] J. W. Negele and H. Orland, *Quantum Many-particle Systems*, Addison-Wesley, RedWood City (1988)

FIGURES

FIG. 1. Schematic diagram of nuclear level systems with spin-orbit coupling, from [8]

FIG. 2. Auto-correlation for different observables in consecutive sweeps in different Hubbard-Stratonovich transformations and Monte Carlo sampling schemes. The continuous HS transformation (2.7) was implemented in the traditional Metropolis and the hybrid-Gaussian random walk, as described in Section VI.A. The discrete HS transformations (2.28) with two-point (2.30) and three-point (2.31) quadrature was carried out as described in Section VI.B.

FIG. 3. The convergence behavior in $\langle H \rangle$ of different HS transformation scheme as $\Delta\beta \to 0$. The cross at $\Delta\beta = 0$ indicates the exact result.

FIG. 4. Grand canonical ensemble for protons only in the *sd* shell with monopole interaction (all six $E_{J=0}$ matrix elements of the Wildenthal interaction), at $\langle N_p \rangle = 3.17$, $\beta = 1$. Shown are $\langle H \rangle$ and $\langle J^2 \rangle$ as functions of $\Delta\beta$ for three different decompositions: pure pairing decomposition, pure density decomposition, and a half-density and half-pairing decomposition. Solid diamonds at $\Delta\beta$ are the exact results obtained by direct diagonalization.

FIG. 5. Zero-temperature calculations of ^{24}Mg with the schematic interaction (6.7). Note the relaxation of $\langle H \rangle$ and $\langle J^2 \rangle$ as β increases. Hollow triangles are static path calculations in the pure density decomposition, solid diamonds are static path calculations by decomposing the pairing interaction into pair operators and the multipole interaction into density operators. Solid circles and hollow squares are both calculations in a pure density decomposition with $\Delta\beta = 0.125$, using the Hartree solution and the maximal prolate state, respectively, as the trial wavefunction. The solid line segments indicate the exact ground state results.

FIG. 6. Canonical ensemble calculations of ^{20}Ne with the schematic interaction (6.7) at $\Delta\beta = 0.25, 0.125$ and 0.0625 and the exact results; $\langle H \rangle$ and $\langle J^2 \rangle$ are shown as functions of β. These calculations were done in a pure density decomposition.

FIG. 7. Similar to Fig. 6 for ^{24}Mg.

FIG. 8. Finite temperature cranked calculations of ^{20}Ne with the schematic interaction (6.7) in canonical ensemble using a pure density decomposition. Here $\beta = 1$, with $\Delta\beta = 0.125, 0.0625$ and 0.03125. The exact cranking curve is also shown.

FIG. 9. Canonical ensemble calculations of the response functions for ^{20}Ne ($\beta = 2.5$) at discrete imaginary time using $\Delta\beta = 0.125, 0.0625$, in a pure density decomposition. The exact results are calculated in the ground state. (a), (c), (e) show the relaxation of isoscalar quadrupole ($Q = Q_p + Q_n$), isovector quadrupole ($Q_v = Q_p - Q_n$) and the isovector angular momentum ($J_v = J_p - J_n$) responses. The corresponding most probable strength functions recovered by the MaxEnt method are shown in (b), (d), (f) respectively. The exact strength functions calculated from ground state are plotted as discrete lines with the height indicating the integrated strength of the delta-functions.

FIG. 10. Similar to Fig. 9. but for the single-particle pickup and stripping response. (a), (c), (e) show the imaginary time stripping response for the $j = \frac{5}{2}$ orbital, and the pickup responses of the $j = \frac{5}{2}$ and $j = \frac{1}{2}$ orbitals respectively. The corresponding most probable strength functions recovered by the MaxEnt method are shown in (b), (d), (f) respectively. The exact response and strength functions are calculated for the ground state.

FIG. 11. Similar to Figs. 9,10. but for the $j = \frac{3}{2}$ orbital. This shows the imaginary time pickup and stripping response of $j = \frac{3}{2}$ orbital. The response functions are in agreement with the exact curve for small τ and then abruptly follows the $j = \frac{5}{2}$ response.

TABLES

TABLE I. The 1st and 2nd moment of the strength function recovered by MaxEnt calculated from (C15) for fig. 9 and 10. The extrapolated total strength and moments ($\Delta\beta \rightarrow$) are compared with the results calculated from the ground state of ^{20}Ne in an exact diagonalization approach.

		$\Delta\beta = 0.125$	$\Delta\beta = 0.0625$	extract	exact
	total strength	27.3 ± 0.2	25.9 ± 0.1	24.5	25.1
$Q(\tau) \cdot Q(0)$	$\langle\omega\rangle$	2.33 ± 0.08	2.77 ± 0.08	3.22	3.46
	$\langle\omega^2\rangle$	8.09 ± 1.2	10.5 ± 1.2	12.9	15.4
	total strength	6.26 ± 0.03	6.78 ± 0.02	7.29	6.96
$Q_v(\tau) \cdot Q_v(0)$	$\langle\omega\rangle$	7.24 ± 0.15	7.77 ± 0.10	8.31	8.38
	$\langle\omega^2\rangle$	59.9 ± 3.9	66.6 ± 2.5	73.4	73.8
	total strength	16.3 ± 0.1	16.05 ± 0.08	15.8	15.9
$J_v(\tau) \cdot J_v(0)$	$\langle\omega\rangle$	8.49 ± 0.25	9.44 ± 0.19	10.39	10.39
	$\langle\omega^2\rangle$	89.8 ± 9.04	107.7 ± 6.4	125.6	119.6
	total strength	1.59 ± 0.01	1.62 ± 0.07	1.64	1.59
$\sum_m a^\dagger_{5/2m}(\tau) a_{5/2m}(0)$	$\langle\omega\rangle$	9.84 ± 0.12	10.32 ± 0.09	10.80	10.98
	$\langle\omega^2\rangle$	98.0 ± 2	107.5 ± 1.4	117	121
	total strength	4.47 ± 0.01	4.42 ± 0.09	4.37	4.41
$\sum_m a_{5/2m}(\tau) a^\dagger_{5/2m}(0)$	$\langle\omega\rangle$	-3.15 ± 0.02	-3.00 ± 0.02	-2.86	-2.81
	$\langle\omega^2\rangle$	10.28 ± 0.05	9.71 ± 0.04	9.14	10.08
	total strength	1.702 ± 0.004	1.745 ± 0.003	1.788	1.773
$\sum_m a_{1/2m}(\tau) a^\dagger_{1/2m}(0)$	$\langle\omega\rangle$	-3.19 ± 0.01	-3.22 ± 0.02	-3.25	-3.16
	$\langle\omega^2\rangle$	10.43 ± 0.06	10.65 ± 0.04	10.87	11.62

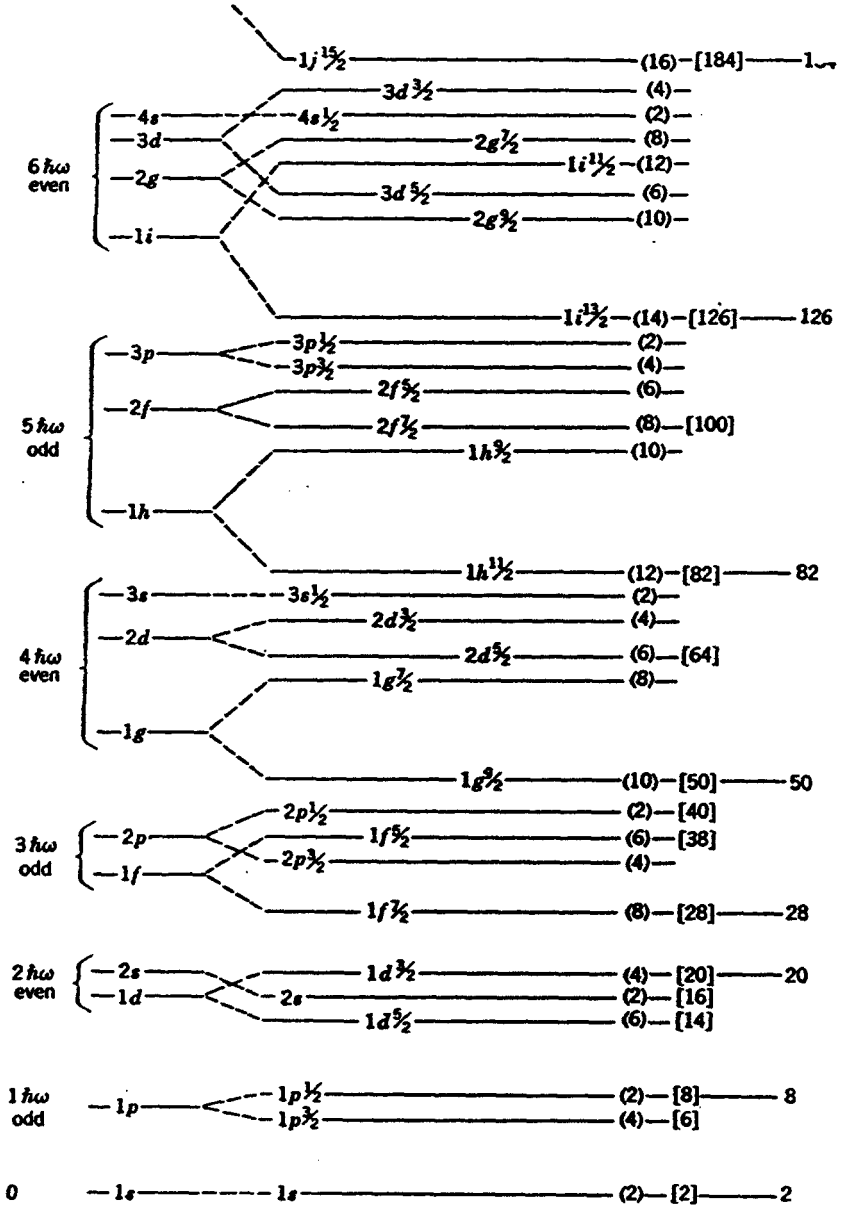
1j15/2 (16) [184]
3d3/2 (4)
4s1/2 (2)
2g7/2 (8)
1i11/2 (12)
3d5/2 (6)
2g9/2 (10)
6ħω even
4s
3d
2g
1i
1i13/2 (14) [126] 126
3p1/2 (2)
3p3/2 (4)
2f5/2 (6)
2f7/2 (8) [100]
1h9/2 (10)
5ħω odd
3p
2f
1h
1h11/2 (12) [82] 82
3s1/2 (2)
2d3/2 (4)
2d5/2 (6) [64]
1g7/2 (8)
4ħω even
3s
2d
1g
1g9/2 (10) [50] 50
2p1/2 (2) [40]
1f5/2 (6) [38]
2p3/2 (4)
1f7/2 (8) [28] 28
3ħω odd
2p
1f
1d3/2 (4) [20] 20
2s (2) [16]
1d5/2 (6) [14]
2ħω even
2s
1d
1p1/2 (2) [8] 8
1p3/2 (4) [6]
1ħω odd
1p
0
1s
1s (2) [2] 2

Fig. 1

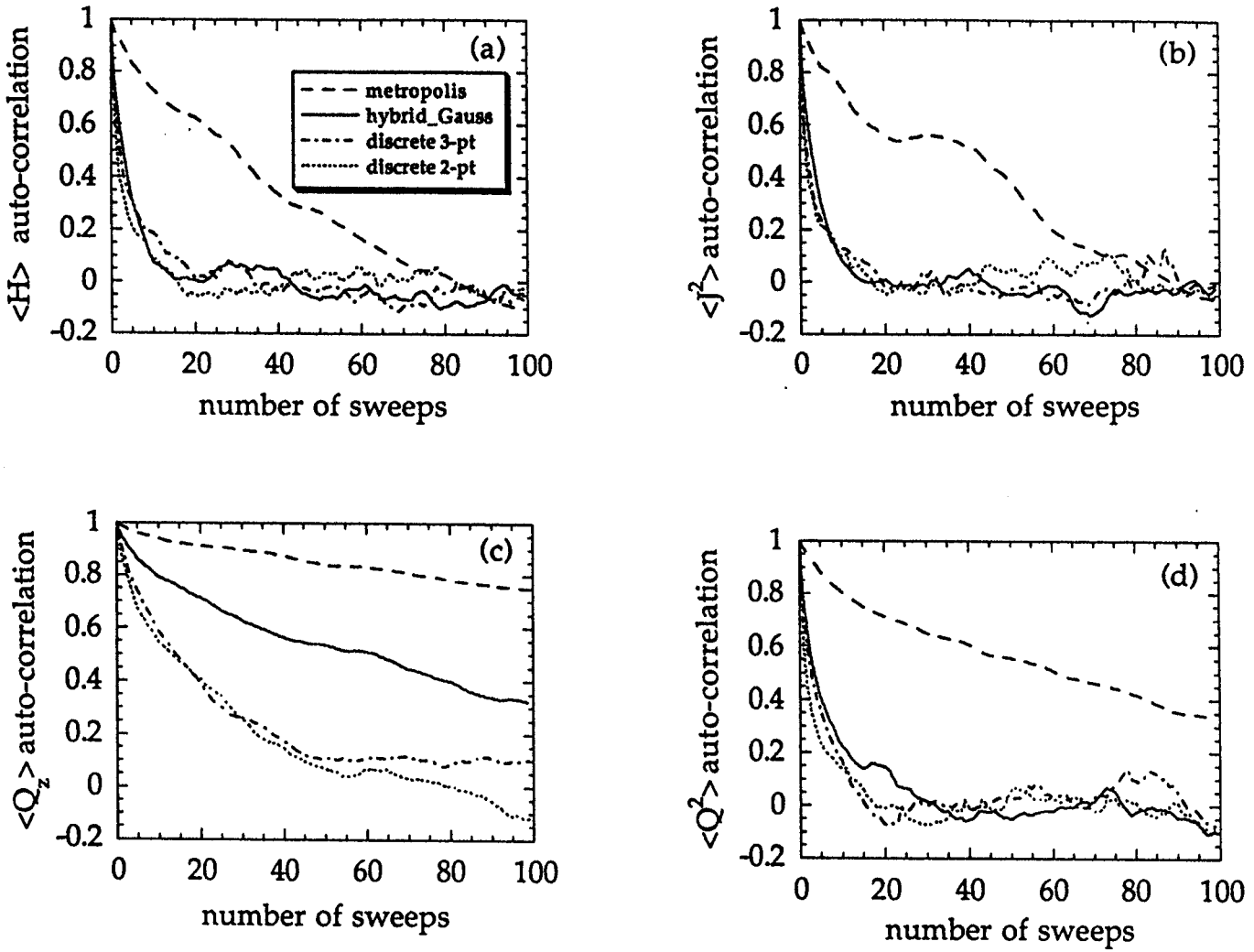
(a)
metropolis
hybrid_Gauss
discrete 3-pt
discrete 2-pt
<H> auto-correlation
number of sweeps
(b)
<J²> auto-correlation
number of sweeps
(c)
<Q_z> auto-correlation
number of sweeps
(d)
<Q²> auto-correlation
number of sweeps

Fig. 2

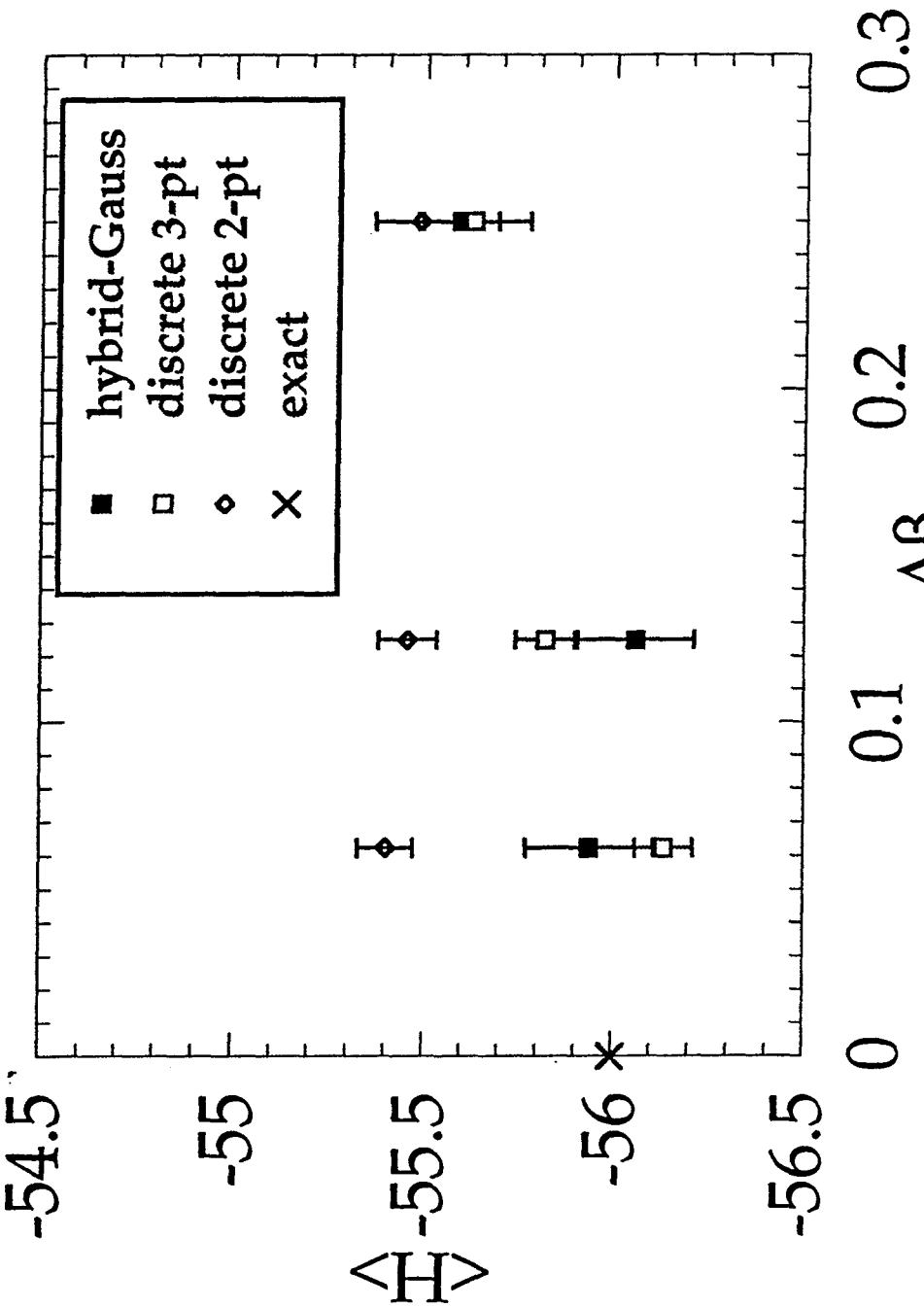
hybrid-Gauss
discrete 3-pt
discrete 2-pt
exact
-54.5
-55
-55.5
-56
-56.5
<H>
0
0.1
0.2
0.3
Δβ

Fig. 3

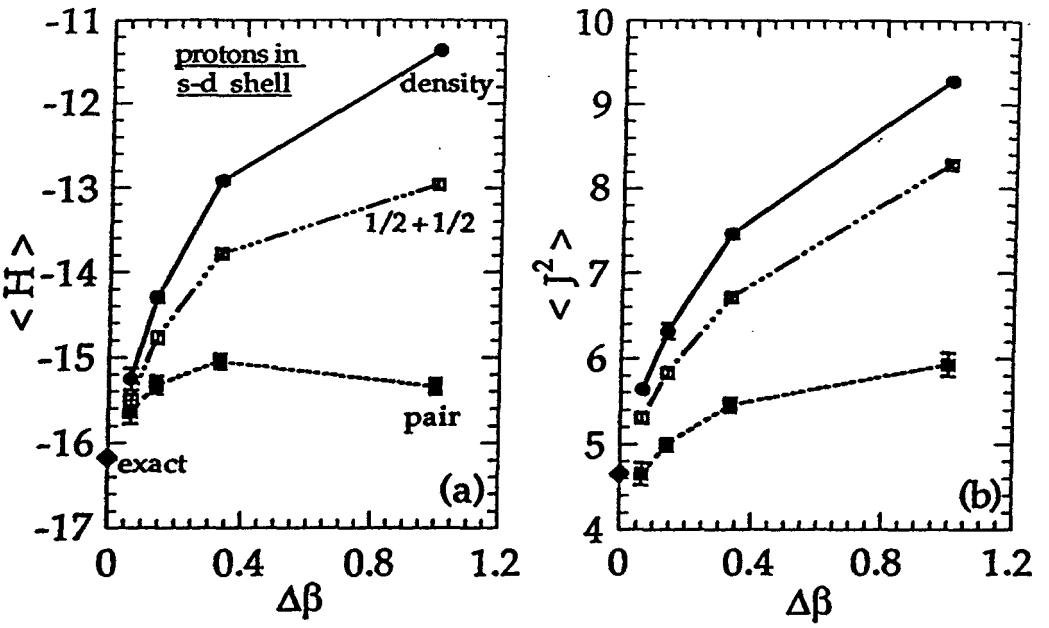
protons in
s-d shell
density
1/2+1/2
pair
exact
(a)
(b)
<H>
<J²>
Δβ
-11
-12
-13
-14
-15
-16
-17
10
9
8
7
6
5
4
0
0.4
0.8
1.2

Fig. 4

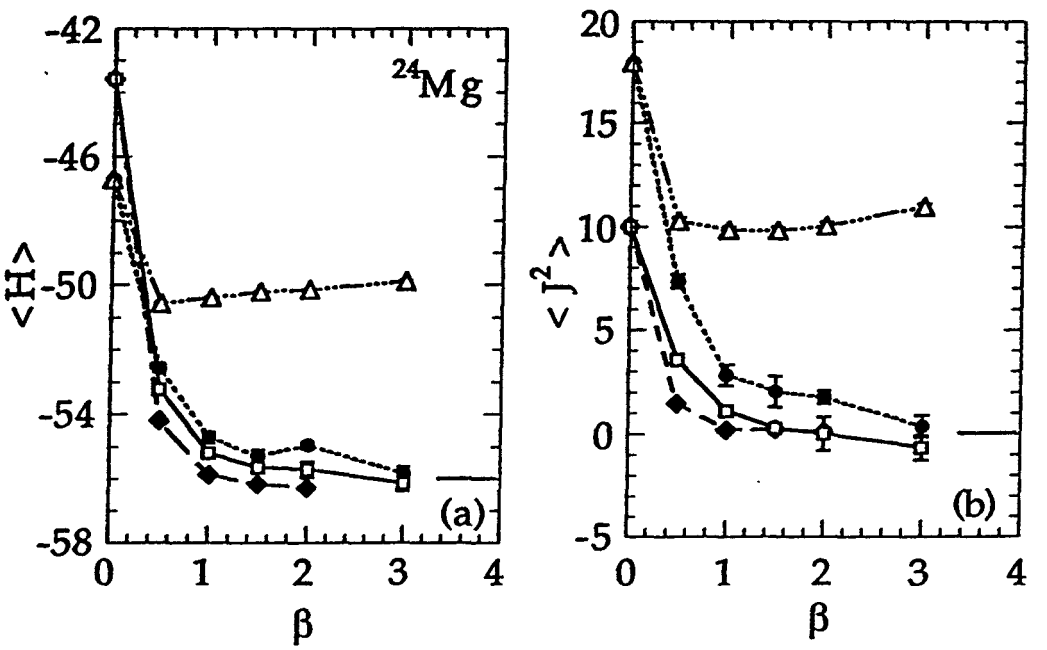
²⁴Mg
(a)
(b)
<H>
<J²>
β
-42
-46
-50
-54
-58
20
15
10
5
0
-5
0
1
2
3
4

Fig. 5

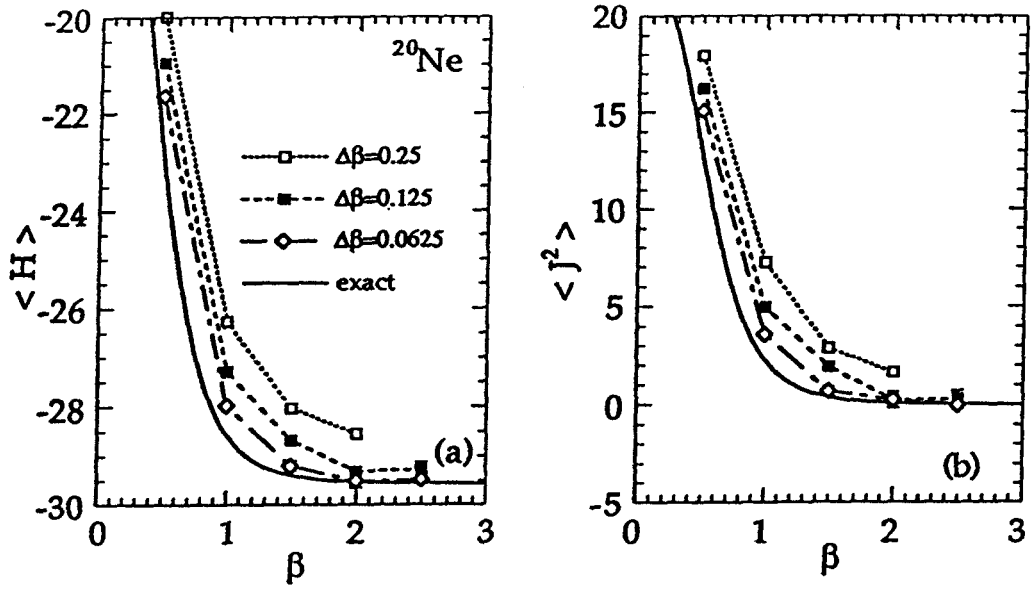
^{20}Ne
Δβ=0.25
Δβ=0.125
Δβ=0.0625
exact
(a)
(b)
< H >
< J^2 >
β

Fig. 6

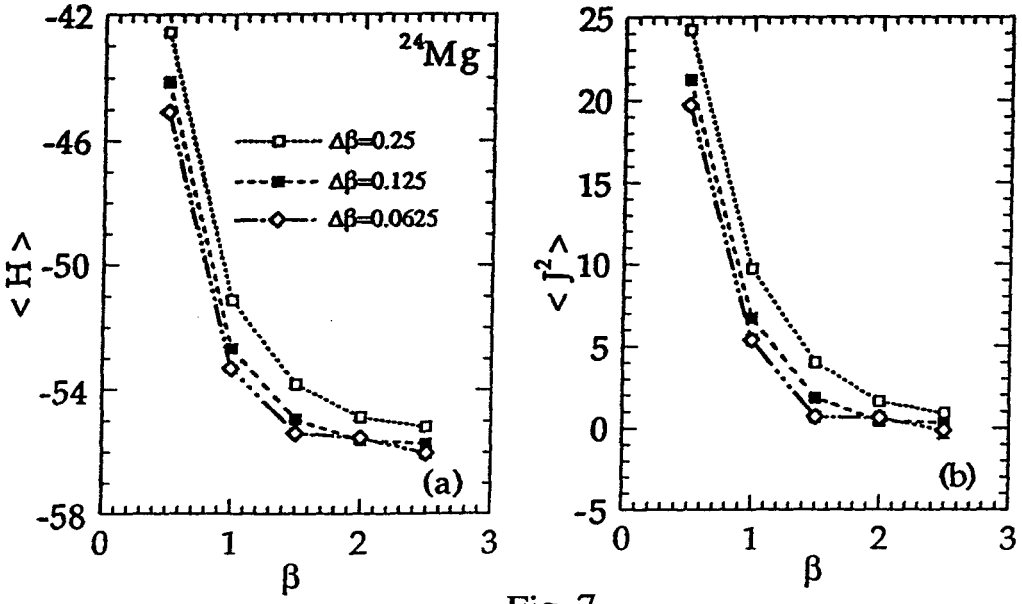
^{24}Mg
Δβ=0.25
Δβ=0.125
Δβ=0.0625
(a)
(b)
< H >
< J^2 >
β

Fig. 7

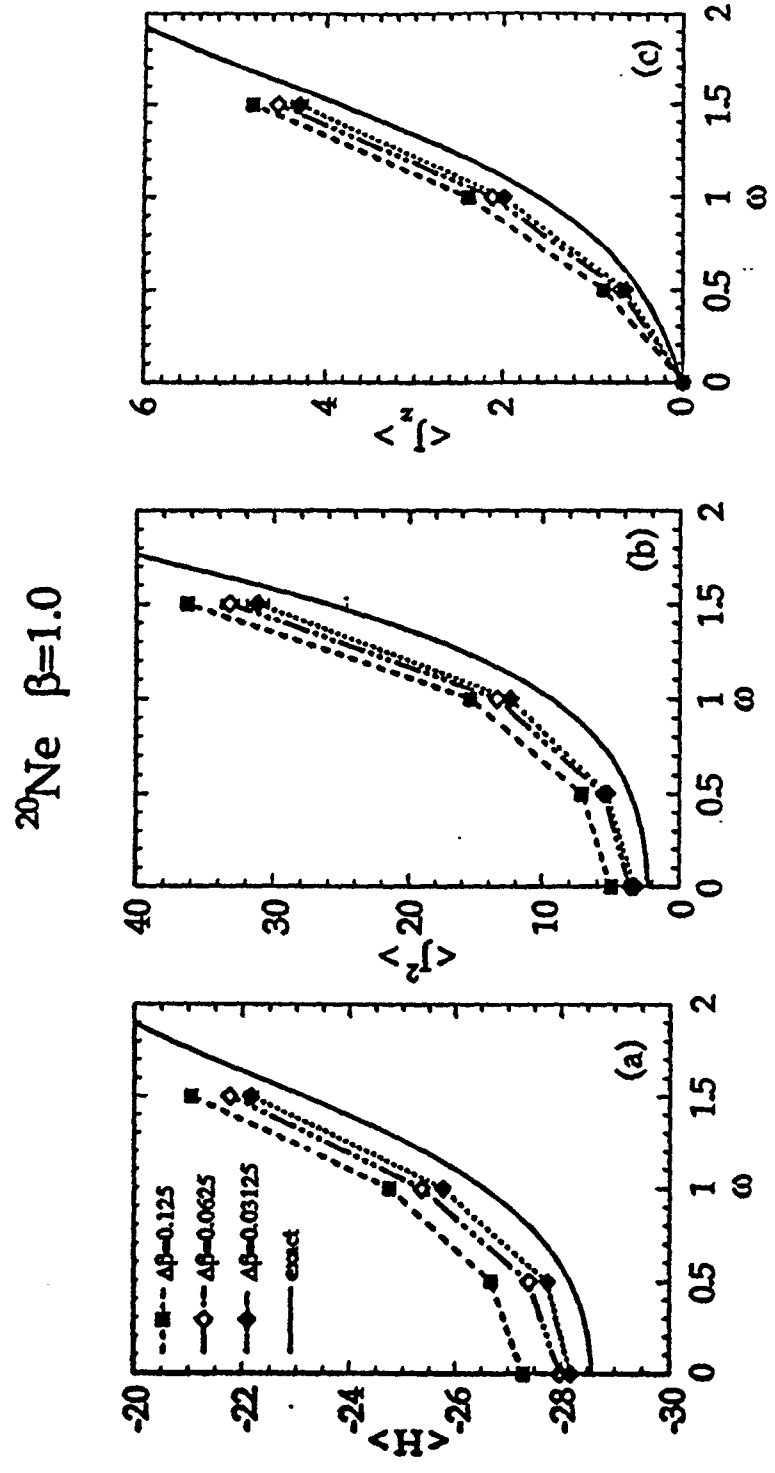

Fig. 8

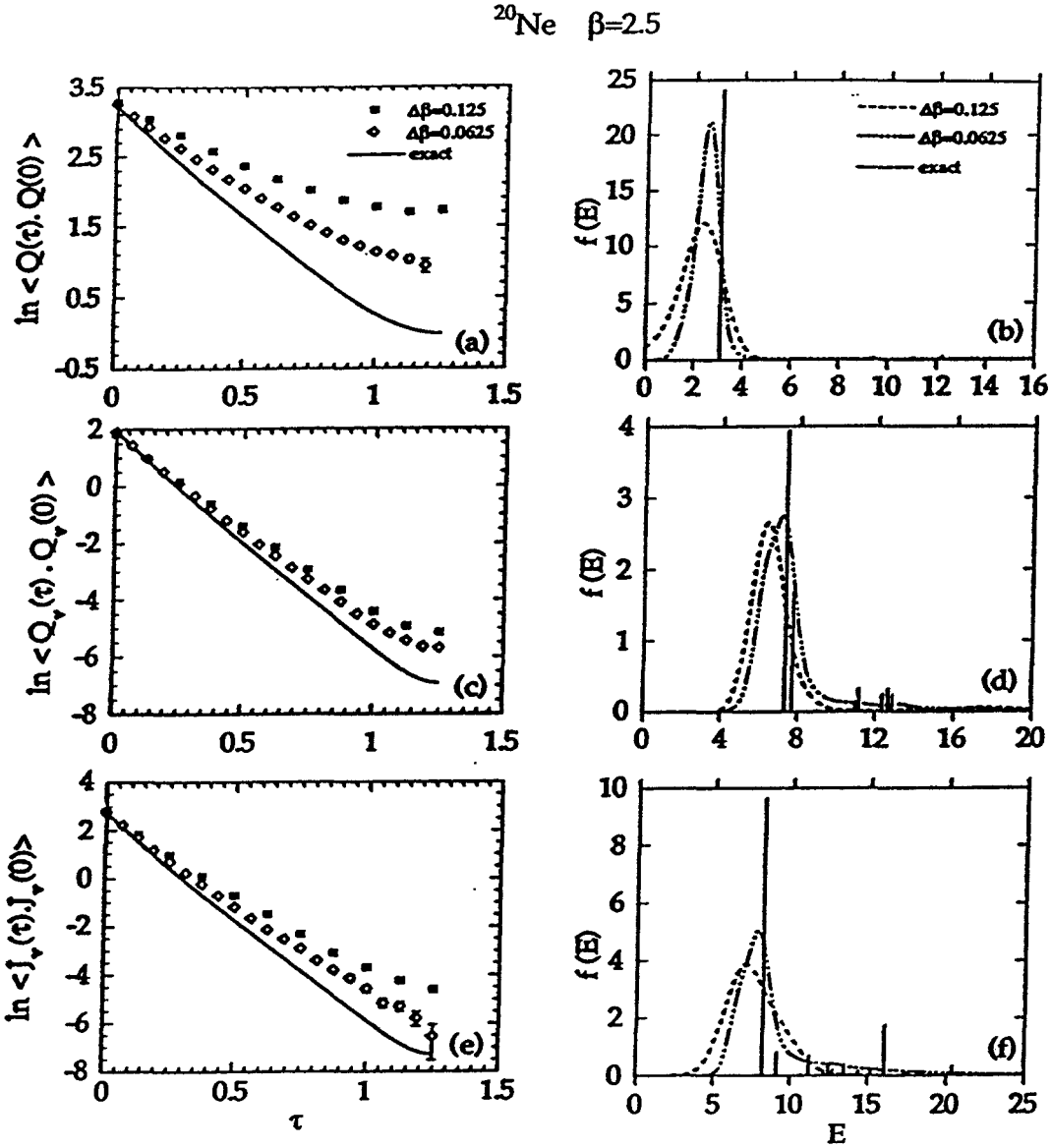
^{20}Ne β=2.5
Δβ=0.125
Δβ=0.0625
exact
ln <Q(τ).Q(0)>
ln <Q_v(τ).Q_v(0)>
ln <J_v(τ).J_v(0)>
f(E)
(a)
(b)
(c)
(d)
(e)
(f)
τ
E

Fig. 9

^{20}Ne β=2.5

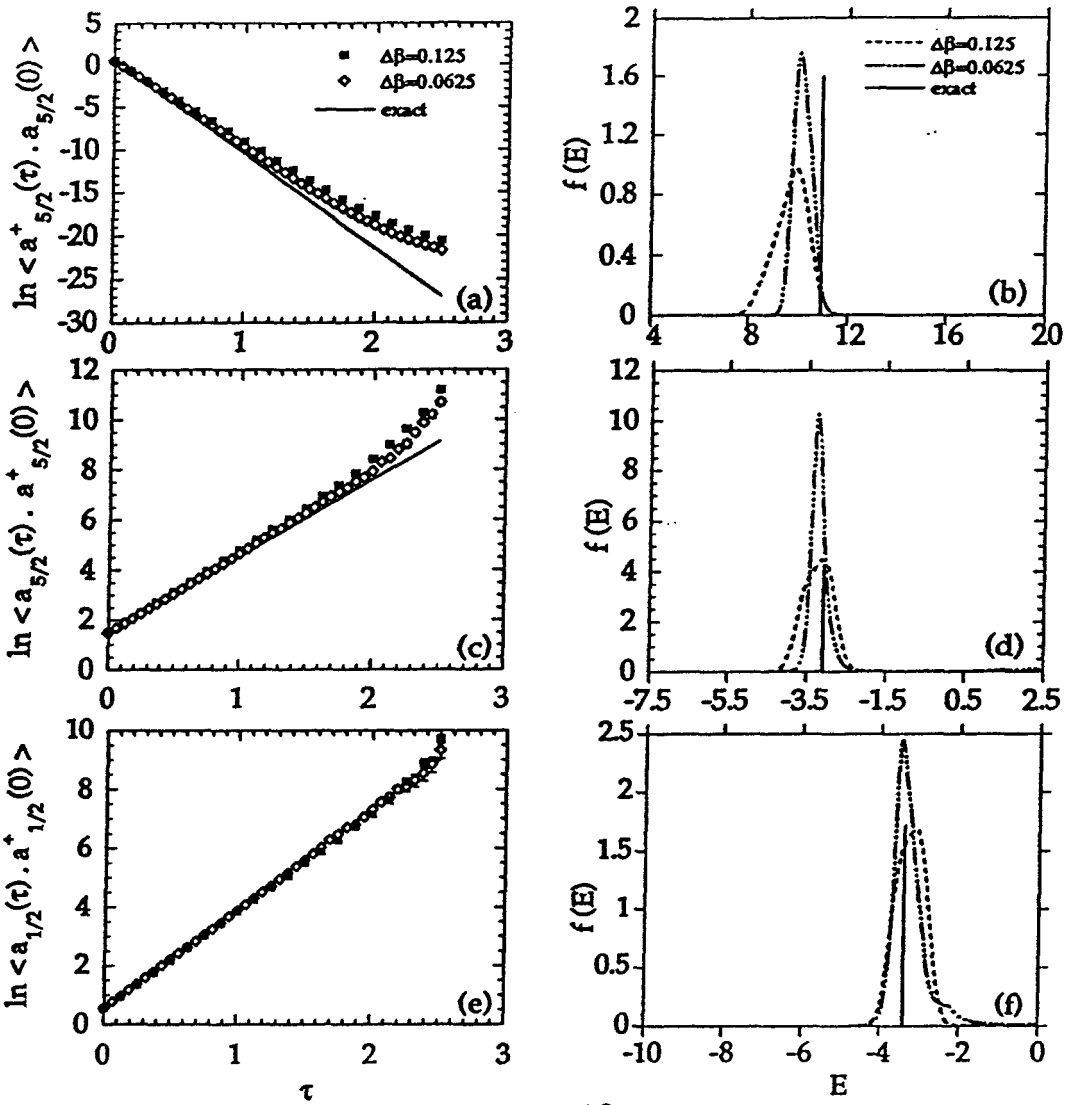

Fig. 10

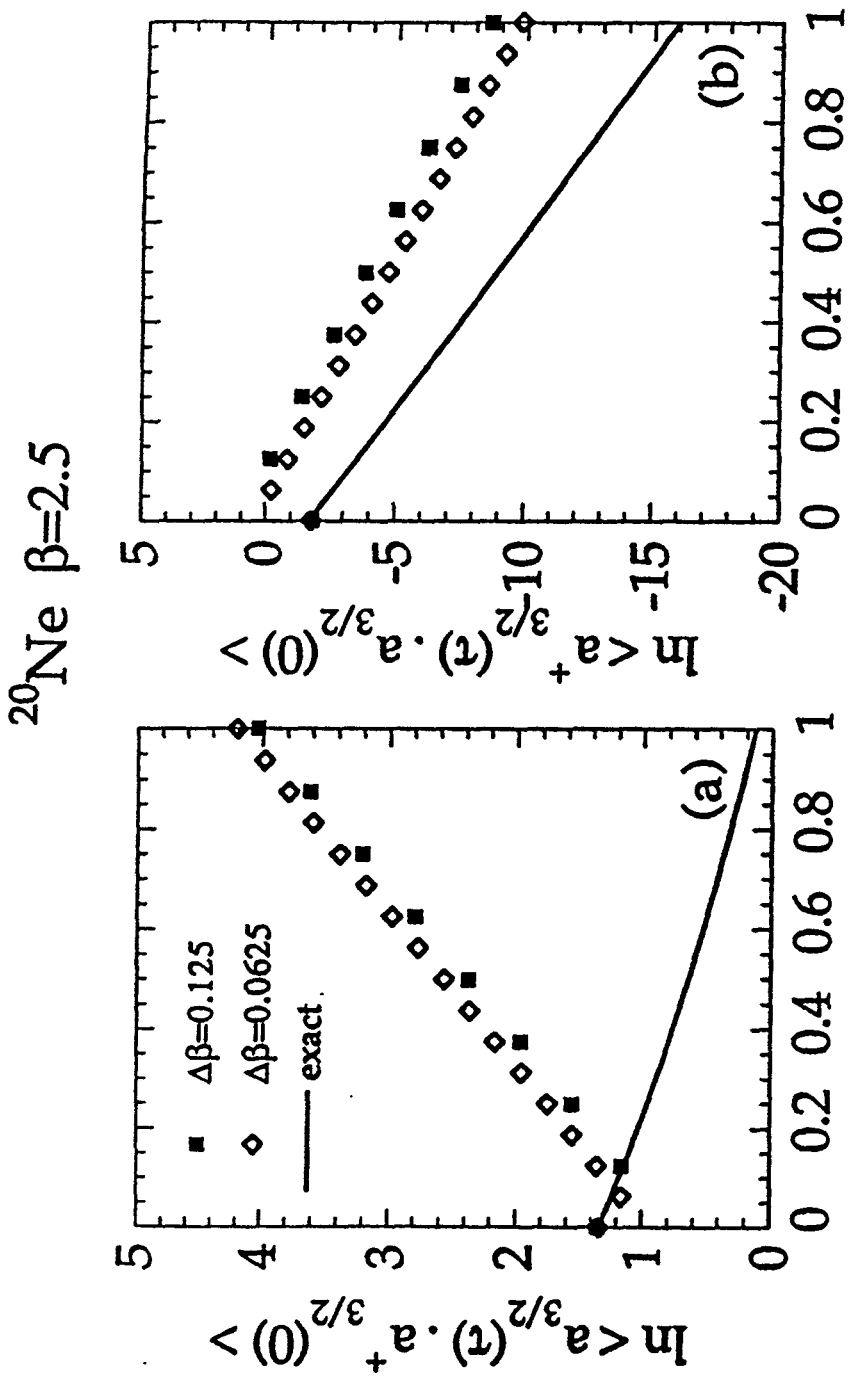

Fig. 11